



BRNO UNIVERSITY OF TECHNOLOGY

VYSOKÉ UČENÍ TECHNICKÉ V BRNĚ

FACULTY OF ELECTRICAL ENGINEERING AND COMMUNICATION

FAKULTA ELEKTROTECHNIKY A KOMUNIKAČNÍCH TECHNOLOGIÍ

DEPARTMENT OF RADIO ELECTRONICS

ÚSTAV RADIOELEKTRONIKY

METHODS OF NUMERICAL INVERSION OF LAPLACE TRANSFORMS FOR ELECTRICAL ENGINEERING AND THEIR APPLICATIONS

METODY NUMERICKÉ INVERZNÍ LAPLACEOVY TRANSFORMACE PRO ELEKTROTECHNIKU A
JEJICH APLIKACE

DOCTORAL THESIS

DISERTAČNÍ PRÁCE

AUTHOR

AUTOR PRÁCE

Nawfal Al-Zubaidi R-Smith, MSc.

SUPERVISOR

ŠKOLITEL

prof. Ing. Lubomír Brančík, CSc.

BRNO 2018

ABSTRACT

Numerical inverse Laplace transform (NILT) methods have become a fundamental part of the numerical toolset of practitioners and researchers in a large number of science and engineering fields, especially in the electrical engineering applied domain. Mainly, NILT techniques assist in getting the time-domain simulations in related applications, e.g. solving ordinary differential equations as those appearing when solving lumped-parameter circuits, solving partial differential equations as in linear distributed-parameter systems or those emerging while investigating signal integrity issues.

Generally, most available 1D NILT methods are very specific, i.e. they perform well on a few type of functions and hence on a limited number of applications; thus the aim of this research is to provide a broad treatment of such numerical methods, the development of universal NILT method and its expansion to multidimensional NILT which can cover a wide field of applications and could provide a practical mechanism for a better diagnosis and analysis of time domain simulations. The reach of the ideas is presented by discussing a wide range of case studies and applications; for example, the NILT methods are applied in solving transmission lines, including multiconductor ones, and even for the solution of weakly nonlinear circuits while utilizing multivariable NILTs. With the assistance of the NILT method an advantage of including frequency dependent parameters and using fractional-order elements in their respective models can be done in a very accurate and simple manner.

KEYWORDS

Numerical inverse Laplace transforms, multidimensional Laplace transforms, transient analysis, accelerated summation, numerical accuracy and efficiency, transmission line modelling, multiconductor transmission line, fractional calculus, frequency domain analysis, frequency dependence, fractional telegraph equation, Matlab language.

Al-Zubaidi R-Smith, N. *Methods of numerical inversion of Laplace transforms for electrical engineering and their applications*: doctoral thesis. Brno: Brno University of Technology, Faculty of Electrical Engineering and Communication, Department of Radio Electronics, 2018. 132 p. Supervised by prof. Ing. Lubomír Brančík, CSc.

DECLARATION

I declare that I have written my doctoral thesis on the topic of “Methods of Numerical Inversion of Laplace Transforms for Electrical Engineering and Their Applications” independently under the guidance of the doctoral thesis supervisor and using the technical literature and other sources of information, which are all quoted in the thesis and detailed in the list of literature at the end of the thesis.

As the author of the doctoral thesis I furthermore declare that, in regard to the creation of this doctoral thesis, I have not infringed any copyright. In particular, I have not unlawfully encroached on anyone’s personal and/or ownership rights and I am fully aware of the consequences in the case of breaking Regulation S 11 and the following of the Copyright Act No 121/2000 Sb., and of the rights related to intellectual property right and changes in some Acts (Intellectual Property Act) and formulated in later regulations, inclusive of the possible consequences resulting from the provisions of Criminal Act No 40/2009 Sb., and of the rights related to intellectual property right and changes in some Acts (Intellectual Property Act) and formulated in later regulations, inclusive of the possible consequences resulting from the provisions of Criminal Act No 40/2009 Sb., Section 2, Head VI, Part 4.

Brno

.....

(Author’s signature)

ACKNOWLEDGEMENT

This doctoral dissertation was only made possible due to the support and advice I have received from numerous people during the last four years.

First and foremost, I would like to express my deepest appreciation to my supervisor prof. Ing. Lubomír Brančík, CSc. for his invaluable guidance and assistance throughout the years.

I would like to thank my fellow Ph.D. colleagues, as we not only shared an office together, but also shared valuable discussions, experiences and found high motivation from one another: Eva Klejmová, Peter Barčík, Aleš Dobesch, Edward Kassem, Chandra Aniruddh, Marek Novák, and Lukáš Janík. I thank the Radio Electronic Department staff especially our Head of Department Prof. Ing. Tomáš Kratochvíl, Ph.D., who has always been a great motivation in my work and was always very friendly and supportive throughout the years.

I would also like to thank the co-authors of the included papers of the international conferences and impacted journals. I thank prof. Ing. Lubomír Brančík, CSc., doc. RNDr. Edita Kolářová Ph.D., Mgr. Aslihan Kartci and Ing. Filip Záplata, Ph.D. for reading, reviewing, engaging in important discussions, and providing valuable remarks and ideas. I thank the great people in Johannes Kepler University Linz for receiving me, inspiring me and helping me advance in my work: prof. Robert Willie, dr. Alexander Paler, Andres Grimmer, Sebastian Pointner and Alwin Zulehner.

In addition, and most importantly I thank my dear mother Elizabeth Smith and my dear father dr. Khamis Al-Zubaidi for their indefatigable support. I thank my gorgeous wife Anna Maria and my charming son Mishal for their endless patience, love and for all the great moments we share together.

Nawfal Al-Zubaidi R-Smith, MSc.

Brno, 2018

ACKNOWLEDGMENT

The research described in this doctoral thesis has been implemented in the laboratories supported by the Sensor, Information and Communication Systems Research Centre (SIX) project; registration number CZ.1.05/2.1.00/03.0072. Operational Program Research and Development for Innovation.

Brno

.....

(author's signature)

Contents

INTRODUCTION	12
1 STATE OF THE ART	14
1.1 One-dimensional NILT methods	14
1.1.1 Fourier series expansion methods	14
1.1.2 Combination of Gaver functional	16
1.1.3 Deforming the Bromwich contour	18
1.1.4 Laguerre function expansion	19
1.2 Overview of the one-dimensional NILTs applications	20
1.3 Two-dimensional NILTs	20
1.3.1 Accelerated <i>FFT</i> and <i>IFFT</i> -based two-dimensional NILTs by partial inversion	21
1.3.2 Two-dimensional NILT by fast Hartley transform computations	23
1.3.3 Two-dimensional NILT by the Fourier series representation . .	23
1.3.4 Two-dimensional NILT based on Zakian's numerical scheme .	25
1.4 Overview of the two-dimensional NILTs applications	26
1.5 Multi-dimensional NILTs	26
1.5.1 Numerical inversion of 3D Laplace transform method based on FFT and IFFT	27
1.5.2 Overview of multi-dimensional NILTs applications	27
1.6 Fractional calculus and applied analysis for NILT applications	28
1.6.1 Basic fractional differential equation definitions	30
1.6.2 Basic fractional calculus of electronic components	31
2 DISSERTATION OBJECTIVES	33
2.1 Theoretical basis analysis and comparative studies	33
2.2 Multivariable integral transforms	33
2.3 Development of effective NILT techniques	34
3 1D HYPERBOLIC NILT METHOD	35
3.1 Original proposed 1D hyperbolic-based NILT method	35
3.1.1 Error analysis of the 1D hyperbolic NILT method	37
3.2 Alternative approach for the derivation of the hyperbolic NILT method	39
3.3 Enhancements on the 1D hyperbolic NILT method	41
3.3.1 Generalization of the 1D hyperbolic NILT method	41
3.3.2 Integration of infinite series convergence acceleration techniques	41
3.3.3 Experimental error analysis	46

3.4	Comparative study for the 1D hyperbolic NILT method	50
3.5	Summary	53
4	APPLICATIONS OF THE 1D HYPERBOLIC NILT METHOD	54
4.1	Lossy transmission line simulation using the hyperbolic NILT method	54
4.2	Incorporation of fractional-order transmission line primary parameters	56
4.3	Incorporation of frequency dependent transmission line parameters . .	59
4.4	Fractional-order TL model simulation	60
4.5	Nonuniform transmission line with fractional-order elements	62
4.6	Multiconductor transmission line systems with linear terminations . .	69
4.6.1	Fractional-order MTL case study	73
4.7	Nonuniform multiconductor transmission line systems with possible external feedback	78
4.7.1	Nonuniform MTL case study	82
4.8	Summary	84
5	EXPANSION OF HYPERBOLIC NILT METHOD INTO THE TWO DIMENSIONAL FORM	85
5.1	Simulation and analysis of some 2D NILT methods	85
5.2	Numerical method of the hyperbolic NILT two-dimensional expansion	90
5.2.1	Theoretical concept and basic formulae	90
5.2.2	The numerical method	91
5.3	Error analysis of devised 2D hyperbolic NILT method	94
5.4	Comparative analysis of the 2D hyperbolic NILT method	96
5.5	Summary	97
6	APPLICATION OF THE MNILT METHODS IN THE ELECTRI- CAL ENGINEERING FIELD	98
6.1	Transmission line simulation using the 2D hyperbolic NILT method .	98
6.1.1	Transmission line via 2D hyperbolic NILT case study	99
6.2	Weakly nonlinear-circuit solution via MNILT	100
6.2.1	Weakly nonlinear circuits using 1D to 3D NILTs case study . .	102
6.3	Summary	105
7	RESEARCH CHALLENGES AND CONCLUSIONS	106
	Bibliography	110
	List of abbreviations	123
	List of appendices	124

A Curriculum Vitae	125
B List of Publications	128
C Achievements	132

List of Figures

1.1	Resulting 3D shifted unit step by utilizing the 3D-NILT method. . . .	28
3.1	The quotient-difference algorithm's lozenge diagram.	44
3.2	The ε -algorithm's lozenge diagram.	45
3.3	Accuracy experiment results of the accelerated hyperbolic NILTs with test function F_1	47
3.4	Accuracy experiment results of the accelerated hyperbolic NILTs with test function F_2	48
3.5	Accuracy experiment results of the accelerated hyperbolic NILTs with test function F_3	49
3.6	Test results of the Zakian, Talbot, Stehfest, FFT-Qd NILT and Hyp-Eul NILT methods with function F_1	51
3.7	Test results of the Zakian, Talbot, Stehfest, FFT-Qd NILT and Hyp-Eul NILT methods with function F_2	51
3.8	Test results of the Zakian, Talbot, Stehfest, FFT-Qd NILT and Hyp-Eul NILT methods with function F_3	52
3.9	Hyp-Eul NILT inversion and corresponding absolute error for function $f(t) = \cos(\omega t)$	53
4.1	Transmission line model in the Laplace domain.	54
4.2	Voltage waveforms conditions along TL by via 1D Hyp-Eul NILT. . .	56
4.3	Current waveforms conditions along TL via 1D Hyp-Eul NILT.	56
4.4	Fractional-order primary parameters of the TL.	57
4.5	Real value of γ_f versus α and β	58
4.6	Real value of Z_{cf} versus α and β	59
4.7	Voltage waveform in the middle of the TL ($x = 1$ m).	61
4.8	Current waveform in the middle of the TL ($x = 1$ m).	61
4.9	Voltage distribution along the TL with fractional-order parameters ($\alpha = \beta = 0.98$).	62
4.10	Voltage distribution along the TL with fractional-order parameters ($\alpha = \beta = 0.95$).	62
4.11	Nonuniform transmission line with linear terminations.	63
4.12	Electrical circuit of an infinitesimal segment of a transmission line. . .	64
4.13	Flow chart with different types of TL.	67
4.14	Voltage distribution along several TL types.	67
4.15	Voltage and current distributions on nonuniform TL with different fractional-order elements.	69
4.16	General $(n + 1)$ -conductor TL system with linear terminations.	70
4.17	A $(3 + 1)$ -conductor TL system.	73

4.18	Voltage distribution on the 1 st and the 3 rd line with integer-orders $\alpha = \beta = 1$	74
4.19	Voltage distribution on the 1 st and the 3 rd line with fractional-orders $\alpha = \beta = 0.97$	74
4.20	Voltage distribution on the 1 st and the 3 rd line with fractional-orders $\alpha = \beta = 0.84$	74
4.21	Current distribution on the 1 st and the 3 rd line with integer-orders $\alpha = \beta = 1$	75
4.22	Current distribution on the 1 st and the 3 rd line with fractional-orders $\alpha = \beta = 0.97$	75
4.23	Current distribution on the 1 st and the 3 rd line with fractional-orders $\alpha = \beta = 0.84$	75
4.24	Voltage distribution on the 2 nd line with integer-orders $\alpha = \beta = 1$. . .	76
4.25	Voltage distribution on the 2 nd line with fractional-orders $\alpha = \beta = 0.97$.	76
4.26	Voltage distribution on the 2 nd line with fractional-orders $\alpha = \beta = 0.84$.	76
4.27	Current distribution on the 2 nd line with integer-orders $\alpha = \beta = 1$. . .	77
4.28	Current distribution on the 2 nd line with fractional-orders $\alpha = \beta = 0.97$.	77
4.29	Current distribution on the 2 nd line with fractional-orders $\alpha = \beta = 0.84$.	77
4.30	MTL system with possible external feedback.	79
4.31	Nonuniform MTL system with linear terminations.	82
4.32	MTL's wires voltage distributions under different conditions.	83
5.1	Inversion and error analysis of 2D NILTs for F_1	87
5.2	Inversion and error analysis of 2D NILTs for F_2	88
5.3	Inversion and error analysis of 2D NILTs for F_3	89
6.1	Transmission line model in Laplace-domain with respect to the time variable.	98
6.2	Voltage distribution along the TL via 2D hyperbolic NILT.	100
6.3	Current distribution along the TL via 2D hyperbolic NILT.	100
6.4	Diagram of a nonlinear circuit solution by using Volterra series ex- pansion and multidimensional ILTs.	102
6.5	Electrical circuit with nonlinear resistive element R_n	102
6.6	Numerical inversions leading to current response Volterra series terms by (a) 1D NILT, (b) 2D NILT, (c) 3D NILT, for an exponential impulse.	104
6.7	Numerical inversions leading to current response Volterra series terms by: (a) 1D NILT, (b) 2D NILT, (c) 3D NILT, for a unit step.	104
6.8	Resulting current response for: (a) an exponential impulse, (b) a unit step.	104
6.9	Resultant current response for the case $a = 1$ by: (a) Volterra series solution, (b) Runge-Kutta method, and (c) the relative error.	105

List of Tables

1.1	List of parameters for Zakian's method	17
3.1	List of test functions with their pre-known originals	46
3.2	1D hyperbolic NILT ξ accuracy measures.	49
3.3	List of test functions and their original-time domain values for the comparative study	50
5.1	List of two variable test functions with their pre-known originals . . .	86
5.2	Accuracy calculations of the simulated 2D NILTs	86
5.3	Parameter optimal choices used for the simulated 2D NILTs	90
5.4	Absolute static errors of the hyperbolic 2D NILT	96
5.5	Accuracy measures of 2D NILT methods using three test functions . .	97

INTRODUCTION

Numerical Inverse Laplace Transforms (NILT) methods are classified by researchers to be methods that are profoundly utilized in time-domain simulations, and they are broadly used in various scientific areas, for instance, applications that require the solution of ordinary differential equations or those dealing with partial differential equations [1–8]. Realizing and solving signal integrity issues, especially in high speed digital systems with sufficiently high-clock frequencies, is often related to the analytic solutions of mathematical governing equations. In such situations the Laplace transform ‘ $\mathbf{L}\{\cdot\}$ ’ is often used, due to its simplicity and effectiveness, to deal with different transient excitation functions (e.g. Dirac, Heaviside, periodic functions), and hence transforming the solution into a linear simplified mathematical description [2]. Primarily these transforms are very attractive in solving differential equations, which arise in fields such as automatics, control theory, and transient process in linear time invariant systems [3]. Nevertheless, the inevitable steps are to obtain the original result in the time domain which is considered to be the most difficult part and, in some situations, can be even impossible to obtain analytically [4], among which we can mention transcendental and/or irrational Laplace transforms. The NILT methods can therefore be a potential tool to overcome these complications by determining the original in a fast and accurate manner. Numerical inverse Laplace transform methods can be generally sorted according to the number of variables or dimensions that the method is derived upon, which can be categorized as follows [5–10]:

- One-dimensional NILT methods (1D NILT):
Most of the NILT methods available in literature are considered to be one-dimensional methods; these methods are fundamental, especially for the solution of ordinary differential equations.
- Two-dimensional NILT methods (2D NILT):
The two-dimensional methods are effective, and the need to use the 2D variables arise mainly for solving problems such as partial differential equations; for instance, solution of transmission line and related analysis.
- Multi-dimensional NILT methods (MNILT):
Multi-dimensional methods are important for solving more complex systems, such as that for nonlinear circuit analysis.

Performing a research on one-dimensional NILT methods shows us that there exist multiple methods, mainly those that are usually related to a specific field of application and hence could be considered as limited methods. The different 1D-NILT methods differ from one another by their range of applicability, stability, accuracy and, last but not least, the speed of computation. The range of applications

of a certain NILT method are usually difficult to anticipate without running some tests on the method and computing their absolute errors. Then, after having performed such tests, then it is possible to classify the method and decide on which field of application or ‘type of functions’ the specific NILT method performs best on. The second characteristic, the stability of the method, which is an important phenomenon of the numerical method, i.e. if a specific method is not stable on some type of function, then the method could lead to very absurd results; mathematically speaking, a reason for instability could be for example when the NILT algorithm is of a fractional form with a difference in the denominator, that could be, in some cases, equal to zero and then infinity is a result at that specific point. Generally, a stable method also means a wider range of application for the numerical method. The third characteristic to list is the accuracy of the method, or in other words, to have relatively small absolute error when performing error analysis for a NILT method. Finally, the computational speed of a NILT method; with the constant development in science and technology, time becomes a more important factor, and hence, the methods with a fast-computational time are preferred. The backbone of the NILT methods is the inverse Laplace transform (ILT) technique, as shown in equation (1) and (2), representing the Laplace transform and its inversion; where s is the Laplace complex variable,

$$F(s) = \int_0^{\infty} f(t)e^{-st} dt, \quad (1)$$

$$f(t) = \frac{1}{2\pi j} \int_0^{\infty} F(s)e^{st} ds, \quad (2)$$

The Laplace transform is an effective tool used in science and engineering specially for solving differential equations or generally assisting in time-domain simulations for different applications; even though, the main difficulty is then inverting the Laplace domain solution back into real time domain, in simple cases it could be done by using the Laplace inverting tables; however, for more sophisticated applications, such as that for systems with distributed parameters, where transcendental or irrational types of functions are involved, then the inversion is very difficult or even impossible [1,11]. In all of these mentioned cases, the NILT methods can play an efficient role in solving these quantities of interest. In research, there exist several one-dimensional NILT methods, as will be described with more details in following sections, which are used for inverting functions of one variable; much less attention was paid to higher dimensional-NILTs, mainly due to the non-existent closed form inversions [9,12–14]. Multi-dimensional NILT methods are of our high interest due to the necessity to solve scientific quantities of concern in deterministic and stochastic models, those especially arising in the fields of electrical engineering, radio communications, and computer sciences [12].

1 STATE OF THE ART

In this chapter, an overall view on different numerical inverse Laplace transform models and their characteristics will be described and categorized, with the highlighting of their fields of applications. The advantages and disadvantages of some of the highly cited NILT methods in research will be summarized in different sections, which are categorized depending on the number of variables that the method deals with, and then on the techniques used for the derivation of approximation of the inversion algorithm.

1.1 One-dimensional NILT methods

There has been a lot of work ongoing in the past years on devising and improving one-dimensional Laplace transform methods, most of which were replicas from other inversion methods; indeed a large review of one-dimensional (1D) methods was done by Davis and Martin [15]. The vast majority of the 1D methods that have a very narrow field of applications did not receive much interest, whereas the most famous 1D methods that had a higher effect in science, and had a role in being considered as origins for 2D inversions can be categorized under the following techniques [3,16],

- Fourier series expansion,
- Deforming the Bromwich contour,
- Laguerre function expansion, and
- Combination of Gaver functional.

Each of these categories will be discussed in more detail in the following subsections.

1.1.1 Fourier series expansion methods

The application of trapezoidal quadrature rule of integration to the real and imaginary parts of the Laplace transform function makes it possible to apply the Fourier series approximation. The first ones to use the Fourier series technique for NILT methods were Dubner and Abate [17]. Methods that are devised based on the Fourier series mainly start by approximating the Laplace inverse by Fourier integrals [16], i.e.

$$f_c(t) = \frac{2e^{at}}{\pi} \int_0^{\infty} \operatorname{Re}\{\hat{f}(a + jy)\} \cos(yt) dy, \quad (1.1)$$

$$f_s(t) = -\frac{2e^{at}}{\pi} \int_0^{\infty} \operatorname{Im}\{\hat{f}(a + jy)\} \sin(yt) dy, \quad (1.2)$$

where ‘Re’ and ‘Im’ denote the real and imaginary parts of a function, respectively. Many methods are based on the Fourier series approximation technique, most of

which are very similar, but have a specific way of identifying the optimum values of the method parameters. Examples of these methods are:

I. Accelerated FFT based NILTs

This method, denoted as ‘*FFT*-Qd NILT’, uses the Fourier series approximation, though modified to enable the usage of the *FFT* algorithm which speeds up the method computational time [18, 19]; furthermore, for convergence acceleration of the infinite series that appears in the method derivation functions, the epsilon or quotient-difference algorithms are adapted to the method. This numerical method was initialized by S. Crump [20], and further modified by using the *FFT* algorithm and then enabling the application of acceleration algorithms [18, 19]. These accelerated *FFT*-based algorithms were developed and implemented using the Matlab language.

The inversion formulae could be summarized as follows, [19]

$$f(t) \approx \tilde{f}(kT) = \frac{e^{ckT}}{NT} \left\{ 2\text{Re} \sum_{n=0}^{N-1} \left[F\left(c - jn \frac{2\pi}{NT}\right) e^{-jnk \frac{2\pi}{N}} \right] - F(c) \right\}, \quad (1.3)$$

by choosing $N = 2^m$, m a natural number, $s = c + j\Omega$ and then applying the *FFT* algorithm, which also has the ability to speed up the calculation of the method.

The error analysis derivation for this method leads us to proper choices of parameters, and thus, theoretically, the error can be adjusted at a desired value, for the derivation details see [21].

$$\varepsilon \leq \varepsilon_M = \frac{Me^{at}}{e^{\tau(c-\alpha)} - 1}, \quad 0 \leq t < \tau. \quad (1.4)$$

The parameter c for a desired relative error could be given as:

$$c = \alpha + \ln\left(\frac{1}{\varepsilon_{Mr} + 1}\right) \approx \alpha - \frac{\ln \varepsilon_{Mr}}{\tau}, \quad (1.5)$$

the parameter α is a free parameter that could be optimized for better results; mainly α should be positioned to the right of all poles of $F(s)$ in the Gaussian complex plane.

Two different acceleration algorithms have been in conjunction applied to this method:

- Epsilon algorithm of Wynn, as presented in [18, 22];
- Quotient difference algorithm of Rutishauser, described in [19].

The utilization of the acceleration algorithms to *FFT*-based NILT has improved its accuracy and speedup the estimated time of the inversion, due to the ability to truncate the infinite series while still obtaining relatively high

accuracy. With different experiments done on both acceleration algorithms, the inversion method gives a similar accuracy in the result though the quotient difference algorithms is generally more stable [23].

II. Honig-Hirdes method

The Honig-Hirdes inversion method [6], is based on Fourier series expansion, by a sophisticated application of the trapezoidal rule to the Bromwich integral. By considering the Laplace transform initial conditions, then the numerical inversion formula is namely:

$$f_N(t) = \frac{e^{ct}}{T} \left[-\frac{1}{2} \operatorname{Re}\{F(c)\} + \sum_{k=0}^N \left\{ \operatorname{Re}\left\{ F\left(c + j\frac{k\pi}{T}\right)\right\} \cos\left(\frac{k\pi}{T}t\right) - \operatorname{Im}\left\{ F\left(c + j\frac{k\pi}{T}\right)\right\} \sin\left(\frac{k\pi}{T}t\right) \right\} \right], \quad (1.6)$$

where $s = c + j\omega$, $\operatorname{Re}(s) > a \in R$ and $|f(t)| \leq ke^{at}$ for $t \geq t_0$.

The convergence of the series is accelerated by the use of the so called ε -algorithm. The method has been described by researchers as a method that is relatively generally applicable, and of relative ease of implementation, but a main drawback of the method is the slow convergence because of series truncation and discretization of the algorithm [24].

There are some more algorithms that are also proposed and based on the Fourier series methods for e.g. the Simon method [25], which is an improvement on the Dubner and Abate method by introducing the Euler summation to speed up the convergence and the De Hoog method [26], which is an improved Fourier series procedure using an epsilon algorithm Padé approximation for accelerating the convergence of infinite series.

1.1.2 Combination of Gaver functional

In this section NILT methods that stem from the Gaver functional, which are indorced by researchers, are described. Briefly, the Gaver functional considers a specific approximation of the expectation of the function in hand with the respect to the probability density [27,28]. The Gaver functionals are given by the following equation [29]

$$f_k(t) = (-1)^k \tau k \binom{2k}{k} \Delta^k \hat{f}(k\tau) = k\tau \binom{2k}{k} \sum_{r=0}^k (-1)^r \binom{k}{r} \hat{f}((k+r)\tau), \quad (1.7)$$

where $\tau = \ln(2)/t$ and Δ represents a forward difference operator, namely

$$\Delta \hat{f}(n\tau) = \hat{f}((n+1)\tau) - \hat{f}(n\tau). \quad (1.8)$$

Nevertheless, Gaver demonstrated that if $f(t)$ is expressed by the Taylor series for all $t > 0$, then $f_k(t)$ has the following convergence behavior $f_k(t) \approx f(t) + \frac{c_1(t)}{k} + \frac{c_2(t)}{k^2} + \dots$ as $k \rightarrow \infty$ with a fixed t .

Two of the most known methods in the category are the Zakian and the Stehfest methods, both are briefly disclosed below:

I. Zakian's method

Zakian's method is based on his derivation of an explicit formula for the numerical inverse Laplace transform [30], in which he approximates the function in time domain using an infinite series of weighted evaluations of domain function [31],

$$\hat{f}(t) = \frac{2}{t} \sum_{j=1}^N \text{Re} \left\{ k_j F \left(\frac{\alpha_j}{t} \right) \right\}. \quad (1.9)$$

From the inversion formula, it can be clearly noticed that the method is easy to implement. k_j and α_j are constant coefficients that could be both real or complex conjugate pairs. Depending on the field of application the parameter N could be optimized to get a better result. In Table 1, the values of parameters k_j and α_j are presented for the case when $N = 5$ terms [17].

Tab. 1.1: List of parameters for Zakian's method

j	α_j	k_j
1	$12.83767675 + j1.666063445$	$-36902.0821 + j196990.4257$
2	$12.22613209 + j5.012718792$	$61277.02524 \sim j95408.62551$
3	$10.93430308 + j8.409673116$	$-28916.56288 + j18169.18531$
4	$8.776434715 + j11.92185389$	$4655.361138 \sim j1.901528642$
5	$5.225453361 + j15.72952905$	$-118.7414011 \sim j141.3036911$

The authors in [32], applied the Zakian method among other methods on an application regarding the solution of the solute transport problems and have concluded that the Zakian method was considered to be relatively efficient and considered among fast computation methods, at least for some specific type of functions used in the solute transport application [33].

II. Stehfest's method

Stehfest's numerical inversion method directly approximates the time domain solution by using the following approximations: [27],

$$F_\alpha = \frac{\ln 2}{T} \sum_{i=1}^N V_i P \left(\frac{\ln 2}{T} i \right), \quad (1.10)$$

where F_α is an approximate value of the inverse $F(t)$ at T , and V_i is given as follows

$$V_i = (-1)^{\left(\frac{N}{2}+i\right)} \sum_{k=\left(\frac{i+1}{2}\right)}^{\min\left(i, \frac{N}{2}\right)} \frac{k^{\left(\frac{N}{2}+1\right)}(2k)!}{\left(\frac{N}{2}-k\right)!k!(i-k)!(2k-1)!}, \quad (1.11)$$

the parameter N is the number of terms used in the summation; it should be given as an even integer and could be optimized for best results.

The Stehfest method is quite popular for solving solute transport problems, such as that in the petroleum engineering field. A related study was done in [33], regarding a case to solving the bottom pressure response curve for well test interpretation. Furthermore, by performing several tests on the Stehfest method, we conceive that this method is more accurate for exponential types of functions in contrast to other types, as will be presented in Chap. 3.

1.1.3 Deforming the Bromwich contour

Another type of methods to derive NILTs are those based on following a specially modified Bromwich contour to derive an approximate algorithm, such a method is the Talbot's method.

I. Talbot's method

Talbot's method is categorized in methods that deform the Bromwich contour to derive an approximation inversion formula. It uses the idea of applying the composite trapezoidal rule to approximate the inverse Laplace transform equation, with consideration to the change of the Bromwich contour by the Talbot contour [15, 32, 34]. Nevertheless, Talbot's method has been recognized as one of the best performing inversion schemes, the algorithm is listed as follows

$$f(t) \approx \tilde{f}(t) = \lambda \frac{e^{\delta t}}{K} T_K(t), \quad (1.12)$$

$$T_N(t) = \frac{v}{2} e^{\lambda t} F(\delta + \lambda) + S_K(t), \quad (1.13)$$

$$S_K(t) = \sum_{i=1}^{K-1} \psi_j \cos(\phi_j) - \sum_{j=1}^{K-1} S_j \sin(\phi_j), \quad (1.14)$$

$$\psi_j = e^{\rho_j} (\alpha_j \gamma_j - \beta_j \delta_j), \quad S_j = e^{\rho_j} (\beta_j \gamma_j - \alpha_j \delta_j), \quad (1.15)$$

$$\rho_j = \lambda t j \frac{\pi}{K} \cos\left(j \frac{\pi}{K}\right), \quad (1.16)$$

$$\phi_j = \lambda t v j \frac{\pi}{K}, \quad F[\delta + \lambda S_v(\phi_j)] = \alpha_j + i\beta_j, \quad (1.17)$$

$$\theta_j = j \frac{\pi}{K}, \quad S_v(\theta_j) = \theta_j \cot(\theta_j) + i v \theta_j, \quad (1.18)$$

$$\dot{S}_v(\theta_j) = i(\gamma_j + i\delta_j). \quad (1.19)$$

The Talbot method is not widely used although it is considered to be among the relatively accurate methods. As mentioned earlier the Talbot method replaces the Bromwich contour of integration with a deformed contour that opens towards the negative axis; on the one hand, this transform allows for a more rapid convergence of a quadrature estimate of the complex inversion integral, but on the other hand the physical system implicitly damps high oscillator terms and thus it is not suitable for conservative problems [15]. The choice of the parameters of the Talbot contour could be considered as a difficulty since there is no straightforward method of determining these parameters, Talbot selection of the parameters was done through experimental results, Patrick O. Kano et al. in [35], present a method to select an optimal rule for the parameters of Talbot's method.

1.1.4 Laguerre function expansion

This category of devised methods imply that the expansion of the original function is approximated by a series of generalized Laguerre functions, with the advantage of having the Laplace transforms directly connected with a bi-linear transformation [15]. One of these methods is the Weeks method described below.

I. Weeks method

William Weeks describes a method in which he utilizes an expansion of orthonormal Laguerre functions [36].

The main inversion formula was suggested originally by Tricomi and is described as [15],

$$f(t) \approx t^\alpha e^{-ct} \sum_{k=0}^N a_k \frac{k!}{(a+k)!} L_k^a\left(\frac{t}{T}\right), \quad (1.20)$$

where the L_k^α are the Laguerre polynomials and α , c and T are parameters. Weeks considers $\alpha = 0$, $c = c_0 + \frac{1}{2T}$, and a_k is the Taylor coefficient; i.e [32]

$$a_0 = \frac{1}{N+1} \sum_{k=0}^M h(\theta_r), \quad (1.21)$$

$$a_k = \frac{2}{M+1} \sum_{k=0}^M h(\theta_r) \cos(k\theta_r), \quad M \neq 0, \quad (1.22)$$

where r is an integer, and θ_r is

$$\theta_r = \frac{\pi 2r + 1}{2M + 1}, \quad (1.23)$$

where $h(\theta_r)$ is

$$h(\theta_r) = \frac{1}{T_m} \left[\operatorname{Re} \left\{ F \left(\psi + \frac{i}{2g} \cot \left(\frac{\theta_r}{2} \right) \right) \right\} - \cot \left(\frac{\theta_r}{2} \right) \operatorname{Im} \left\{ F \left(\psi + \frac{i}{2g} \cot \left(\frac{\theta_r}{2} \right) \right) \right\} \right]. \quad (1.24)$$

1.2 Overview of the one-dimensional NILTs applications

Some of the applications of one-dimensional NILTs in the field of engineering that have been used in research, including, but not limited to, are as follows:

- Generally used for the solution of ordinary differential equations [37].
- Solving systems with distributed parameters including transcendental and/or irrational functions, e.g. lossy transmission lines [1, 38].
- Solving the optical wave equation for propagating light in materials with nontrivial dispersion relations [39].
- Estimating the exponential of a complex matrix through the inversion of the corresponding resolvent matrix [35].

There exist many more applications in the engineering field for one-dimensional NILTs and furthermore, it is highly used for solving applications in the physics, chemistry and mathematics fields.

1.3 Two-dimensional NILTs

Minor attention has been paid to finding two-dimensional NILT methods, especially when compared to 1D NILT methods, and most of these methods are devised upon an expansion of a one-dimensional method; based upon this research, several of these methods are observed and some of them are highlight [8, 10, 14, 16, 40–44]. In this section, some of these best known two-dimensional inversions of importance are emphasized; with the focus on their main concept of derivation, the mathematical analysis and the free parameters for optimization. The first method described will be

the accelerated method based on *FFT* and *IFFT* algorithms by partial inversions [42].

1.3.1 Accelerated *FFT* and *IFFT*-based two-dimensional NILTs by partial inversion

In this section, an effective two-dimensional NILT method will be described, the method has an approach of evaluating the double Bromwich integral by the repeated application of partial inverse Laplace transforms while using *FFT* and *IFFT* algorithms that help speed up the calculations [42]; this method has the leverage of being able to deal with complex images of two variables that result in complex originals. Following is the description of the inversion algorithm.

Considering the Bromwich integral properties (2), and introducing the partial inverse Laplace transforms as follows,

$$L_2^{-1}\{F(s_1, s_2)\} = F_2(s_1, t_2) = \frac{1}{2\pi j} \int_{c_2-j\infty}^{c_2+j\infty} F(s_1, s_2) e^{s_2 t_2} ds_2, \quad (1.25)$$

and,

$$L_1^{-1}\{F(s_1, s_2)\} = F_1(t_1, s_2) = \frac{1}{2\pi j} \int_{c_1-j\infty}^{c_1+j\infty} F(s_1, s_2) e^{s_1 t_1} ds_1, \quad (1.26)$$

and thus the following expressions are obtained:

$$f(t_1, t_2) = L_1^{-1}\{F_2(s_1, t_2)\} = \frac{1}{2\pi j} \int_{c_1-j\infty}^{c_1+j\infty} F_2(s_1, t_2) e^{s_1 t_1} ds_1, \quad (1.27)$$

$$f(t_1, t_2) = L_2^{-1}\{F_1(t_1, s_2)\} = \frac{1}{2\pi j} \int_{c_2-j\infty}^{c_2+j\infty} F_1(t_1, s_2) e^{s_2 t_2} ds_2, \quad (1.28)$$

by applying the double partial Laplace transform the two-dimensional inversion algorithm becomes, [42]

$$\begin{aligned} \tilde{f}_k(s) = \tilde{f}(kT, s) = C_k \left[\sum_{n=0}^{N-1} F_n(s) z_k^n + \sum_{n=0}^{\infty} G_n(s) z_k^n + \sum_{n=0}^{N-1} F_{-n}(s) z_k^{-n} \right. \\ \left. + \sum_{n=0}^{\infty} G_{-n}(s) z_k^{-n} - F_0(s) \right], \quad (1.29) \end{aligned}$$

where $k = 0, 1, \dots, N-1$, $N = 2^m$, and the following parameters are considered [42],

$$T = \frac{2t_m}{N-2}, \quad (1.30)$$

$$C_k = \frac{\Omega e^{ckT}}{2\pi}, \quad (1.31)$$

$$z_k = e^{-jkT\Omega}, \quad (1.32)$$

$$F_n(s) = F(c - j\Omega n, s), \quad (1.33)$$

$$\Omega = \frac{2\pi}{NT}, \quad (1.34)$$

$$G_n(s) = F_{N+n}(s), \quad (1.35)$$

considering the equality $z_k^N = e^{-2j\pi k} = 1$, where t_m is the maximum time interval and s is the Laplace variable.

By performing error analysis for the method and choosing a limiting relative error, then the value of the parameter c for best results is chosen as $c_i = \alpha_i - \frac{1}{\tau_i} \ln \frac{\varepsilon_{M_r}}{2}$, $i = 1, 2$, where the τ_i represent the sampling periods in the original time domain and ε_{M_r} is the desired limiting relative error.

The process considered to evaluate the inversion equation (1.29) is done by using the *FFT* and the *IFFT* to evaluate the finite sums, i.e. first and third summation in the equation and then using the quotient-difference algorithm by Rutishauser (Qd algorithm) to accelerate the infinite summation terms, i.e. the second and fourth summation in (1.29). The principle of the Qd algorithm is considered to be a continued fraction form of the rational Padé approximation, which helps in improving the inversion algorithm by means of accuracy and computational speed as will be implemented in the following sections.

By using the Qd algorithm for accelerating the infinite series only $2P + 1$ terms are used with P being a free choice parameter that could be optimized for higher accuracy. An error analysis study conducted in [23] shows that the optimal choice of P is 3. Consequently, an infinite series is then described as

$$y(z_k, P) = \sum_{n=0}^{2P} G_n z_k^n, \quad \forall k, \quad (1.36)$$

which has the continued fraction form

$$x(z_k, P) = \frac{d_0}{\left(1 + \frac{d_1 z_k}{(1 + \dots + d_{2P} z_k)}\right)}, \quad \forall k, \quad (1.37)$$

where the coefficients $d_n, n = 0, 1, \dots, 2P$, are evaluated according to the Qd algorithm lozenge diagram [42].

1.3.2 Two-dimensional NILT by fast Hartley transform computations

The numerical inversion of 2D Laplace transforms by fast Hartley transform computations is proposed by Hwang et al. [43].

This method was extended from the 1D inversion method based on the evaluation of the Bromwich integral by using the computational algorithm of fast Fourier transform *FFT*. The expansion was performed by first applying the trapezoidal approximation considering a specific step size, and then efficiently applying 2D fast Hartley transform (FHT), which is an analogue of the discrete Fourier transform for real data [43].

The method is constructed by efficiently applying multiple sets of FHT computations to evaluate the 2D inverted function on the rectangular grids of the plane. The final transform algorithm is given as follows

$$f_a(i_1\Delta T_1, i_2\Delta T_2) = (-1)^{i_1n_1+i_2n_2} \frac{\exp(\sigma_1 i_1 \Delta T_1 + \sigma_2 i_2 \Delta T_2)}{4m_1m_2T_1T_2} \hat{f}(i_1, i_2), \quad (1.38)$$

where

$$\begin{aligned} \hat{f}(i_1, i_2) = & h_{0,0}(i_1, i_2) + 2 \sum_{r_1=1}^{u_1} \sum_{r_2=-u_2}^{u_2} \left[h_{r_1,r_2}(i_1, i_2)(C_{r_1}C_{r_2} - S_{r_1}S_{r_2}) \right. \\ & \left. + h_{-r_1,-r_2}(C_{r_1}S_{r_2} - C_{r_2}S_{r_1}) \right] + 2 \sum_{r_2=1}^{u_2} \left[h_{0,r_2}(i_1, i_2)C_{r_2} + h_{0,-r_2}(i_1, i_2)S_{r_2} \right], \quad (1.39) \end{aligned}$$

where the coefficients are

$$\begin{aligned} C_{r_1} = \cos\left(\frac{2\pi i_1 r_1}{m_1 N_1}\right), \quad C_{r_2} = \cos\left(\frac{2\pi i_2 r_2}{m_2 N_2}\right), \quad S_{r_1} = \sin\left(\frac{2\pi i_1 r_1}{m_1 N_1}\right), \\ S_{r_2} = \sin\left(\frac{2\pi i_2 r_2}{m_2 N_2}\right). \quad (1.40) \end{aligned}$$

Detailed derivation of the algorithms are found in [43]. The authors also show that this method requires much less computational requirements than with a similar method using *FFT* techniques instead.

1.3.3 Two-dimensional NILT by the Fourier series representation

M.V. Moorthy developed a 2D inversion method, presented in [44]. The method is an expansion of the one-dimensional inversion method proposed by Dubner and

Abate [17]. These methods are based on using Fourier cosine series and with properly choosing the contour of integration of the Laplace integral. The method starts by considering the following preliminary conditions

$$s_1 = c_1 + j\omega_1, \quad s_2 = c_2 + j\omega_2, \quad (1.41)$$

by properly choosing the values of c_1 and c_2 a better approximation of the inversion algorithm can be achieved.

Furthermore, considering that

$$|f(t_1, t_2)| \leq Me^{\alpha_1 t_1 + \alpha_2 t_2}, \quad (1.42)$$

such that M is a positive constant, α_1 and α_2 are real numbers and the Laplace domain of the function $F(s_1, s_2)$ is analytic for $\text{Re}\{s_1\} > \alpha_1$ and $\text{Re}\{s_2\} > \alpha_2$.

When applying the Fourier series and using basic mathematical techniques, as described in [44], the inversion algorithm becomes

$$\hat{f}(t_1, t_2) = e^{c_1 t_1 + c_2 t_2} g(t_1, t_2), \quad (1.43)$$

where $\hat{f}(t_1, t_2)$ is the approximate result in time domain of $F(s_1, s_2)$; then by taking the sum of the resulting series over j and k and formally interchanging the order of sums,

$$\begin{aligned} \sum_{j=0}^{\infty} \sum_{k=0}^{\infty} g^{jk}(t_1, t_2) &= \frac{1}{2T^2} \left\{ \frac{1}{2} F(c_1, c_2) + \sum_{m=1}^{\infty} \left[\text{Re} \left\{ F \left(c_1, c_2 + \frac{im\pi}{T} \right) \right\} \cos \left(\frac{m\pi t_2}{T} \right) \right. \right. \\ &- \text{Im} \left\{ F \left(c_1, c_2 + \frac{im\pi}{T} \right) \right\} \sin \left(\frac{m\pi t_2}{T} \right) \left. \right] + \sum_{n=1}^{\infty} \left[\text{Re} \left\{ F \left(c_1 + \frac{in\pi}{T}, c_2 \right) \right\} \cos \left(\frac{n\pi t_1}{T} \right) \right. \\ &- \text{Im} \left\{ F \left(c_1 + \frac{in\pi}{T}, c_2 \right) \right\} \sin \left(\frac{n\pi t_1}{T} \right) \left. \right] + \sum_{n=1}^{\infty} \sum_{m=1}^{\infty} \left[\text{Re} \left\{ F \left(c_1 + \frac{in\pi}{T}, c_2 + \frac{im\pi}{T} \right) \right\} \right. \\ &\cdot \cos \left(\frac{n\pi t_1}{T} + \frac{m\pi t_2}{T} \right) + \text{Re} \left\{ F \left(c_1 + \frac{in\pi}{T}, c_2 - \frac{im\pi}{T} \right) \right\} \cos \left(\frac{n\pi t_1}{T} - \frac{m\pi t_2}{T} \right) \\ &- \text{Im} \left\{ F \left(c_1 + \frac{in\pi}{T}, c_2 + \frac{im\pi}{T} \right) \right\} \sin \left(\frac{n\pi t_1}{T} + \frac{m\pi t_2}{T} \right) \\ &\left. \left. - \text{Im} \left\{ F \left(c_1 + \frac{in\pi}{T}, c_2 - \frac{im\pi}{T} \right) \right\} \cdot \sin \left(\frac{n\pi t_1}{T} - \frac{m\pi t_2}{T} \right) \right] \right\} \quad (1.44) \end{aligned}$$

where ‘Re’ and ‘Im’ represent the real and imaginary parts, respectively, and the right-hand side of (1.44) is denoted as $g(t_1, t_2)$. As it is evident from the approximate formula (1.44) it is a relatively complex formulae, and it mainly requires a long

computational time in contrast with other similar methods with less number of computations.

The error analysis shows that for higher accuracy of the inversion, the best choice of c_1 and c_2 is to be larger than α_1 and α_2 respectively, and thus for example by first choosing $c_1 > \alpha_1$, then the result is

$$c_2 = \alpha_2 - \frac{1}{2T} \ln \left(\frac{\varepsilon - e^{-2T(c_1 - \alpha_1)}}{1 - e^{-2T(c_1 - \alpha_1)}} \right). \quad (1.45)$$

For the best choices of the parameter T , after considering $t_{max} < 2T$, M.V. Moorthy [44] recommends, based on experiments in his research work, to choose its values between $0.5t_{max} \leq T \leq 0.8t_{max}$.

1.3.4 Two-dimensional NILT based on Zakian's numerical scheme

Singhal et al. in [14] developed a two-dimensional inversion method for inverting Laplace transforms with two variables based on the numerical scheme of Zakian [16, 45]. The method was devised by using a Padé approximation and the residual theorem. The final inversion algorithm is stated as follows, [14]:

$$\hat{f}(t_1, t_2) = \frac{1}{t_1 t_2} \sum_{i=1}^{M_1} \sum_{l=1}^{M_2} K_{1i} K_{2l} F \left(\frac{z_{1i}}{t_1}, \frac{z_{2l}}{t_2} \right), \quad (1.46)$$

where K_{1i} and K_{2l} are the residues of approximating the exponential kernel e^{st} of the Bromwich integral, and z_{1i}, z_{2l} are the equivalent poles, they are described by using a rational Padé approximation as [14]:

$$e^{s_r t_r} \approx \zeta N_k, M_k(z_k) = \frac{\sum_{i=0}^{N_k} (M_k + N_k - i)! \binom{N_k}{i} z_k^i}{\sum_{i=0}^{M_k} (-1)^i (M_k + N_k - i)! \binom{M_k}{i} z_k^i}, \quad (1.47)$$

where $r = 1, 2$, and k is the number of variable in the list of terms chosen for the computation. Generally, this method gives the best results when tested with relatively smooth functions.

A promising 2D NILT method developed is a method based on the *FFT* algorithm and improved significantly by using the ε -algorithm which effectively improves the result's precision [10]. Moreover, another 2D NILT method described in [40] is based on the Fourier series of a periodic function constructed by aliasing and applying the Poisson summation formula and then integrated with the Euler transform. Recently, there was proposed by Gomez et al. (2016) a 2D NILT method based on the

MATLAB function ‘*ifft2*’ and the method was successfully tested for an application of the computation of transients along power transmission lines [46].

1.4 Overview of the two-dimensional NILTs applications

Two-dimensional NILTs play an important role in solving electrical engineering applications; some of these best-known examples are:

- General applications related to solving partial differential equations with two variables.
- Simulation of voltage and current waves along transmission lines [13].
- Determining sensitivities of voltage/current waves propagating down multi-conductor transmission lines [47].
- Applications of 2D continuous space-time (CST) systems described by linear 2D partial equations [48].
- Fast computation of transient profiles along power transmission lines [46].
- Steady-state processes in PWM inverters with a sinusoidal output [49].

1.5 Multi-dimensional NILTs

Performing a research in several scientific databases (e.g. Web of Science, Scopus, IEEE) or even a general search in Google web search engine, it can be easily noticed that feeble attempts have been tried so far for developing multi-dimensional NILT (MNILT) methods. This makes it important to develop a method that can be of high value due to its outstanding applications in the electrical engineering field, for instance assisting in solving nonlinear systems.

The basic n -dimensional Laplace transform of a function with multiple variables $f(t_1, \dots, t_m)$ is given as, [13, 50],

$$F(s_1, \dots, s_m) = \int_0^\infty \dots \int_0^\infty f(t) e^{-st^T} \prod_{k=1}^m dt_k, \quad (1.48)$$

where T is the transpose operator, and the following assumptions are considered,

$$|f(t_1, \dots, t_n)| < M e^{\alpha_1 t_1^T \dots \alpha_m t_m^T}, \quad (1.49)$$

such that M is a real positive and α is a minimal abscissa of convergence.

The n -dimensional Laplace transform $F(s_1, \dots, s_m)$ is defined on a region $\{(s_1, \dots, s_n) \in (c_1, \dots, c_n) : \text{Re}[(s_1, \dots, s_n)] > (\alpha_1, \dots, \alpha_n)\}$; where c_n as an abscissa

of convergence, and considering the inequality component-wise. Consequently, the original function is obtained by applying the n -fold Bromwich integral

$$f(t_1, \dots, t_m) = \frac{1}{(2\pi j)^m} \int_{c_1 - j\infty}^{c_n - j\infty} F(s_1, \dots, s_m) e^{(s_1 t_1^T \dots s_m t_m^T)} \prod_{i=1}^m ds_i, \quad (1.50)$$

Some of the attempts to develop an MNILT done so far are the 3D NILT based on FFT and IFFT proposed by L. Brančík [51], another MNILT is one based on the development of multidimensional Laplace transforms by the Laguerre method in [12], and a method based on Fourier series in conjunction with the Poisson summation formula, as described in [52]. Following is the technique for the developed 3D NILT based on *FFT* and *IFFT*, [51].

1.5.1 Numerical inversion of 3D Laplace transform method based on FFT and IFFT

This section describes a technique for numerically inverting 3D Laplace transforms developed from the 1D and 2D methods based on the *FFT* and *IFFT* algorithms integrated with the quotient-difference algorithm, which were presented in the previous sections (1.2.1 and 1.3.1), [51].

In [51], two procedures to derive the method are shown: one is based on using the rectangular rule of integration with generalized frequency steps and substituting $s_i = c_i + j\omega_i$, $i = 1, 2, 3$. The second procedure is based on using partial inverse Laplace transforms, such that the following expression is used $f(t_1, t_2, t_3) = L_3^{-1}\{L_2^{-1}\{L_1^{-1}\{F(s_1, s_2, s_3)\}\}\}$, such that it follows the properties of the triple Bromwich integral.

The final inversion resultant formula is [51],

$$\tilde{F}_i(\mathbf{P}_{i+1}^k) = \frac{e^{c_i k T_i}}{\tau_i} \sum_{n=-\infty}^{\infty} \tilde{F}_{i-1}(\mathbf{P}_i^k) e^{2j\pi n k T_i / \tau_i}, \quad (1.51)$$

with $i = 1, 2, 3$, $F_0(\mathbf{P}_1) \equiv F(s_1, s_2, s_3)$ and $F_3(\mathbf{P}_4) \equiv f(t_1, t_2, t_3)$, and having $p_j = s_j$ for $j \geq i$ or otherwise $p_j = t_j$, $j = 1, 2, 3$.

The 3D shifted unit step is applied on the 3D method as a test function and is shown in Fig. 1, [51]. In order to display the three variable functions, the results are shown as three 2D cuts while considering one different variable as a constant each time.

1.5.2 Overview of multi-dimensional NILTs applications

In the electrical engineering field the applications of MNILTs can be a powerful tool for the solution of nonlinear circuits and some other related applications. Below are some of these MNILTs applications that have been used:

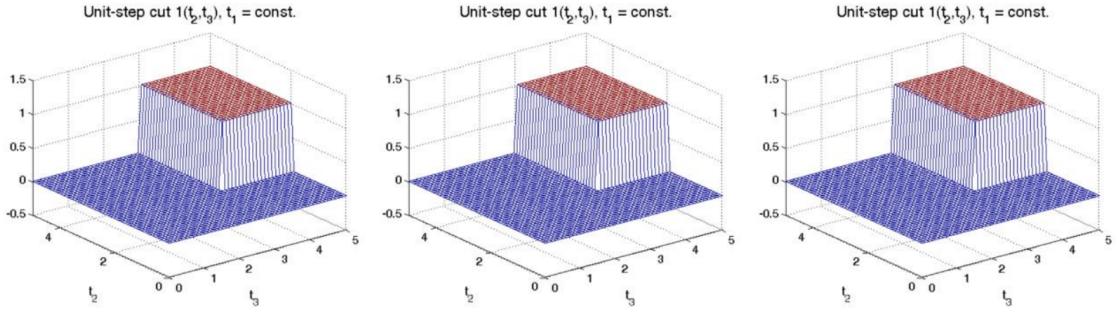


Fig. 1.1: Resulting 3D shifted unit step by utilizing the 3D-NILT method.

- Application of MNILT for solving a weakly nonlinear circuit with the use of the Volterra series expansion; an application of an electrical circuit with a nonlinear element is described [51].
- Application to calculate time-dependent distributions in the transient BMAP/G/1 queue, to calculate the inversion of the two-dimensional transforms of the joint distribution of the duration of a busy period and the time-dependent transient queue-length and workload distributions in the M-G-1 queue [52].

Traditionally, in the design of analog circuits, the Laplace operator s is raised to an integer order, such as s, s^2, s^3, \dots ; nevertheless, it is mathematically valid to raise it to a non-integer order α , that is s^α , [53]. This leads us to the following section, where an introduction to fractional calculus is presented. In the next chapters, with utilizing a proposed NILT method, fractional-order primary elements will be incorporated to enhance the modeling and simulation of distributed systems, for e.g. TL and MTL. Hence, in order to keep this work self-contained, the following sections briefly review the basics of fractional calculus and electronic components.

1.6 Fractional calculus and applied analysis for NILT applications

Fractional calculus, which covers irrational or complex integration and differentiation orders, may be considered an old and yet a novel topic which can be simply included in several applications in the electrical engineering field due to the benefit of using the NILT methods. The the basics of differentiation and integration to a non-integer order dates to the early stages of the 19th century [54],

scientists were inspired by the fractal models found in the nature. The origins go back to the year 1695 when L'Hôpital wrote a letter to Leibniz inquiring about the meaning of $D^n y$ when $n = 1/2$, [55]. Considering Leibniz ideas, many important mathematicians developed the theoretical concepts. Henceforth, more systematic studies evolved; A. K. Grünwald studied the fractional operations in 1867. Afterwards, G. F. B. Riemann developed the concept of fractional integrations and presented his results on 1892. Several papers in this field were then written by A. V. Letnikov between 1868 and 1872. An important next step was the development of operational calculus of Heaviside to solve some problems of electromagnetic theory. Heaviside introduced fractional differentiation in his study of transmission line theory. Several applications of fractional calculus are related to the transcendental functions of the Mittag-leffler and Wright type, or rather more generally by the Meijer G-functions and the Fox H-functions, [56–58]. In the last years, fractional calculus emerged as a 'novel' tool for the analysis of dynamical systems.

As of now, higher attention is being paid to fractional calculus and its large field of applications with methods of fractional derivative and integral approximations. In many applications, among which are: using fractional-order derivatives to express the anomalous diffusion in space and time domain, provided by Metzler and Klafter [59], applications in bioengineering [60–63], fractional-order filters [64, 65], control theory [66], signal processing [67], oscillators [68–74], transmission lines [75–78], and many more. Generally, the mathematical descriptions and properties of fractional-order derivatives can be found in the monographs of Podlubny [79], Herman [80], and Meerschaert and Sikorskii [81].

The principle of fractional derivatives and integrals is a very interesting topic, though hard to imagine, because, unlike commonly used differential operators, fractional ones are not related to some common geometrical meaning. Yet, many physical phenomena have an intrinsic fractional-order description, and hence fractional-order calculus is needed to explain them. For example, a semi-infinite lossy transmission line current is related to applied voltage as, $I(s) = \sqrt{s}V(s)$. In the case of diffusion of heat into the semi-infinite solid, the temperature exhibited at the boundary of the surface is related to half-integral of heat [82]. Signal propagation on an RC TL can be described by a partial differential equation (PDE) that is equivalent in form to the equations describing the classical Gaussian diffusion. Fractional order generalizations of this model reflect the onset of anomalous, non-Gaussian diffusion. Anomalous diffusion has been characterized in both space and time using a rich variety of fractional order derivatives when the line or skin effect is described by fractional differential equations [83]. In recent decades, scientists and engineers

have recognised that the fractional differential equations provide a better approach to describe the complex phenomena in nature such as the skin effect, dielectric relaxation, and chaos. In Ref. [84], Liu et al. considered the inherent fractional order characteristics of the skin effect and achieved a fractional order cable model using the Levy's fitting method [85], and the numerical solution for the fractional differential equations.

The main advantages of fractional derivatives when compared to the classical integer-order ones, is that they provide better results for the description of memory, materials, and processes. In principle, fractional-order systems are characterized by infinite memory, whereas they are finite for integer order systems [82]. Lately, electronic circuits have become one of the fields of practical applications that is showing significant good results, for instance in the fabrication of fractional-order capacitors by using silicon. Furthermore, the behavior of the three well-known elements: the resistor, the capacitor, and the inductor are designed today in the time domain based on integer-order differential equations [86]. Integer-order algebraic equations in the complex frequency s -domain are used to describe the linear dynamical systems via Laplace transform. Hence, the circuit order is directly proportional to the number of energy storage elements in the circuit.

1.6.1 Basic fractional differential equation definitions

To recall some basic FDE, a certain definition of a fractional derivative of a function $f(t)$ with κ as its order, and a zero lower limit [79, 87], is a method proposed by M. Caputo in his book [88], Caputo's definition can be written as

$${}_0^c D_t^\kappa f(t) = \frac{1}{\Gamma(\kappa - n)} \int_0^t \frac{f^{(n)}(\tau) d\tau}{(t - \tau)^{\kappa+1-n}}, \quad (1.52)$$

where $n - 1 < \kappa < n$, n is an integer, and $\Gamma(\cdot)$ denotes the Gamma function. Considering natural conditions on the function $f(t)$, for $\kappa \rightarrow n$ the Caputo derivative becomes a conventional n -th derivative of the function $f(t)$. This definition (1.52) is beneficial for physical applications, since the initial conditions of FDEs with Caputo's derivatives correspond to those of classical ones having integer-order derivatives, in other words, contain the limit values of integer-order derivatives of unknown functions at the lower terminal $t = \kappa$.

The formula for the Laplace transform of the Caputo's definition fractional derivative (1.52) is given as

$$\mathbf{L}\left\{{}_0^c D_t^\kappa f(t)\right\} = s^\kappa F(s) - \sum_{k=0}^{n-1} s^{\kappa-k-1} f^{(k)}(0), \quad (1.53)$$

where $f^{(k)}(0)$ represents the initial conditions (i.e. the k -th order derivatives at $t = 0$, k integer).

1.6.2 Basic fractional calculus of electronic components

In principle, a system which is defined by fractional-order differential equations is named as a Fractional Order System; while a fractance device is an electrical element which exhibits fractional order impedance properties. As known, in the conventional circuit elements, the impedance Z can be expressed as follows

$$Z \propto (j\omega)^r, \quad (1.54)$$

having ω as the angular frequency, and r taking the values $-1, 0, +1$ for the capacitance, the resistance, and the inductance, accordingly. However, a device which does not follow the conventional class is named as a fractance device, which has the impedance characterized by the following relation [89],

$$Z \propto \omega^\alpha \exp(j\theta), \quad (1.55)$$

A fractance device finds its applications in hard disk drives, robotics, signal processing circuits, fractional-order control, filters and so forth.

Some of the essential points about a fractance device are [89,90]:

- (a) The phase angle is constant independent of the frequency but depends only on the value of fractional order, α . Thus, this device is also known as constant phase angle device or simply fractor.
- (b) Moderate characteristics between inductor, resistor, and capacitor can be obtained using fractance device.
- (c) With the use of an operational amplifier, a fractional order differentiation and integration can be accomplished easily.

Considering the above, the immittances (impedance and admittance) of fractional-order capacitor and inductor are defined according to fractional calculus of electrical components as

$$Z_\alpha = s^\alpha L_\alpha, \quad (1.56)$$

$$Y_\beta = s^\beta C_\beta, \quad (1.57)$$

where L_α is the pseudo-inductance with order $\alpha \in (0,1]$, and C_β is the pseudo-capacitance with order $\beta \in (0,1]$, [89]. While α and β are not equal to one, there exist frequency-dependent losses in the real part called dispersion loss of the

fractional-order inductance/capacitance expressions [91].

The Laplace transform, as is well known, is considered an efficient method for solving differential equations of integer order as well as those with fractional orders. However, for differential equations with fractional orders, the Laplace transform works effectively for relatively simple equations, due to the difficulty of calculating the inversion of Laplace transform [92]. This difficulty has been bypassed by using numerical inversion of Laplace transform in fractional calculus; as shown in [93], where three methods (invlap, gavsteh and FFT-NILT) were described and verified. As will be shown in further chapters, fractional calculus is introduced and successfully incorporated in specific modeling techniques by using the proposed NILT method.

2 DISSERTATION OBJECTIVES

It has been demonstrated so far, in this doctoral thesis, the importance of the numerical inverse Laplace transform (NILT) methods for 1D, 2D and n -dimensions and their relation to a large field of applications in science, physics, and chemistry and especially, our field of focus, the electrical and electronics engineering field [8,16,46]. This brings us up to the open-ended question, could we develop a relatively universal NILT method with one or more variables that is verified to be stable and accurate enough for terms of electrical engineering? All this and more open issues will be addressed shortly. The emphasis, in this dissertation, is to characterize and study the current developed methods and to further devise a relatively universal, stable and accurate method which could be easily applied and implemented for electrical engineering applications, such as transmission lines analysis, multi-conductor lines or more sophisticated like non-linear circuit simulation [8, 46].

2.1 Theoretical basis analysis and comparative studies

- I. Research of the theoretical basis of the numerical inversion methods, review and comparative study of different developed NILT methods.
- II. The development of single-variable NILT methods and their successful program implementation.
- III. Categorization of the different methods with regard to their applicability on electrical engineering topics and their relevance to the scientific field.
- IV. Incorporation of fractional-order calculus in the different applications of NILT methods, e.g. fractional-order TL modeling and simulation using NILT method.

2.2 Multivariable integral transforms

- I. Research study of the theoretical basis of multivariable integral transforms, review of numerical methods of two and more variable inverse Laplace transformation methods, and development of their program codes.
- II. Application of MNILT in electrical engineering field, and utilizing Volterra series theory with the possibility of its application into non-linear systems analysis.
- III. Inclusion of fractional-order calculus for the applications of MNILT, e.g. fractional-order multiconductor transmission lines modeling and simulation.

2.3 Development of effective NILT techniques

- I. Development of effective numerical techniques for the inversion of Laplace transforms of one-variable and multi-variables.
- II. Integration of efficient acceleration techniques to the proposed NILT methods, which yield to result enhancements.
- III. Development and implementation of the corresponding program codes.
- IV. Error analysis and accuracy tests for each of the above mentioned cases.
- V. Verification by successful application in linear and non-linear systems analysis.
- VI. Incorporation of fractional-order elements for related NILT applications.
- VII. Innovative approaches to the solution of PDE's describing lossy coupled multiconductor transmission lines (MTL).

3 1D HYPERBOLIC NILT METHOD

With the inspiration to develop a numerical inverse Laplace transform, which is characterised by having a high accuracy, computationally efficient, and relatively universal, hence the hyperbolic NILT method is presented. Most available methods of the numerical calculation of the inverse Laplace transformations $f(t) = \mathbf{L}^{-1}\{F(s)\}$, have significant limitations regarding the class of functions that can be inverted, the achievable accuracy, and the computational time. This can be also noticed by checking the results of several comparative studies on 1D NILT performance (see for example [29, 93, 94], and references therein). Most of these methods are based on the necessity that the inverse transform of polynomial time functions up to a certain high power are accurate; since most of the time this order is determined through a table of coefficients, it is then not practically easy to be changed whenever it is needed [5]. In this chapter, a potential method, which is relatively universal and has a desirable accuracy, is presented and described. An advantage of this method is that its accuracy can be improved simply without changing the algorithm but only on the cost of the computational time.

In the following sections, the hyperbolic NILT method presented in detail, including the mathematical derivation of the algorithms and the related error analysis is studied. The NILT method of interest, is endorsed by deriving the resulting algorithm through following a different process, while resulting in the same final algorithm. Afterwards, an enhancement to the proposed method is done by integrating several infinite series convergence accelerating algorithms, which improve the accuracy and computational time of the method. Moreover, the corresponding analysis and tests are shown by using relevant test functions of known originals. The method is then applied on many examples including transients in lumped/distributed systems.

3.1 Original proposed 1D hyperbolic-based NILT method

I. Principle formula and basic assumptions

The hyperbolic NILT method is based on approximating the Laplace transform definition Bromwich integral, [1, 5, 95, 96],

$$f(t) = \frac{1}{2\pi j} \int_{c-j\infty}^{c+j\infty} F(s)e^{st} ds, \quad (3.1)$$

where $s = c + j\omega$, while considering the basic assumptions,

- $F(s)$ is regular for $\text{Re}\{s\} > 0$,
- when $|s| \rightarrow \infty$ then $F(s) \rightarrow 0$, and
- $F^*(s) = F(s^*)$, where the symbol $*$ represents the complex conjugate.

II. Recapitulation of original hyperbolic NILT

The Laplace transform's inverse kernel e^{st} in (3.1) can be approximated by two hyperbolic relations, namely

$$K_{sh}(st, a) = \frac{e^a}{2 \sinh(a - st)}, \quad (3.2)$$

$$K_{ch}(st, a) = \frac{e^a}{2 \cosh(a - st)}, \quad (3.3)$$

Henceforth, the reciprocal hyperbolic functions are expressed by the infinite sum of rational functions in $z = a - st$,

$$\frac{1}{\sinh z} = \frac{1}{z} + 2z \sum_{n=1}^{\infty} \frac{(-1)^n}{n^2\pi^2 + z^2}, \quad (3.4)$$

$$\frac{1}{\cosh z} = 2\pi \sum_{n=0}^{\infty} \frac{(-1)^n(n + 0.5)}{(n + 0.5)^2\pi^2 + z^2}. \quad (3.5)$$

Further, continuing the derivation with the successive application of the residual theorem and performing simple mathematical manipulations, described in more detail in [5], we obtain the following approximate formulae

$$f_{sh}(t, a) = \frac{e^a}{t} \left(\frac{1}{2} F\left(\frac{a}{t}\right) + \sum_{n=1}^{\infty} (-1)^n \text{Re} \left\{ F\left(\frac{a}{t} + \frac{n j \pi}{t}\right) \right\} \right), \quad (3.6)$$

$$f_{ch}(t, a) = \frac{e^a}{t} \sum_{n=1}^{\infty} (-1)^n \text{Im} \left\{ F\left(\frac{a}{t} + \frac{(n - 0.5) j \pi}{t}\right) \right\}, \quad (3.7)$$

There exists an alternative way to express the hyperbolic functions, i.e. their definition exponential functions, (3.2) and (3.3) can be rearranged into the form of the sum of infinite geometric series, and hence, from that, the absolute errors of formulae (3.6) and (3.7) can be obtained, respectively, as listed bellow,

$$\varepsilon_{sh}(t, a) = \sum_{n=1}^{\infty} e^{-2na} f((2n + 1)t), \quad (3.8)$$

$$\varepsilon_{ch}(t, a) = \sum_{n=1}^{\infty} (-1)^n e^{-2na} f((2n + 1)t), \quad (3.9)$$

where the detailed study of the error is presented in the next section in more detail. By performing several tests it is found that the arithmetic mean of

both NILT approximations (3.6) and (3.7) results in an even more enhanced and accurate inversion algorithm, namely

$$f_{en}(t, a) = \frac{e^a}{2t} \left(\frac{1}{2} F\left(\frac{a}{t}\right) + \sum_{n=1}^{\infty} (-1)^n \left(\operatorname{Re} \left\{ F\left(\frac{a}{t} + \frac{nj\pi}{t}\right) \right\} \dots \right. \right. \\ \left. \left. + \operatorname{Im} \left\{ F\left(\frac{a}{t} + \frac{(n-0.5)j\pi}{t}\right) \right\} \right) \right), \quad (3.10)$$

the absolute error of (3.10) can be analytically obtained

$$\varepsilon_{en}(t, a) = \sum_{n=1}^{\infty} e^{-4na} f((4n+1)t). \quad (3.11)$$

3.1.1 Error analysis of the 1D hyperbolic NILT method

There exist two types of errors which can be conceived when investigating the resulting hyperbolic NILT algorithms; the first is the ‘static error’, caused by the approximation of the exponential kernel e^{st} , and the second is the ‘dynamic error’, which results from the practical truncation of the infinite series appearing in each of the hyperbolic NILT final algorithms. Below in greater detail are the errors and the possibilities of improvement discussed [5].

I. The static error:

In order to investigate the static error for each of the cases, i.e. (3.6) and (3.7), lets start by approximating the exponential kernel by a different way, namely, equation (3.3) can be approximated as follows

$$K_{ch}(st, a) = \frac{e^a}{2 \cosh(a-st)} = \frac{e^{st}}{1 + e^{-2a}e^{2st}}, \quad (3.12)$$

assuming $a > \gamma t$, then $|e^{-2a}e^{2st}| \ll 1$ and hence the fraction $1/(1 + e^{-2a}e^{2st})$ is possible to expand as a convergent MacLaurin series as follows,

$$K_{ch}(st, a) = e^{st} + \sum_{n=1}^{\infty} (-1)^n e^{-2na} e^{(2n+1)st}, \quad (3.13)$$

from (3.13) it can be seen that the sum expression represents the error of the approximation, it is obvious that this error can be highly suppressed by a proper choice of the parameter a . Substituting (3.13) in (3.1) we have

$$\begin{aligned} f(t) \approx f_{ch}(t, a) &= \frac{1}{2\pi j} \int_{c-j\infty}^{c+j\infty} F(s) K_{ch}(st, a) ds \\ &= \frac{1}{2\pi j} \int_{c-j\infty}^{c+j\infty} F(s) e^{st} ds + \frac{1}{2\pi j} \int_{c-j\infty}^{c+j\infty} F(s) \sum_{n=1}^{\infty} (-1)^n e^{-2na} e^{(2n+1)st} ds \\ &= f(t) + \sum_{n=1}^{\infty} (-1)^n e^{-2na} f[(2n+1)t] = f(t) - e^{-2a} f(3t) + e^{-4a} f(5t) - \dots \\ &= f(t) + \varepsilon_{ch}(t, a). \end{aligned} \quad (3.14)$$

From (3.14) the absolute static error of (3.7) is then

$$\begin{aligned}\varepsilon_{ch} &= f_{ch}(t, a) - f(t) = \sum_{n=1}^{\infty} (-1)^n e^{-2na} f[(2n+1)t] \\ &= -e^{-2a} f(3t) + e^{-4a} f(5t) - \dots .\end{aligned}\quad (3.15)$$

Similarly, the static error of (3.6) approximation can be obtained by first approximating the exponential kernel in (3.2) as follows

$$K_{sh}(st, a) = \frac{e^a}{2 \sinh(a-st)} = \frac{e^{st}}{1 - e^{-2a} e^{2st}}, \quad (3.16)$$

then, by expanding as a convergent MacLaurin series and substituting back to (3.1), we get

$$\begin{aligned}f(t) &\approx f_{sh}(t, a) = \frac{1}{2\pi j} \int_{c-j\infty}^{c+j\infty} F(s) E_{sh}(st, a) ds \\ &= f(t) + e^{-2a} f(3t) + e^{-4a} f(5t) + \dots = f(t) + \varepsilon_{sh}(t, a).\end{aligned}\quad (3.17)$$

From (3.17) the absolute static error of (3.6) is then

$$\begin{aligned}\varepsilon_{sh} &= f_{sh}(t, a) - f(t) = \sum_{n=1}^{\infty} e^{-2na} f[(2n+1)t] \\ &= e^{-2a} f(3t) + e^{-4a} f(5t) + \dots .\end{aligned}\quad (3.18)$$

Equivalently, the absolute static error for the arithmetic mean formula (3.10) can be derived, and it is given as follows

$$\varepsilon_{en}(t, a) = \sum_{n=1}^{\infty} e^{-4na} f((4n+1)t). \quad (3.19)$$

Assigning M as a maximum absolute value of an original function $f(t)$, and using the formula of the sum of infinite geometric series, the limiting absolute errors of (3.6), (3.7) and (3.10), respectively, are given as follows

$$\varepsilon_{shM}(a) = \varepsilon_{chM}(a) = \frac{Me^{-2a}}{1 - e^{-2a}} \approx Me^{-2a}, \quad (3.20)$$

$$\varepsilon_{enM}(a) = \frac{Me^{-4a}}{1 - e^{-4a}} \approx Me^{-4a}. \quad (3.21)$$

ensuing the results in [1], it is conceived that the absolute error is adjustable by optimizing the choice of the parameter $a > 0$; it is also evident that this error suppression effect is higher for the arithmetic mean absolute error formula (3.21), as the exponent is raised to the power of ‘ $-4a$ ’, in contrast to ‘ $-2a$ ’ for the other two approximations, and thus (3.10) provides higher accuracy results.

II. The dynamic error:

The ‘dynamic’ error can be explained as the error caused by the truncation, in practice, of the NILT infinite series. Mainly, this error depends highly on the number of terms used to compute the method, n_{sum} . This error can be highly reduced by incorporating a suitable technique of infinite series convergence acceleration, as will be shown in Sect. 3.3.

3.2 Alternative approach for the derivation of the hyperbolic NILT method

An alternative approach to derive the hyperbolic NILT method is performed as a further confirmation of this algorithm [1, 95]. It starts from the ILT Bromwich integral (3.1), and takes into account the same presumptions. Taking the integration contour to be a vertical line, i.e. $s = c + j\omega$, where c is the distance from the imaginary axis in a way that $F(s)$ has no singularities on or to the right of this vertical line. Then the original time-domain function can be obtained as follows

$$f(t) = \frac{e^{ct}}{2\pi} \int_{-\infty}^{\infty} F(c + j\omega)(\cos \omega t + j \sin \omega t) d\omega . \quad (3.22)$$

Changing the integration to a summation and replacing the differential $d\omega$ with the difference Ω , then we have

$$\tilde{f}(t) = \frac{e^{ct}\Omega}{2\pi} \sum_{k=-\infty}^{\infty} F(c + jk\Omega)(\cos k\Omega t + j \sin k\Omega t) . \quad (3.23)$$

Furthermore, if the distance from the imaginary axis, c , and the integration step, Ω , are selected as time-dependent parameters, i.e. inversely proportional to time in which the original is to be computed parameters,

$$c = \frac{a}{t} , \quad (3.24)$$

$$\Omega = \frac{\pi}{t} , \quad (3.25)$$

neglecting the initial time point, i.e. $t \neq 0$, then (3.23) becomes,

$$\tilde{f}(t) = \frac{e^a}{2t} \sum_{k=-\infty}^{\infty} F\left(\frac{a}{t} + jk\frac{\pi}{t}\right)(\cos k\pi + j \sin k\pi) . \quad (3.26)$$

Henceforth, two cases are considered:

I. Integer values are used for the summation index in (3.26)

If the summation index in (3.26) takes integer values, i.e. $k = \dots, -2, -1, 0, 1, 2, \dots$, then,

$$\tilde{f}(t) = \frac{e^a}{2t} \sum_{k=-\infty}^{\infty} (-1)^k F\left(\frac{a}{t} + jk\frac{\pi}{t}\right) . \quad (3.27)$$

Having the assumption $F^*(s) = F(s^*)$, then $F(s) + F^*(s) = 2\text{Re}\{F(s)\}$ is valid, and hence

$$\tilde{f}_1(t) = \frac{e^a}{t} \left(\frac{1}{2} F\left(\frac{a}{t}\right) + \sum_{k=1}^{\infty} (-1)^k \text{Re} \left\{ F\left(\frac{a}{t} + jk\frac{\pi}{t}\right) \right\} \right), \quad (3.28)$$

noting that this formula corresponds to (3.6), i.e. the first hyperbolic NILT method approximation $f_{sh}(t, a)$.

II. Fractional values are used for the summation index in (3.26)

If the summation index in (3.26) takes fractional values, i.e. $k = \dots - 3/2, -1/2, 1/2, 3/2, \dots$, or for simplicity assuming $k = r - 1/2$ and then taking an integer index as $r = \dots, -2, -1, 0, 1, 2, \dots$, then

$$\tilde{f}_2(t) = \frac{e^a}{2jt} \sum_{r=-\infty}^{\infty} (-1)^r F\left(\frac{a}{t} + j\left(r - \frac{1}{2}\right)\frac{\pi}{t}\right). \quad (3.29)$$

Having the assumption $F^*(s) = F(s^*)$, then $F(s) - F^*(s) = 2j \text{Im}\{F(s)\}$, is valid, and hence we get

$$\tilde{f}_2(t) = \frac{e^a}{t} \sum_{r=1}^{\infty} (-1)^r \text{Im} \left\{ F\left(\frac{a}{t} + j\left(r - \frac{1}{2}\right)\frac{\pi}{t}\right) \right\}, \quad (3.30)$$

noting that this formula corresponds to (3.7), i.e. the second hyperbolic NILT method approximation $f_{ch}(t, a)$, and thus both approximations of the hyperbolic NILT methods are confirmed. Furthermore, the arithmetic mean of the hyperbolic NILT method (3.10) can be also verified by the second approach, namely, assuming the integration step is half of that from (3.25), i.e

$$\Omega = \frac{\pi}{2t}, \quad (3.31)$$

though, keeping the Bromwich integration path as in (3.24), then (3.23) becomes

$$\tilde{f}(t) = \frac{e^a}{4t} \sum_{k=-\infty}^{\infty} F\left(\frac{a}{t} + jk\frac{\pi}{2t}\right) \left(\cos k\frac{\pi}{2} + j \sin k\frac{\pi}{2} \right). \quad (3.32)$$

similarly, taking integer index for the summation value, i.e. $k = \dots, -2, -1, 0, 1, 2, \dots$, then we get

$$\tilde{f}(t) = \frac{e^a}{4t} \sum_{k=-\infty}^{\infty} j^k F\left(\frac{a}{t} + jk\frac{\pi}{2t}\right). \quad (3.33)$$

Taking the assumption $F^*(s) = F(s^*)$, and both the identities $F(s) + F^*(s) = 2\text{Re}\{F(s)\}$, $F(s) - F^*(s) = 2j \text{Im}\{F(s)\}$, and then pairing the terms with neighboring indexes

$$\begin{aligned} \tilde{f}(t) = \frac{e^a}{2t} \left(\frac{1}{2} F\left(\frac{a}{t}\right) + \sum_{k=1}^{\infty} (-1)^k \left(\text{Re} \left\{ F\left(\frac{a}{t} + jk\frac{\pi}{t}\right) \right\} \right. \right. \\ \left. \left. + \text{Im} \left\{ F\left(\frac{a}{t} + j\left(k - \frac{1}{2}\right)\frac{\pi}{t}\right) \right\} \right) \right). \quad (3.34) \end{aligned}$$

As can be noticed, the formulae (3.34) corresponds with (3.10), thus the arithmetic mean formulae of the hyperbolic NILT method, $f_{en}(t, a)$ is also verified.

3.3 Enhancements on the 1D hyperbolic NILT method

In this section, the progress on generalizing the hyperbolic NILT method together with the integration of the quotient difference acceleration algorithm are presented.

3.3.1 Generalization of the 1D hyperbolic NILT method

The work, presented in reference [1], describes the possibility for a generalization of the method for a better accuracy, which basically allows to increase the accuracy of the method by the reduction of the integration step with the possibility to predict the absolute limit error [95]. This alternative approach to improve the accuracy provides a broader range of application to the hyperbolic NILT method, with the ability of optimizing the free parameter a to attain a marginally absolute error. Mainly, the integration step is reduced by $\Omega = \pi/mt$, where m is an integer, while maintaining the parameter c as it was originally defined [1].

3.3.2 Integration of infinite series convergence acceleration techniques

With the motivation to reduce the ‘static’ error effect, discussed above, and further enhancing the proposed hyperbolic NILT original method, the idea of adapting some infinite series convergence acceleration techniques is proposed, and then after several tests, using the Matlab programming language, their performance on the hyperbolic NILT method and compare their results.

Specific convergence acceleration techniques are available and suitable to be integrated with the proposed method. Namely, the techniques incorporated to the hyperbolic NILT method are: the Euler transform, the quotient-difference algorithm of Rutishauser and the epsilon algorithm of Wynn; this will be shown in the following sections.

In practice, the computation of formula (3.10) is done as follows; first it can be formally rewritten as a combination of three parts, i.e. an initial, a finite sum and

an infinite sum,

$$f_{en}(t, a) = \frac{e^a}{2t} \left(\frac{1}{2} F\left(\frac{a}{t}\right) + \sum_{n=1}^{n_{sum}} (\dots) + \sum_{n=n_{sum}+1}^{\infty} (\dots) \right), \quad (3.35)$$

the initial part and the finite part are computed normally as they are, whereas the infinite part, in practice, can be computed up to a relatively high number of terms, e.g. 500 terms or higher. Nevertheless, by adapting suitable infinite series convergence acceleration techniques, the number of computed terms can be highly reduced, and in the same time, providing an increase in the accuracy of the method's results, saving valuable memory storage, and reducing the computational time.

I. By means of the Euler transform:

The infinite series in (3.10) for practical computation is truncated into a finite number of terms n_{sum} , as shown in (3.35), which leads to a decrease in the accuracy of the inversion result. To suppress this effect the Euler transform (ET) is incorporated.

The ET is a well-known technique for accelerating the convergence of infinite series [97]. This technique performs at its best for alternating infinite series [1, 5, 7]. Practically, the ET is applied after n_{sum} terms are computed numerically by the hyperbolic NILT algorithm then n_{eul} terms are added, but weighted by factors, namely

$$2^{(-n_{eul})} V_{(n_{eul}-k+1)}, \quad (3.36)$$

where $k = 1, 2, \dots, n_{eul}$, and V_r is given by the recursive formula

$$V_{r+1} = V_r + \binom{n_{eul}}{r}, \quad V_1 = 1. \quad (3.37)$$

The final result obtained is then added as a replacement to the infinite series part of (3.35). The Euler transform gives a high improvement on the proposed method, for both the accuracy and computational speed, as will be verified in following sections from the several performed simulation test results. Mainly, an improvement on the accuracy of the inversion, computational speed and less memory usage are achieved by introducing the Euler transform to the proposed hyperbolic NILT method. Hereon, the hyperbolic NILT method in conjunction with the Euler convergence acceleration technique is denoted as 'Hyp-Eul NILT'.

II. By means of the quotient-difference algorithm:

The quotient-difference algorithm (QdA) of Rutishauser is considered to be

a highly stable and efficient acceleration method [98]. The QdA gives, under certain conditions, the roots as the limits of similar quotient sequences [99]; for a power series, this algorithm corresponds to a rational Padé approximation expressed as a continued fraction.

Practically, the infinite sum is computed up to n_{sum} number of terms and the QdA requires only $n_{qd} = 2P + 1$ additional terms above n_{sum} as input data. Namely, considering (3.10) the ‘finite’ term is computed normally as it is, whereas, the ‘infinite’ term is rearranged, for simplicity, as follows

$$\begin{aligned} \sum_{n=1}^{\infty} (-1)^n \left[\operatorname{Re} \left\{ F \left(\frac{a + jn\pi}{t} \right) \right\} + \operatorname{Im} \left\{ F \left(\frac{a + j(n - 0.5)\pi}{t} \right) \right\} \right] \\ = \sum_{n=1}^{\infty} z^n Q_n \approx \sum_{n=1}^{n_{sum}} z^n Q_n + y(z, P), \end{aligned} \quad (3.38)$$

where $z = -1$, Q_n is the expression in the square brackets, and the term $y(z, P)$ represents the result of the QdA applied on additional n_{qd} terms of the residual original infinite series,

$$y(z, P) = \frac{d_0}{1 + \frac{d_1 z}{1 + \frac{d_2 z}{1 + \frac{d_3 z}{1 + \dots + d_{2P}}}}} , \quad (3.39)$$

which considerably improves the precision of the results.

In order to evaluate the coefficients $d_n = 0, \dots, 2P$, a clear demonstration can be based on the quotient-difference algorithm diagram illustrated in Fig. 3.1, [42, 98, 100].

The coefficients $d_n = 0, 1, \dots, 2P$ in (3.39) are based on the QdA lozenge diagram, see Fig. 3.1, which is computed by the following process; the first two columns are filled by

$$e_0^{(k)} = 0, \quad k = 0, \dots, 2P, \quad (3.40)$$

$$q_1^{(k)} = \frac{Q_{k+1}}{Q_k}, \quad k = 0, \dots, 2P - 1, \quad (3.41)$$

the consequent columns are formed by the following relations for $r = 1, \dots, P$,

$$e_r^{(k)} = q_r^{(k+1)} - q_r^{(k)} + e_{r-1}^{(k+1)}, \quad k = 0, \dots, 2P - 2r, \quad (3.42)$$

for $r = 2, \dots, P$,

$$q_r^{(k)} = \frac{q_{r-1}^{(k+1)} e_{r-1}^{(k+1)}}{e_{r-1}^{(k)}}, \quad k = 0, \dots, 2P - 2r - 1, \quad (3.43)$$

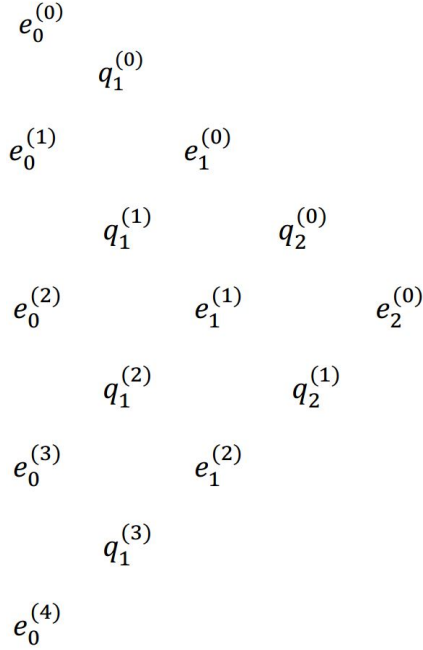


Fig. 3.1: The quotient-difference algorithm's lozenge diagram.

now it is possible to obtain the coefficients $d_n = 0, 1, \dots, 2P$ by the following relations

$$d_0 = Q_0, \quad d_{2m-1} = -q_m^{(0)}, \quad d_{2m} = -e_m^{(0)}, \quad m = 1, \dots, P. \quad (3.44)$$

A practical computation to get the solution of $y(z, P)$ can be done by processing the following recursive formulae,

$$A_n(z) = A_{n-1}(z) + d_n z A_{n-2}(z), \quad (3.45)$$

$$B_n(z) = B_{n-1}(z) + d_n z B_{n-2}(z), \quad (3.46)$$

where $n = 1, \dots, 2P$, and the initial coefficients given are $A_{-1} = 0, B_{-1} = 1, A_0 = d_0$, and $B_0 = 1$. Finally, the continued fraction (3.39) can be given as $y(z, P) = A_{2P}(z)/B_{2P}(z)$, for any z . The simulation of the quotient-difference algorithm adaption to the proposed NILT method is performed in the universal Matlab programming language.

III. By means of the ε -algorithm of Wynn:

The next convergence acceleration technique integrated is the ε -algorithm of Wynn [101]. The ε -algorithm is categorized as a nonlinear technique used to accelerate the convergence of infinite series and iterations. It has also been used to obtain useful results from divergent series/iterations and to assist in

the solution of differential and integral equations [101, 102].

The process followed to adapt the ε -algorithm to the 1D hyperbolic NILT method is theoretically similar to the QdA process, i.e. using a few number terms n_{eps} above n_{sum} which are used as input data to the ε -algorithm. In its turn, the ε -algorithm samples the additional terms and extrapolates them by fitting them to a polynomial multiplied by a decaying exponential [103].

Mathematically, the ε -algorithm can be described first by illustrating the lozenge diagram of the method, illustrated in Fig. 3.2. The diagram describes the case where $P = 2$, such that the total number of additional terms used is $2P + 1$ terms.

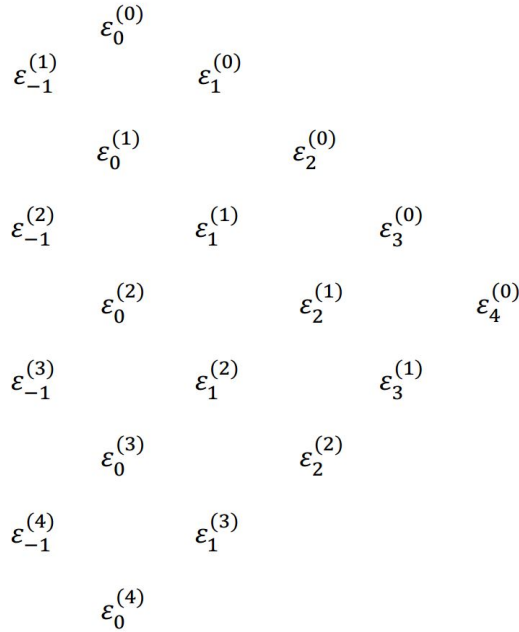


Fig. 3.2: The ε -algorithm's lozenge diagram.

To obtain the values of the lozenge diagram symbols used the following formulas will be used [10, 102]. Namely, to construct the first column $\varepsilon_{-1}^{(k)} = 0, k = 1, \dots, 2P$ is used. The initial term in the second column $\varepsilon_0^{(0)}$ represents the result of the truncated finite sum (3.35). Subsequently, the remaining entries of the second column represent partial sums computed recurrently by

$$\varepsilon_0^{(k)} = \varepsilon_0^{(k-1)} + F_{(n_{sum}+k)} z^k, \quad k = 1, \dots, 2P. \quad (3.47)$$

where $F_{n_{sum}}$ is the result of the finite part of (3.35) computed up to n_{sum} terms, and $z = -1$. The following columns for $r = 1, \dots, 2P$, are obtained by

the formula

$$\varepsilon_r^{(k)} = \varepsilon_{r-2}^{(k+1)} + [\varepsilon_{r-1}^{(k+1)} - \varepsilon_{r-1}^{(k)}]^{-1}, k = 0, \dots, 2P - r. \quad (3.48)$$

When finishing the recurrent steps according to (3.48) the sequence of successive approximations $\varepsilon_0^{(0)}, \varepsilon_2^{(0)}, \varepsilon_4^{(0)} \dots$ is obtained. This sequence converges much faster than the original sequence of partial sums. The required result from the EA transform is the entry $\varepsilon_{2P}^{(0)}$. Nevertheless, the algorithm can be under instability if P is chosen too high, based on previous experiments $P = 2$ or $P = 3$ seem to be sufficient [10].

3.3.3 Experimental error analysis

In this section, an experimental error analysis is performed, with the intention to confirm the theoretical error analysis (3.19). Moreover, it is interesting to investigate the effect of the different acceleration techniques presented earlier on the proposed hyperbolic-NILT method, namely, these techniques are the Hyp- ε NILT, the Hyp-Qd NILT and the Hyp-Eul NILT. The test functions used, shown in Tab. 3.1, are chosen intentionally to be of different mathematical types, i.e. rational, irrational and transcendental types with pre-known originals, to test the method's performance.

Tab. 3.1: List of test functions with their pre-known originals

	Functions in the Laplace domain	Original functions in the time domain
1	$F_1(s) = \frac{2 \cdot \omega^3}{[s^2 + \omega^2]^2}$	$f_1(t) = \sin(\omega t) - \omega t \cos(\omega t)$
2	$F_2(s) = \frac{e^{-\sqrt{s}}}{s}$	$f_2(t) = \operatorname{erfc}\left(\frac{1}{2\sqrt{t}}\right)$
3	$F_3(s) = \frac{1 - e^{-s}}{2s} e^{-s}$	$f_3(t) = 0.5$ if $1 \leq t \leq 2$, and 0 elsewhere .

The results of testing functions ($F_1 - F_3$) in conjunction with their absolute error plots are displayed in Fig. 3.3 to Fig. 3.5 [104]. These results illustrate the inversions done by proposed accelerated NILT methods discussed above. Respective adapted acceleration techniques have been algorithmized in the Matlab language and were analyzed as for their accuracy, numerical stability and optimal choice of their parameters. Generally, the following statements can be conceived as for the hyperbolic NILT method; the quotient-difference is more numerically stable, mainly

when compared to the epsilon algorithm, i.e. due to the mathematical structure of the epsilon algorithm, a probability exists that in the denominator two big numbers of near values are subtracted, which leads to the denominator to approach zero and hence cause some instability [102]. On the other hand, the Euler transform gives a high impact on the accuracy of the method's results, it can be clearly noticed by checking the absolute error in Fig. 3.3 to Fig. 3.5; this is mainly due to the characteristics of the Euler transform when it behaves at its best for alternating power series, which is the case of the hyperbolic NILT method.

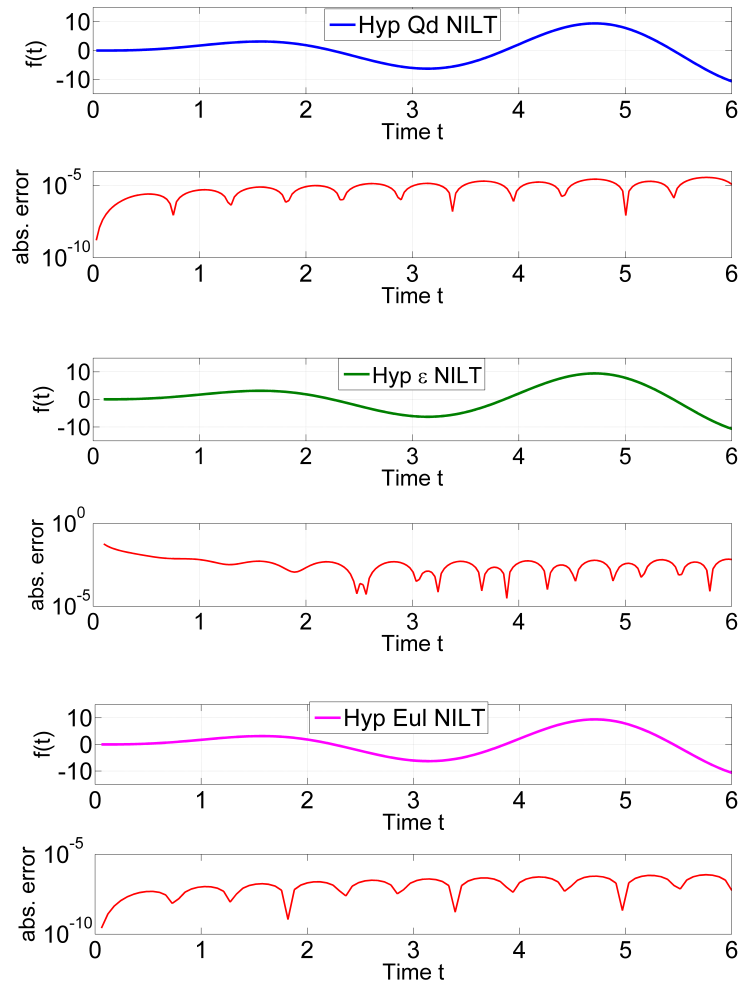


Fig. 3.3: Accuracy experiment results of the accelerated hyperbolic NILTs with test function F_1 .

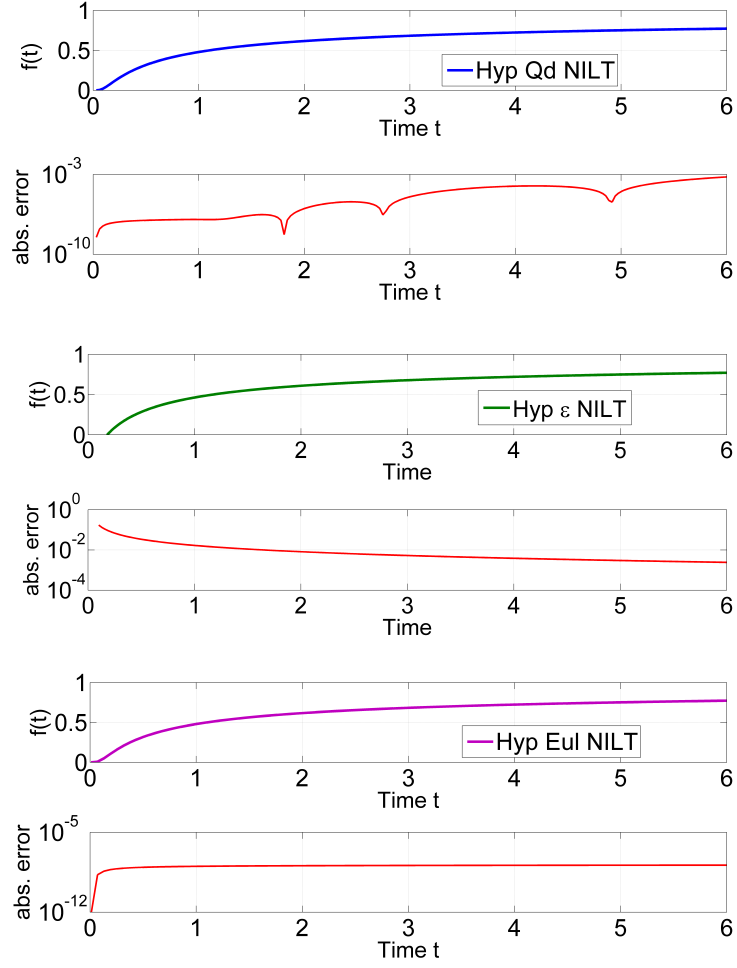


Fig. 3.4: Accuracy experiment results of the accelerated hyperbolic NILTs with test function F_2 .

Furthermore, a precise quantitative conclusion of the accuracy of the hyperbolic NILT method with the adapted acceleration techniques can be observed by introducing the accuracy measure ξ , while considering a number of 200 points, namely

$$\xi = \sqrt{\frac{\sum_{i=1}^{200} [f(t_i) - \hat{f}(t_i)]^2}{200}}, \quad (3.49)$$

where $f(t_i)$ is the pre-known original and $\hat{f}(t_i)$ is the result of the hyperbolic NILT inversion. The results are shown in Tab. 3.2 for each of the acceleration techniques.

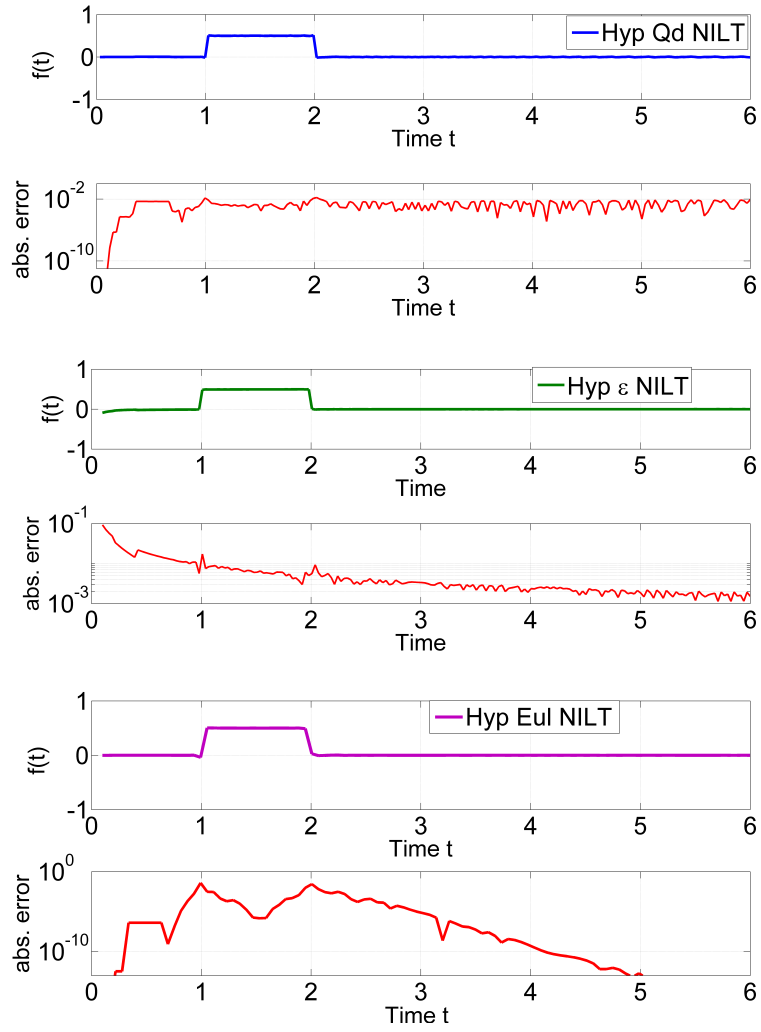


Fig. 3.5: Accuracy experiment results of the accelerated hyperbolic NILTs with test function F_3 .

Tab. 3.2: 1D hyperbolic NILT ξ accuracy measures.

F_r	Hyp- ε NILT	Hyp-Qd NILT	Hyp-Eul NILT
1	0.8×10^{-2}	1.34×10^{-5}	2.25×10^{-7}
2	2.3×10^{-2}	1.42×10^{-4}	1.18×10^{-8}
3	1.2×10^{-2}	7.9×10^{-2}	4.9×10^{-3}

3.4 Comparative study for the 1D hyperbolic NILT method

The 1D NILT methods analyzed in this section include:

- The Zakian 1D method [30],
- the Talbot 1D method [105],
- the Stehfest method [27],
- the 1D accelerated FFT-based method (FFT-Qd NILT) [19], and
- the NILT method based on inverse Laplace transform kernel hyperbolic approximations (Hyp-Eul NILT), [1, 5, 96, 102].

These methods were implemented by using the Matlab mathematical language and were verified as for their accuracy, stability, range of application as well as their computational speed. The methods were verified by using test functions in the Laplace domain with their pre-known originals. Tab. 3.3 shows the functions and their known originals respectively [96].

The methods were implemented by using the Matlab mathematical language and verified as for their accuracy, stability, range of application as well as their computational speed.

Tab. 3.3: List of test functions and their original-time domain values for the comparative study

r	Functions in the Laplace domain $F_r(s)$	Functions in the time domain $f_r(t)$
1	$F_1(s) = \frac{\omega}{s^2 + \omega^2}$	$f_1(t) = \sin(\omega t)$
2	$F_2(s) = \frac{e^{-a\sqrt{s}}}{\sqrt{s}}$	$f_2(t) = \frac{1}{\sqrt{\pi t}} \cdot e^{-\frac{a^2}{4t}}$
3	$F_3(s) = \frac{1}{s} \cdot \frac{1}{\exp(s)-1}$	Staircase Function.

The results of inverting the test functions on each of the described 1D NILT methods are displayed in Fig. 3.6 to Fig. 3.8; each method was tested independently on the time interval $t = (0, 9)$ sec, [96]. The results show that for the chosen test functions, the Zakian method generally lacks accuracy for the exponential and for the staircase function; as for the sinusoidal function $f_1(t)$, the Zakian method is inverted correctly for about six oscillations and then is slowly damped. The Talbot method is more accurate on the whole-time interval, except for the staircase function, the

function has jump discontinuities, and the Gibbs effect is easily noticed, as is the case with function $f_3(t)$.

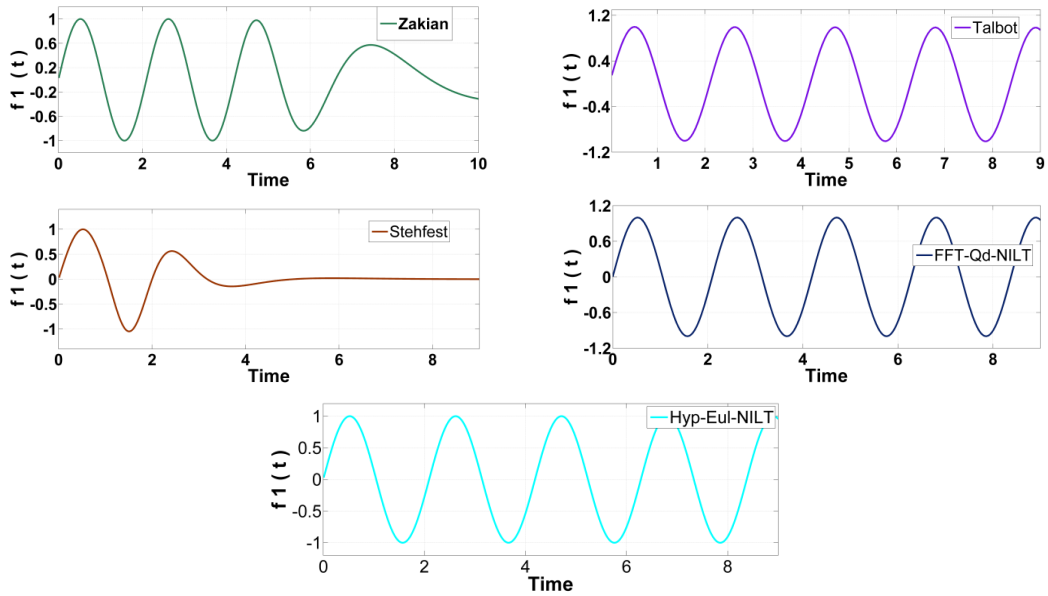


Fig. 3.6: Test results of the Zakian, Talbot, Stehfest, FFT-Qd NILT and Hyp-Eul NILT methods with function F_1 .

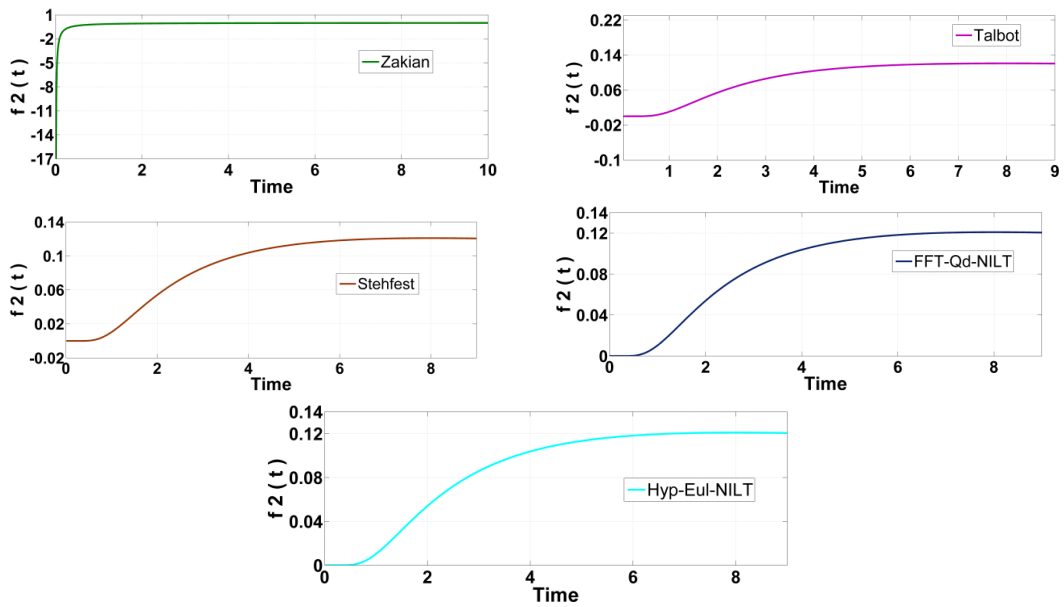


Fig. 3.7: Test results of the Zakian, Talbot, Stehfest, FFT-Qd NILT and Hyp-Eul NILT methods with function F_2 .

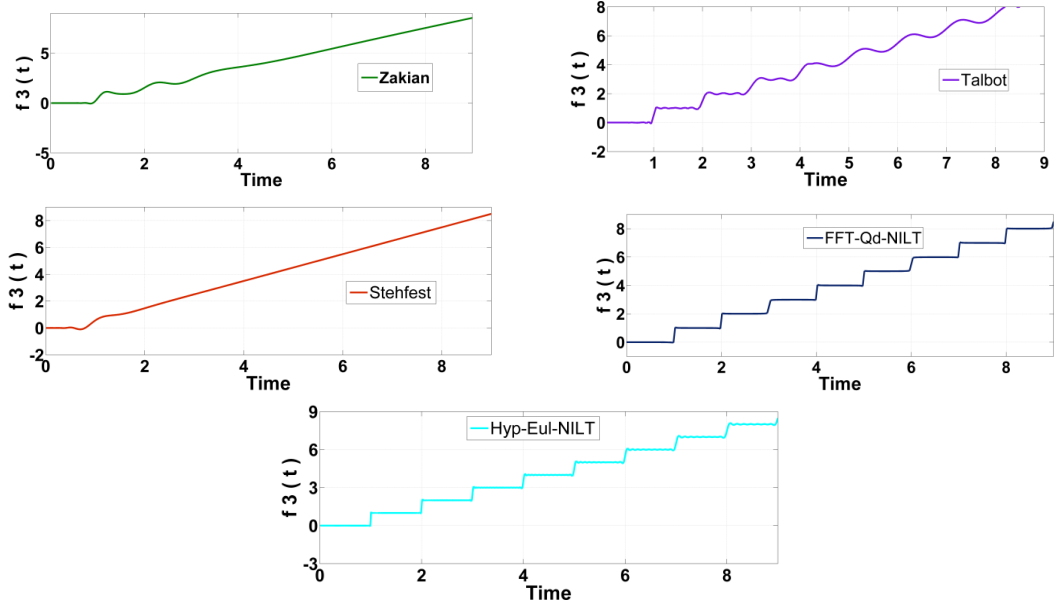


Fig. 3.8: Test results of the Zakian, Talbot, Stehfest, FFT-Qd NILT and Hyp-Eul NILT methods with function F_3 .

The simulation results of the Stehfest NILT method are programmed in the Matlab language. The inversion is relatively good for the exponential function $f_2(t)$, although the results of the other two functions, $f_1(t)$ and $f_3(t)$ are not possible to be considered for practical uses due to the lack of accuracy [96]. Nevertheless, the method showed positive results in other types of functions in other fields of applications, such as the solute transport or the applications in the petrol engineering field [33]. Regarding the performed tests using the FFT-Qd NILT and the Hyp-Eul NILT, as can be noticed, their results exhibit a high accuracy and stability on the whole-time interval for all the tested functions. The staircase function is an important case to look at as, due to its several discontinuities, it is usually difficult to invert such functions, but both the FFT-Qd NILT and the Hyp-Eul-NILT provide very accurate inversions for it. The Hyperbolic NILT accuracy measurement, incorporated with different accelerating techniques, has been performed by the experimental error analysis and the results have been published in [1, 102, 104]. From the error analysis performed the accuracy of the Hyp-Eul NILT is shown to be relatively very high. This is verified by the low absolute error measurements, such a case is illustrated in Fig. 3.9, where the inversion result and its corresponding error graph are displayed. In this figure it is shown that the absolute error for the Hyp-Eul NILT inversion of function $f(t) = \cos(\omega t)$ is below 10^{-10} ; on average, along the time interval, this error decreases even further on some regions of the function.

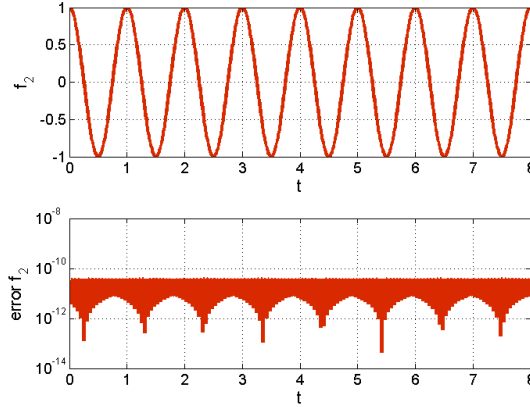


Fig. 3.9: Hyp-Eul NILT inversion and corresponding absolute error for function $f(t) = \cos(\omega t)$.

3.5 Summary

In this chapter, the 1D hyperbolic NILT method was presented, and its algorithms were devised. This method differs from other algorithms for the numerical inversion of the Laplace transform, as it behaves as a nearly ideal lowpass filter with time-variable cutoff frequency. These final algorithms have been derived further by following a different manner, i.e. by the direct numerical integration of the ILT Bromwich definition integral, while achieving the same final 1D hyperbolic NILT algorithms. The second approach leads to a possibility of a generalization of the method by decreasing the integration step, while enabling to predict a limiting absolute error. Furthermore, the numerical error analysis of the method was computed and studied. The proposed method was developed by the incorporation of several different infinite series convergence acceleration techniques; namely, the Euler transform, the quotient-difference algorithm, and the Epsilon algorithm. These techniques were adapted separately each to the 1D hyperbolic NILT method and simulated and their absolute errors were tested with the goal to find the finest technique which provides the highest accuracy and stability to the method. It was clear, after a comparative study with different NILT methods was conducted, that the method provides relatively a very high accuracy and stability and covers a high range of types of functions that can be inverted; for instance, transcendental, rational and irrational Laplace transforms which occur in systems with distributed parameters. All the simulations in this chapter, including other NILT methods, were programmed by the author in the Matlab programming language.

4 APPLICATIONS OF THE 1D HYPERBOLIC NILT METHOD

In this chapter, several applications using the 1D hyperbolic NILT method, among others, are successfully implemented. These applications are focused on the simulation of voltage/current waveforms along lossy transmission lines (TL), frequency dependent TL, multiconductor TL (MTL), and including fractional-order elements in the modeling of these applications. Results of each of these applications are programmed in Matlab and illustrated in respective figures.

4.1 Lossy transmission line simulation using the hyperbolic NILT method

The NILT's field of applications are, mainly, used to process Laplace transforms that arise from the solution of systems with distributed parameters, in which their mathematical structures result in transcendental and/or irrational Laplace transforms. A practical application of the proposed 1D hyperbolic NILT method is here presented; this application involves the solution of a lossy TL and a simulation the conditions of the voltage/current waveforms along the TL wires.

The TL model in the Laplace domain is shown in Fig. 4.1 below [96]. The Laplace

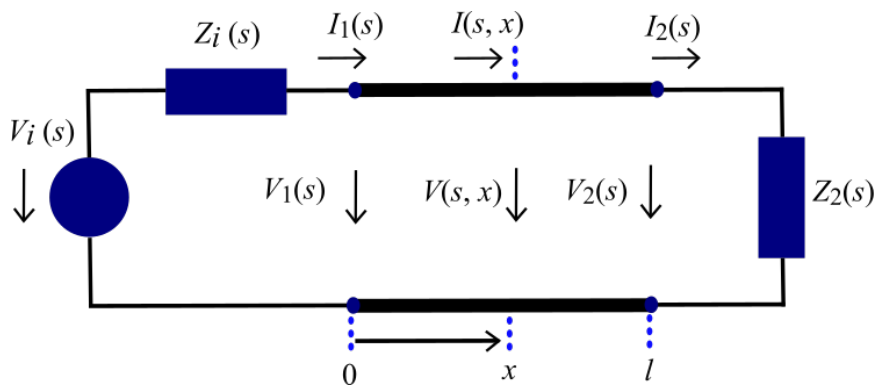


Fig. 4.1: Transmission line model in the Laplace domain.

model of the transmission line results from the application of the Laplace transform of one variable (the time t) on the pair of telegrapher equations

$$-\frac{\partial v(t, x)}{\partial x} = R_0 i(t, x) + L_0 \frac{\partial i(t, x)}{\partial t}, \quad (4.1)$$

$$-\frac{\partial i(t, x)}{\partial x} = G_0 v(t, x) + C_0 \frac{\partial v(t, x)}{\partial t}, \quad (4.2)$$

where R_0 , L_0 , G_0 and C_0 are per-unit-length (p.u.l.) elements and represent resistance, inductance, conductance and capacitance, respectively.

The Laplace transform of the solution with considering zero initial conditions, i.e. $v(0, x) = 0$ and $i(0, x) = 0$, and by incorporating boundary conditions then we get [1],

$$V(s, x) = V_i(s) \frac{Z_c(s)}{Z_i(s) + Z_c(s)} \cdot \frac{e^{-\gamma(s)x} + \rho_2(s)e^{-\gamma(s)[2l-x]}}{1 - \rho_1(s)\rho_2(s)e^{-2\gamma(s)l}}, \quad (4.3)$$

$$I(s, x) = V_i(s) \frac{1}{Z_i(s) + Z_c(s)} \cdot \frac{e^{-\gamma(s)x} - \rho_2(s)e^{-\gamma(s)[2l-x]}}{1 - \rho_1(s)\rho_2(s)e^{-2\gamma(s)l}}, \quad (4.4)$$

where $Z_c(s)$ and $\gamma(s)$ represent the characteristic impedance and the propagation constant of the line, respectively, and are given as

$$Z_c(s) = \sqrt{\frac{Z_0(s)}{Y_0(s)}} = \sqrt{\frac{R_0 + sL_0}{G_0 + sC_0}}, \quad (4.5)$$

$$\gamma(s) = \sqrt{Z_0(s) \cdot Y_0(s)} = \sqrt{(R_0 + sL_0)(G_0 + sC_0)}, \quad (4.6)$$

where $Z_0(s) = R_0 + sL_0$ and $Y_0(s) = G_0 + sC_0$ are p.u.l. series impedance and shunt admittance, respectively.

The reflection coefficients at the beginning and end of the TL $\rho_1(s)$ and $\rho_2(s)$ accordingly, are

$$\rho_1(s) = \frac{Z_i(s) - Z_c(s)}{Z_i(s) + Z_c(s)}; \quad \rho_2(s) = \frac{Z_2(s) - Z_c(s)}{Z_2(s) + Z_c(s)}. \quad (4.7)$$

In this test, the simulation of a uniform transmission line with length l is performed and the following parameters are considered; $l = 2$ m, $R_0 = 10$ m Ω /m, $L_0 = 227$ nH/m, $G_0 = 2$ mS/m, $C_0 = 90.9$ pF/m, $Z_i = 30$ Ω , $Z_2 = 3$ k Ω . The transmission line is tested with an excitation wave $v_i(t) = \sin^2\left(\frac{\pi t}{4 \cdot 10^{-9}}\right)$ with $0 \leq t \leq 4 \cdot 10^{-9}$, and $v_i(t) = 0$, otherwise. The corresponding Laplace domain of the excitation voltage waveform is $V_i(s) = \frac{2\pi^2[1 - \exp(-4 \cdot 10^{-9}s)]}{s[(4 \cdot 10^{-9}s)^2 + 4\pi^2]}$. The time-domain conditions of the voltage, and current waveforms are obtained by using the hyperbolic 1D NILT method, the results are depicted in Fig. 4.2 and Fig. 4.3 for the beginning, middle and end of the transmission line [96].

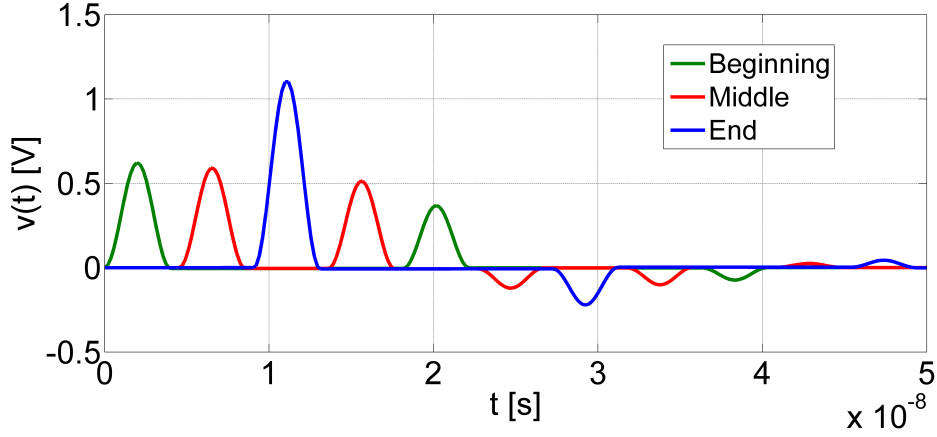


Fig. 4.2: Voltage waveforms conditions along TL by via 1D Hyp-Eul NILT.

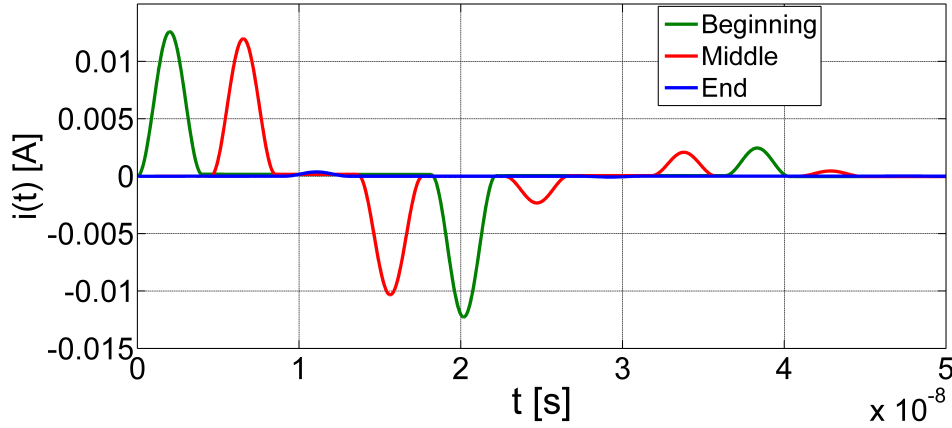


Fig. 4.3: Current waveforms conditions along TL via 1D Hyp-Eul NILT.

The parameters used for the Hyp-Eul NILT to obtain the results are: $n_{sum} = 200$, $n_{euler} = 100$ and $m \cdot a = 9$.

4.2 Incorporation of fractional-order transmission line primary parameters

Research of fractional-order calculus was introduced more than 300 years ago, with a vast field of applications benefiting from the introduction of fractional-order calculus, and still many potential topics in this field that are open for further research and discussion. Due to the advantage of having the NILT methods in hand,

it is thus possible to introduce the fractional-order domain of different application models in the Laplace domain and thus highly simplifying the solution process. In the following subsections, we introduce the fractional-order primary parameters to the TL mode, with detailed analysis being performed. Following, the fractional-order TL resulting model is tested via an excitation waveform, and with the assistance of the Hyp-Qd NILT, we can simulate the voltage/current waveforms along the TL in the time-domain.

I. Fractional-order primary parameters

Considering a TL of length l with distributed elements, as in Fig. 4.1, the TL has the elementary section shown in Fig. 4.4. The primary parameters L'_0 , C'_0 have the fractional orders α and β , respectively, where the dash designation represents only the fractional order immittances, keeping into account the numerical value of parameters is unchanged.

As it will be demonstrated, imposing fractional parameters give a higher

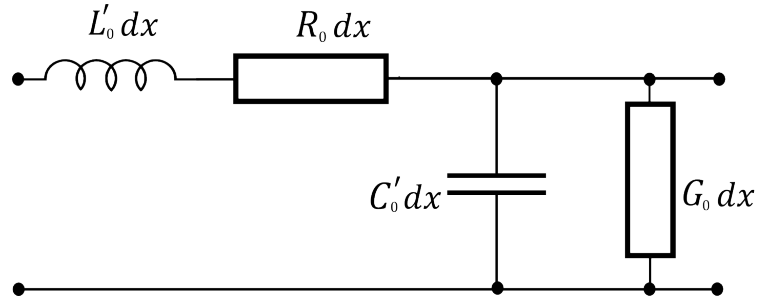


Fig. 4.4: Fractional-order primary parameters of the TL.

degree of freedom for TL modeling and optimization, enabling the realization of the losses, especially those resulting from high frequencies [81], and furthermore building on the fact that the solution of the TL traveling waveforms continuously depends on the fractional derivative.

Incorporating the fractional-order primary parameters into transmission line systems of equations results in

$$Z_{cf} = \sqrt{\frac{Z_{0f}(s)}{Y_{0f}(s)}} = \sqrt{\frac{R_0 + s^\alpha L'_0}{G_0 + s^\beta C'_0}}, \quad (4.8)$$

where $Z_{cf}(s)$ annotates the fractional-order characteristic impedance, which is replaced instead of the integer-order characteristic impedance $Z_c(s)$ in (4.5).

Consequently, the propagation constant $\gamma(s)$ changes accordingly with fractional parameters as

$$\gamma_f(s) = \sqrt{Z_{0f}(s) \cdot Y_{0f}(s)} = \sqrt{(R_0 + s^\alpha L'_0)(G_0 + s^\beta C'_0)}. \quad (4.9)$$

II. Fractional-order model analysis and results

R. Ismail et al. [77], discuss the effects of the fractional parameters α and β on the real part of the propagation constant (the attenuation) and the real part of the characteristic impedance (the resistive element). Moreover, in the recent work in [91], we argue that by checking the sign of the real part of the propagation constant γ , which should remain negative as it represents attenuation and in practice $0 < \alpha, \beta < 2$, then the region of the fractional parameters α and β are found to be in the range $1 < \alpha + \beta < 3$; illustrations of this study are shown in Fig. 4.5, [91]. Furthermore, it is interesting to notice, when analyzing the fractional-order characteristic impedance, that the real part of Z_{cf} , which represents the resistive element, is affected by the fractional parameters α and β . Mainly, with a constant load, the TL response to applied voltage is resistive rather than reactive, despite being composed of inductive, capacitive and resistive elements. The integer-model case of characteristic impedance can be noticed in the Fig. 4.6 (a) and that is when $\alpha = 1$ and $\beta = 1$. Interestingly, the real value of the characteristic impedance (resistive element) is positive and increasing when the fractional values are in the range $0 < \alpha, \beta < 1$ and hence we bound our choices in this region; above this range the real value of the characteristic impedance is negative and decreasing as shown in Fig. 4.6 (c).

The relation of $Z_{cf}(s)$ and $\gamma_f(s)$ with the fractional parameters α and β are shown in Fig. 4.5 and Fig. 4.6, accordingly. The sub-figures (a), (b) and (c) illustrate the real value with the regions of interest which bound the selection of α , β . The simulations are done in Matlab with $s = j\omega$, where ω is the angular frequency and is chosen as $\omega = 1 \times 10^9 \text{ rad} \cdot \text{s}^{-1}$.

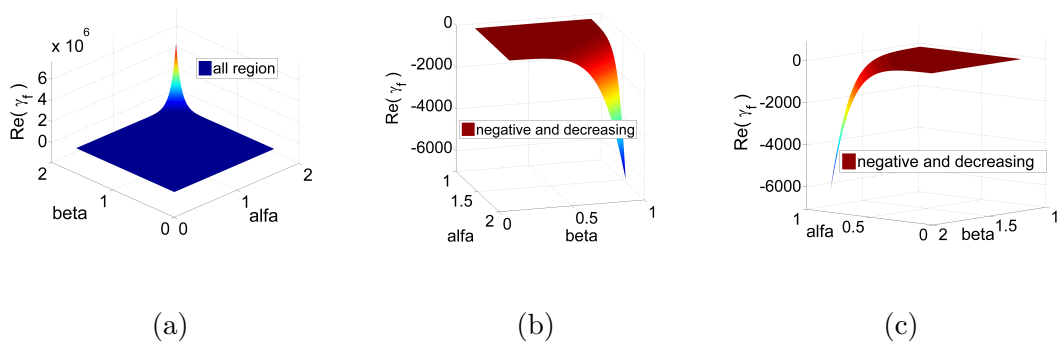


Fig. 4.5: Real value of γ_f versus α and β .

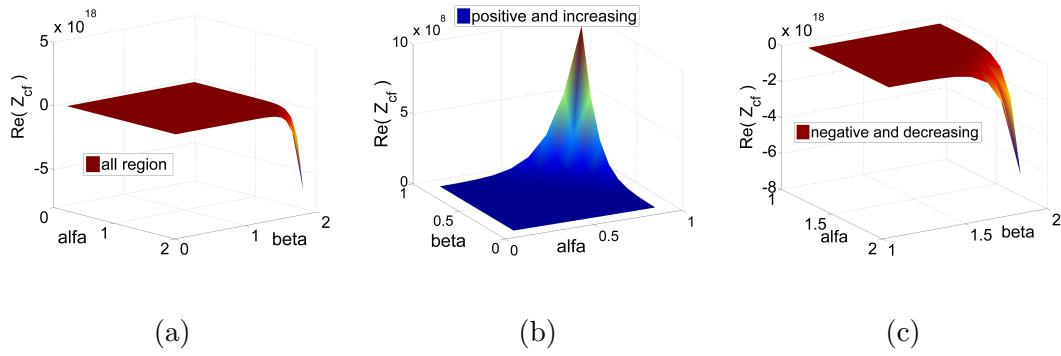


Fig. 4.6: Real value of Z_{cf} versus α and β .

4.3 Incorporation of frequency dependent transmission line parameters

Due to continuous rapid increase in operational frequencies and transmission speeds in power systems, an essential characteristic to be considered is the frequency dependence properties. Generally, skin effect (SE) is an important frequency dependent parameter to be considered when dealing with high frequency applications [106]; its impact is usually higher than the polarization effect on the surrounding medium [107]. Mainly, skin effect increases the resultant losses of the TL. By transforming the skin effect into the Laplace-domain the solution is effectively simplified, rather than solving in the time-domain. The fractional-order series impedance is supplemented by the term $K\sqrt{s}$, to give

$$Z_{0f}(s) = R_0 + s^\alpha L'_0 + K\sqrt{s} \quad , \quad (4.10)$$

where the added rightmost term represents both high-frequency internal resistance and internal inductive reactance. Skin effect can be described as the tendency of a high-frequency electric current to distribute itself in a conductor so that the current density near the surface is greater than at its core. The transmission line parameters have obvious frequency-dependent phenomena due to the skin and edge effect on high frequencies. Taking into account the SE and other conditions, the calculation and analysis of frequency-dependent transmission line gives more accurate transmission characteristics. Therefore, (4.10) will be used in (4.8) and (4.9) in the following analysis.

4.4 Fractional-order TL model simulation

For this study, let us consider a lossy transmission line of length $l = 2$ m, $R_0 = 0.35$ Ω/m , $L_0 = 265$ nH/m, $G_0 = 0.1$ mS/m, $C_0 = 95$ pF/m, $Z_i = 10$ Ω , $Z_2 = 2.5$ k Ω , and the skin effect parameter $K = 4.5 \cdot 10^{-4}$ $\Omega\sqrt{\text{s}}/\text{m}$ for frequency dependent line or $K = 0$ is used for the frequency independent line [108], and with the fractional parameters α and β used for the inductance and capacitance, accordingly. The fractional-order characteristic impedance with incorporating the skin effect is given as

$$Z_{cf} = \sqrt{\frac{R_0 + s^\alpha L'_0 + K\sqrt{s}}{G_0 + s^\beta C'_0}} . \quad (4.11)$$

Consequently, the fractional-order propagation constant with the skin effect is given as

$$\gamma_f(s) = \sqrt{(R_0 + s^\alpha L'_0 + K\sqrt{s})(G_0 + s^\beta C'_0)} . \quad (4.12)$$

After substituting the characteristic impedance and the propagation constant, in their fractional-order form, into (4.3) and (4.4), then the voltage/current waveforms are effectively obtained in the time-domain by undergoing the proposed hyperbolic numerical inverse Laplace transform (Hyp-Qd NILT) method, accelerated with the quotient-difference algorithm. For this analysis the TL was excited with the voltage waveform [91]

$$v_i(t) = \begin{cases} \sin^2\left(\frac{\pi t}{2 \cdot 10^{-9}}\right), & \text{for } 0 < t < 2 \cdot 10^{-9} \text{ ,} \\ 0, & \text{elsewhere .} \end{cases}$$

The excitation waveform is first converted to the Laplace domain i.e:

$$V_i(s) = \frac{2\pi^2(1 - \exp(-2 \cdot 10^9 s))}{s((2 \cdot 10^{-9} s)^2 + 4\pi^2)} ,$$

and then the voltage/current waveforms are simulated for three cases; the integer TL model, the integer TL model with frequency dependence parameters and the fractional-order TL model with frequency dependent parameters; results are illustrated in Fig. 4.7 and Fig. 4.8 for voltage and current waveforms, respectively. By observing these and comparing the fractional-order model including skin effect with the integer-model, it is noticed that the results capture more realistically the TL properties which are neglected in the integer model.

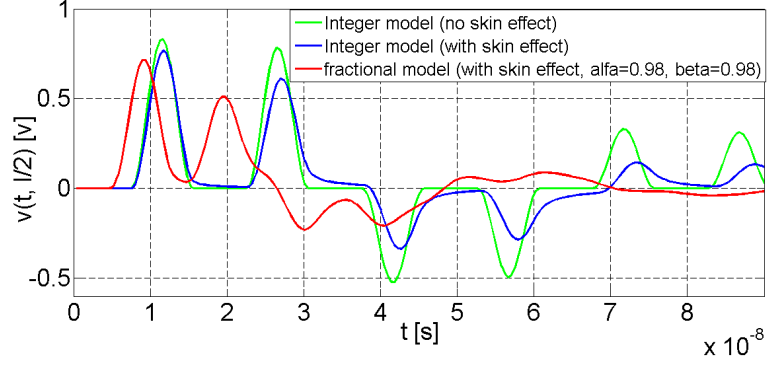


Fig. 4.7: Voltage waveform in the middle of the TL ($x = 1$ m).

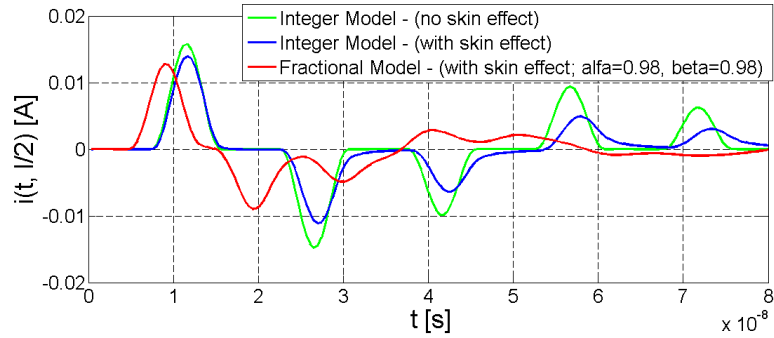


Fig. 4.8: Current waveform in the middle of the TL ($x = 1$ m).

In Fig. 4.9 and Fig. 4.10 are illustrated the voltage distributions, along the same TL example described above, with the choices of fractional parameters $\alpha, \beta = 0.98$ in Fig. 4.9, and $\alpha, \beta = 0.95$ in Fig. 4.10; these values are selected to be in the range bounded by checking the sing of the real value of Z_{cf} and γ_f . It is evident that when $\alpha, \beta = 0.95$ the diffusion is faster than when $\alpha, \beta = 0.98$, [91].

These results are consistent with the behavior of fractional order systems. In essence, as the forward wave and reflected wave travel in opposite directions, this leads to a change in the traveling wave shape and range. As a result, the fractional transmission line model captures the abnormal diffusion phenomena of the voltage wave in the TL much more precisely than the classical integer mode. The simulation results shown in Fig. 4.7 and Fig. 4.8 were computed using the 1D hyperbolic NILT method accelerated with the QdA, on the other hand the 3D voltage and current distributions in Fig. 4.9 and Fig. 4.10, respectively, were obtained by the 2D FFT-NILT method.

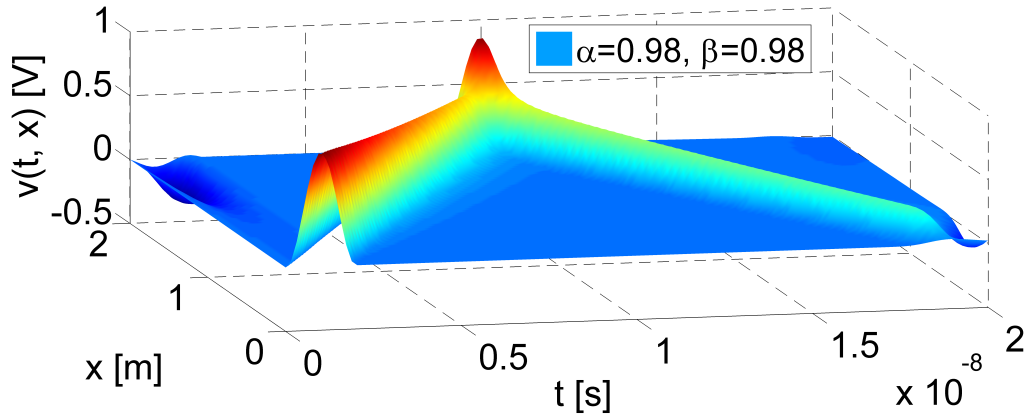


Fig. 4.9: Voltage distribution along the TL with fractional-order parameters ($\alpha = \beta = 0.98$).

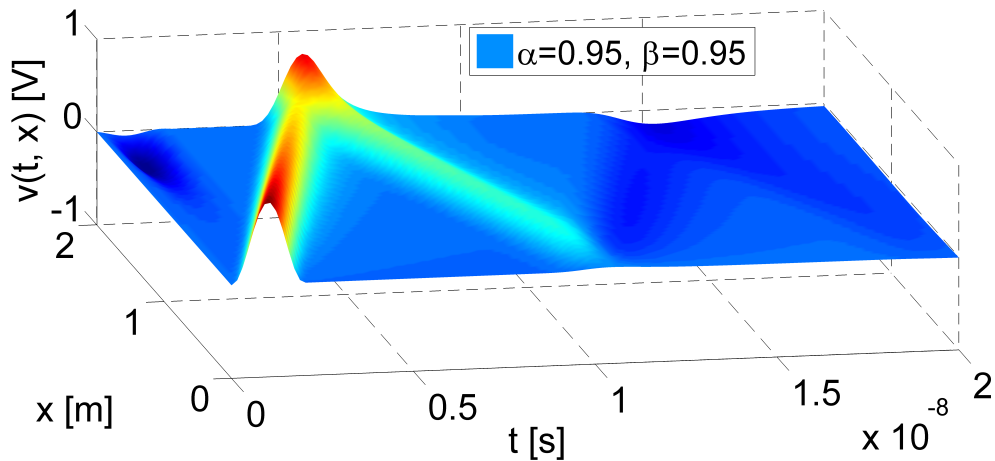


Fig. 4.10: Voltage distribution along the TL with fractional-order parameters ($\alpha = \beta = 0.95$).

4.5 Nonuniform transmission line with fractional-order elements

In high-speed electronics, the design of large integrated circuits includes analysis and verification steps, where interconnect structures between functional blocks are used, e.g. printed circuit boards (PCB) or inside electronic chips are often modeled as general nonuniform TL and, therefore, the transmission line theory is used [106,

107]. In this section, with the use of the hyperbolic NILT method, we will present a developed solution of the nonuniform TL model with including fractional-order elements. Consider the nonuniform TL system, illustrated in Fig. 4.11, [109]. The

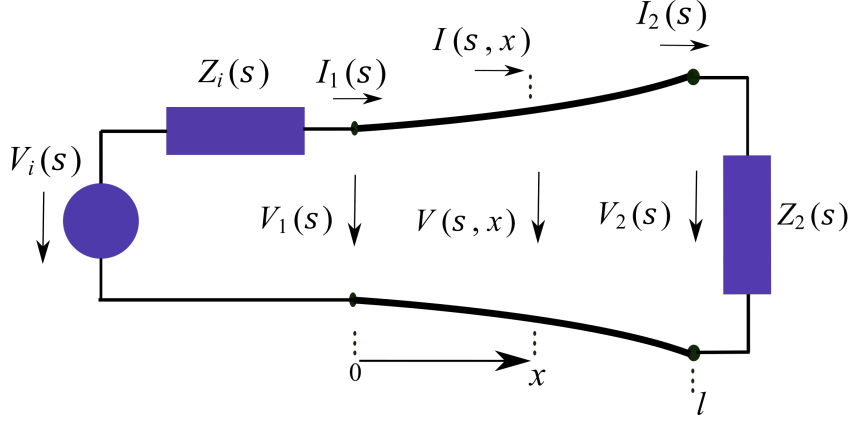


Fig. 4.11: Nonuniform transmission line with linear terminations.

TL has a length l , with linear terminal loads $Z_i(s)$ and $Z_2(s)$ and an excitation source $V_i(s)$. The terminal loads can be represented by their Thévenin or Norton equivalent circuits. Telegraphic equations representing TL, which can be easily found in literature [13, 76], are expressed for nonuniform TL as follows

$$-\frac{\partial v(t, x)}{\partial x} = R_0(x)i(t, x) + L_0(x)\frac{\partial i(t, x)}{\partial t}, \quad (4.13)$$

$$-\frac{\partial i(t, x)}{\partial x} = G_0(x)v(t, x) + C_0(x)\frac{\partial v(t, x)}{\partial t}, \quad (4.14)$$

in which $v(t, x)$ and $i(t, x)$ are the voltage and current waveforms traveling along the TL, and $R_0(x)$, $L_0(x)$, $G_0(x)$ and $C_0(x)$ are p.u.l. primary parameters of the nonuniform TL. The telegrapher system of equations described earlier can be simplified by applying the Laplace transform with respect to time. Therefore, considering zero initial conditions then (4.13) and (4.14) become, respectively

$$-\frac{dV(s, x)}{dx} = (R_0(x) + sL_0(x))I(s, x) = Z_0(s, x)I(s, x), \quad (4.15)$$

$$-\frac{dI(s, x)}{dx} = (G_0(x) + sC_0(x))V(s, x) = Y_0(s, x)V(s, x), \quad (4.16)$$

where $Z_0(s, x)$ and $Y_0(s, x)$ are p.u.l. series impedance and shunt admittance, respectively. In the following sections we incorporate the skin effect, and further expand the work done in [87] by considering fractional-order primary LC elements, with the assistance of the 1D FFT/IFFT NILT method [13].

I. Incorporation of Skin Effect

Based on theory of fractional differential equations, it is shown in [106], where the p.u.l. series impedance is modified to include the skin effect as follows

$$Z_0(s, x) = R_0(x) + sL_0(x) + K(x)\sqrt{s} , \quad (4.17)$$

the terms in (4.17) represent, respectively, the dc p.u.l. resistance, the external inductive reactance, and the later term denotes the high-frequency resistance and the internal inductive reactance.

II. Incorporation of Fractional-Order Elements

Fractional calculus is a potential branch of mathematics that is involved in the non-integer differentiation and integration. Recently, more attention has been paid to this field, as various applications are benefiting from it. The Caputo definition of the fractional derivative of a function $f(t)$, with order κ and zero lower limit is defined by the equation (1.52) and has the Laplace transform given by (1.53). Based on fractional calculus of electrical components, the immittances of fractional-order, inductance and capacitance in the s -domain, for a ‘nonuniform’ TL are given as

$$Z_\alpha(s, x) = s^\alpha L_\alpha(x) , \quad (4.18)$$

$$Y_\beta(s, x) = s^\beta C_\beta(x) , \quad (4.19)$$

where $L_\alpha(x)$ is the pseudo-inductance with order $\alpha \in (0, 1]$ and $C_\beta(x)$ is the pseudo-capacitance with order $\beta \in (0, 1]$, [89]. In consideration of the foregoing, let us investigate a transmission line system with a nonuniform TL of length l , and distributed elements as in Fig. 4.11. The TL has an elementary section illustrated in Fig. 4.12. The primary parameters $L_\alpha(x)$, $C_\beta(x)$ have the fractional orders α and β , respectively, where the superscripts denote that immittances are of fractional-order types, rather than integer ones.

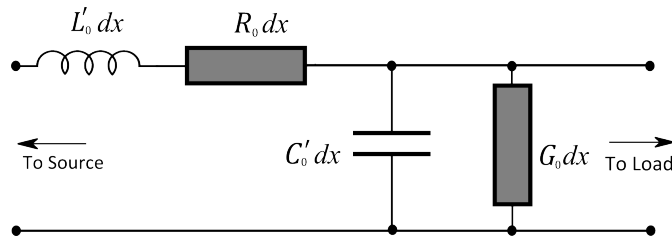


Fig. 4.12: Electrical circuit of an infinitesimal segment of a transmission line.

The two-coupled s -domain first-order ordinary differential equations, (4.15) and (4.16), with varying coefficients can be more effectively solved when composed into a compact matrix form as follows

$$\frac{d}{dx} \begin{bmatrix} V(s, x) \\ I(s, x) \end{bmatrix} = \begin{bmatrix} 0 & -Z(s, x) \\ -Y(s, x) & 0 \end{bmatrix} \cdot \begin{bmatrix} V(s, x) \\ I(s, x) \end{bmatrix}, \quad (4.20)$$

where $V(s, x)$ and $I(s, x)$ are the Laplace transforms of instantaneous voltage and current at distance x from the left side ‘the beginning’ of the TL, respectively. By incorporating fractional-order elements into the nonuniform TL system of equations, we get

$$Z_f(s, x) = R_0(x) + s^\alpha L' + K(x)\sqrt{s}, \quad (4.21)$$

$$Y_f(s, x) = G_0(x) + s^\beta C'_0, \quad (4.22)$$

where $Z_f(s, x)$ and $Y_f(s, x)$ denote fractional-order p.u.l. series impedance and shunt admittance, respectively. The compact matrix form (4.19) can be expressed more formally, for simplicity, as follows

$$-\frac{d\mathbf{W}(s, x)}{dx} = \mathbf{M}(s, x) \mathbf{W}(s, x). \quad (4.23)$$

A known solution for the ordinary differential equation (ODE) (4.22) can be given as [110],

$$\mathbf{W}(s, x) = \mathbf{\Phi}_0^x(s) \mathbf{W}(s, 0), \quad (4.24)$$

where $\mathbf{\Phi}_0^x(s)$ is the integral matrix also known as the matrizant, which can be defined by the Volterra product integral [110], and $\mathbf{W}(s, 0)$ is obtained by the boundary condition, which is the solution at $x = 0$ (the nonuniform TL input). If the nonuniform TL is divided into m small segments, see Fig. 4.12, it is then possible to consider them as nearly uniform segments. This is based on the fact that for a uniform TL the matrizant is then converted to a matrix exponential function. By considering the property of a matrizant, $\mathbf{\Phi}_0^x = \mathbf{\Phi}_y^x \mathbf{\Phi}_0^y$, $x > y > 0$, it is possible to divide the TL on m small segments, namely $\Delta x_q = x_q - x_{q-1}$, where $q = 1, 2, \dots, x_0 = 0$ and $x_m = l$, considering each as a uniform segment. In the light of this, an approximated matrizant of the whole TL is represented by products of respective matrix exponentials,

$$\tilde{\mathbf{\Phi}}_0^d(s) = e^{-\mathbf{M}(\zeta_m, s)\Delta x_m} e^{-\mathbf{M}(\zeta_{m-1}, s)\Delta x_{m-1}} \dots e^{-\mathbf{M}(\zeta_1, s)\Delta x_1} \quad (4.25)$$

here $\zeta_p \in \Delta x_p$, for instance $\Delta x_p = h = l/m, \forall p$. Henceforth, to solve (4.23) it is required to incorporate a boundary condition $\mathbf{W}(s, 0) = [V_1(s), I_1(s)]^T$, which is given by the linear circuit terminations connected to the TL. These

linear networks can be represented by their Thévenin or Norton equivalents. Here the former is considered, and then we get

$$V_1(s) = V_i(s) - Z_i(s)I_1(s) \quad (4.26)$$

where $V_i(s)$ and $Z_i(s)$ are the internal voltage and impedance of the Thévenin model. Considering Thévenin models on both sides of the TL, the current $I_1(s)$ entering the TL left side can be obtained

$$I_1(s) = \frac{(\Phi_{11}(s) - Z_2(s)\Phi_{21}(s))V_i(s)}{(\Phi_{11}(s) - Z_2(s)\Phi_{21}(s))Z_i(s) + Z_2(s)\Phi_{22}(s) - \Phi_{12}(s)}, \quad (4.27)$$

where $\Phi_{ij}(s)$, $i, j = 1, 2$, are elements of the chain matrix, in case the $x = l$ (nonuniform TL output), and it is given as follows

$$\Phi(s) = \begin{bmatrix} \Phi_{11}(s) & \Phi_{12}(s) \\ \Phi_{21}(s) & \Phi_{22}(s) \end{bmatrix}. \quad (4.28)$$

Substituting (4.26) back to (4.25) we get

$$V_1(s) = V_i(s) \left(1 - \frac{Z_i(s)(\Phi_{11}(s) - Z_2(s)\Phi_{21}(s))}{(\Phi_{11}(s) - Z_2(s)\Phi_{21}(s))Z_i(s) + Z_2(s)\Phi_{22}(s) - \Phi_{12}(s)} \right), \quad (4.29)$$

and hence (4.23) is successfully obtained.

By utilizing the NILT method, we can, at this point, get the time domain voltage/current terminal waveforms from (4.23), i.e. by considering $\mathbf{w}(t, 0) = [v_1(t), i_1(t)]^T$ and $\mathbf{w}(t, l) = [v_2(t), -i_2(t)]^T$, then $\mathbf{W}(s, x)$ undergoes the NILT method to get $\mathbf{w}(t, x) = [v(t, x), i(t, x)]^T$.

III. Analysis and simulation results

Let us investigate a nonuniform TL with length $l = 0.6$ m as in Fig. 4.11. The nonuniform TL has the following specifications: The terminating circuits are obtained by their Thévenin equivalents, with the parameters $R_1 = 1 \Omega$, $R_2 = 1 \text{ k}\Omega$. Moreover, the p.u.l. parameters are set to be exponentially nonuniform by using the formula $D(x) = D_0 e^{dx}$, where the parameter $D_0 \in \{L_0, R_0, G_0, C_0\}$, and $d \in \{d_L, d_R, d_G, d_C\}$, while the nonuniform skin effect is given as $K(x) = K_0 e^{kx}$. The p.u.l. parameters specifications are as follows: $L_0 = 500 \text{ nF/m}$, $R_0 = 0.1 \Omega/\text{m}$, $C_0 = 60 \text{ pF/m}$, and $G_0 = 20 \text{ mS/m}$. The transmission line is excited by the following pulse

$$v_i(t) = \begin{cases} \sin^2\left(\frac{\pi t}{2 \cdot 10^{-9}}\right), & \text{if } 0 \leq t \leq 2 \cdot 10^{-9} \text{ s,} \\ 0, & \text{otherwise.} \end{cases} \quad (4.30)$$

with its Laplace transform given as,

$$V_i(s) = \frac{2\pi^2(1 - \exp(-2 \cdot 10^{-9}s))}{s((2 \cdot 10^{-9}s)^2 + 4\pi^2)}. \quad (4.31)$$

The simulation results are done for several cases as illustrated in Fig. 4.13.

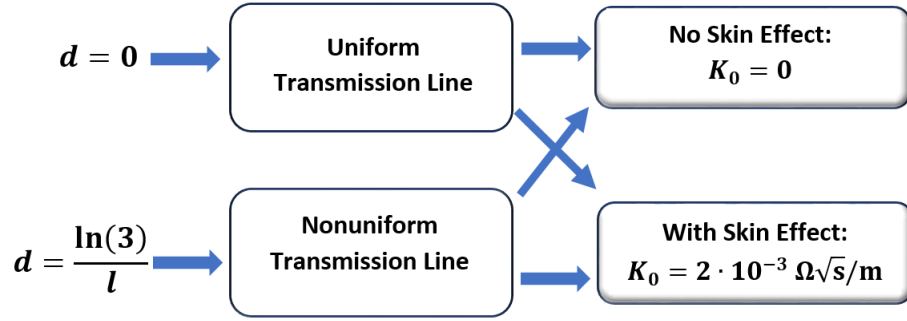


Fig. 4.13: Flow chart with different types of TL.

Namely, when $d = 0$ then the TL is uniform, otherwise the inhomogeneity is chosen as $d = \ln(3)/l = 2.75$; as for the skin effect the parameter $K_0 = 2 \cdot 10^{-3} \Omega\sqrt{s}/m$ and $K_0 = 0$, when no skin effect is considered.

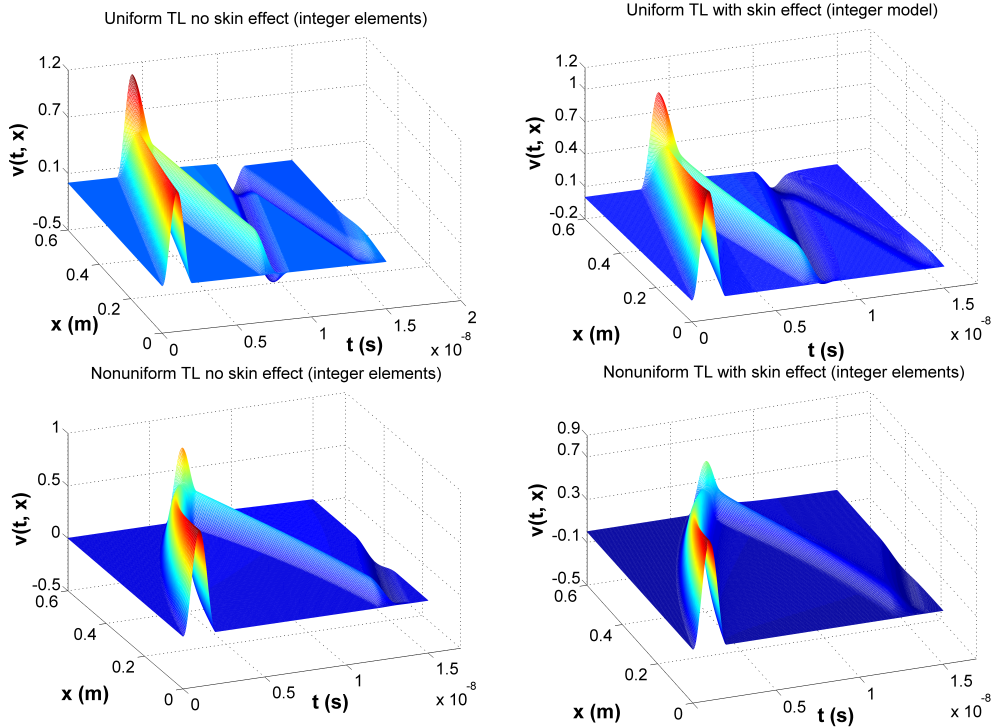


Fig. 4.14: Voltage distribution along several TL types.

The results for the earlier-mentioned cases are shown in Fig. 4.14; the simulations are done in Matlab language by utilizing the 1D FFT/IFFT NILT method accelerated with the quotient-difference algorithms [13]. The 3D results are obtained, in contrast to 2D ones, by utilizing the Matlab capabilities, i.e. using 3D arrays. In Fig. 4.15, the nonuniform TL with skin effect and different fractional-order cases are shown. The range limits of the fractions α and β were investigated earlier in Sect. 4.2; and the study was based on the relation of the changes in the fractions, α , β , with the characteristic impedance or with the propagation constant; namely, the fractions are bounded by the following relations

$$0 < \alpha, \beta < 1 , \quad (4.32)$$

$$1 < \alpha + \beta < 3 , \quad (4.33)$$

Fig. 4.15 illustrates the simulations of the TL model for the fractions α and β with several choices, i.e., 0.98, 0.95 and 0.85, respectively, for both voltage and current waveforms. The following can be concluded; the distributed parameter system of the nonuniform TL can be modeled using the fractional-calculus effectively, and it provides a better representation of the transmission line phenomena.

Moreover, imposing fractional parameters can provide higher degrees of freedom for the TL representation and better control in its characteristics. In the comparison of sub Fig. 4.15, it is noticed that by decreasing the value of the fractions, a faster waveform diffusion is exhibited. This agrees with the work in [111,112], where the incidence wave, with time, acts on the reflected wave, which corresponds with the fact that the solution continuously depends on the fractional derivative. Furthermore, it is clear that modeling with fractional orders can compensate for power losses as the envelope of the voltage/current waves decreases correspondingly with changing fraction orders.

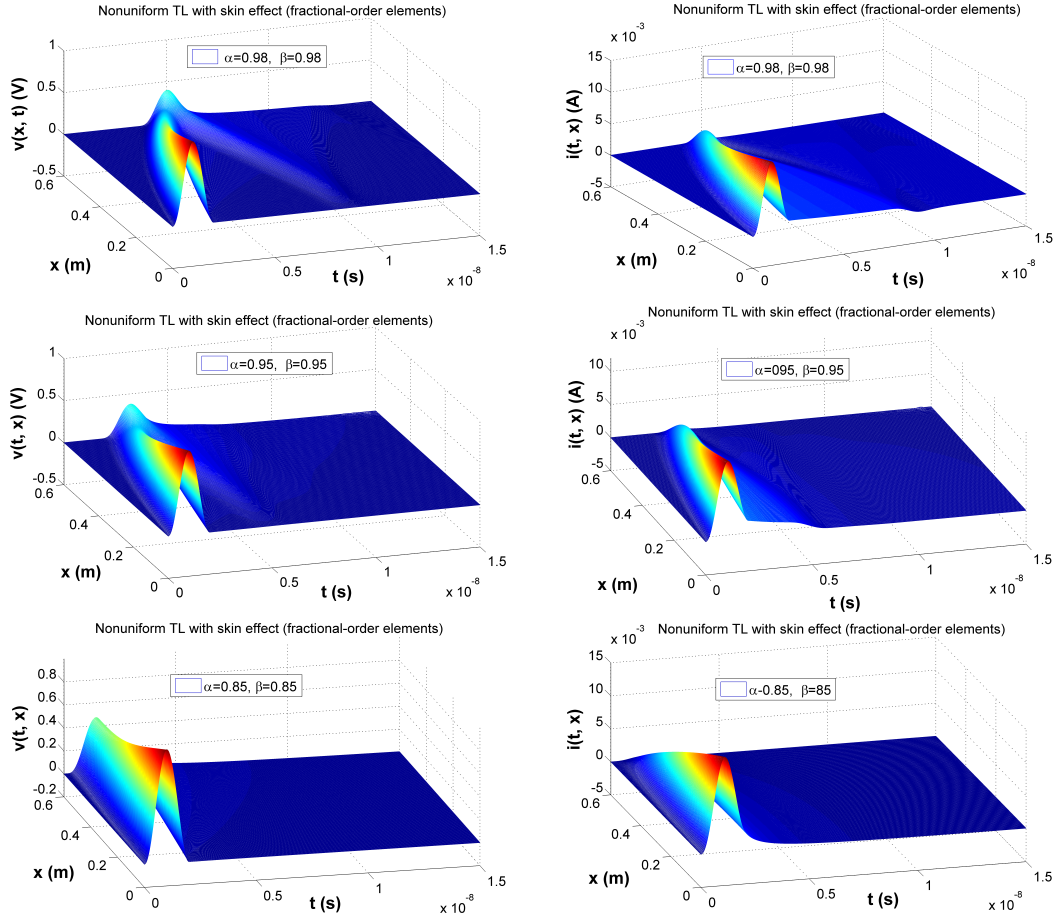


Fig. 4.15: Voltage and current distributions on nonuniform TL with different fractional-order elements.

4.6 Multiconductor transmission line systems with linear terminations

Multiconductor transmission lines (MTLs) are often found in communication systems, power distribution systems, and digital computers, [86]. Thus, the analysis of such systems comes out to be of high practical importance. In the previous sections, we examined the time-domain analysis of the TL system equations and incorporated frequency dependences, nonuniformity, and fractional-order elements. In this section, we will focus on MTLs, which consist of more than two conductors, with linear terminations. It will be shown that the process to expand the result obtained for the TL to the MTL is straightforward, mainly done by introducing the matrix notation. Generally, there are many methods that can be considered when simulating MTL, such as the derivation of the MTL equations from the integral form of Maxwell's equations, derivation of the MTL equations from the

p.u.l. equivalent circuit, utilizing the ‘implicit Wendroff and state variable’ method and others, [107, 113, 114]. Nevertheless, by the advantage of using NILT method, the analysis of MTLs can be done much more time effectively and enable us to introduce all different losses and effects on the modeling, including fractional-order elements, in a simple and fast manner.

This section will be dedicated to an advanced solution of MTLs terminated on both ends with linear networks; these terminations can be modeled by generalized Thevenin and/or Norton equivalents. In the next section MTLs with more complex terminations and possible external feedbacks, describable with a modified nodal analysis and utilizing the NILT method, will be addressed. In this analysis, we will

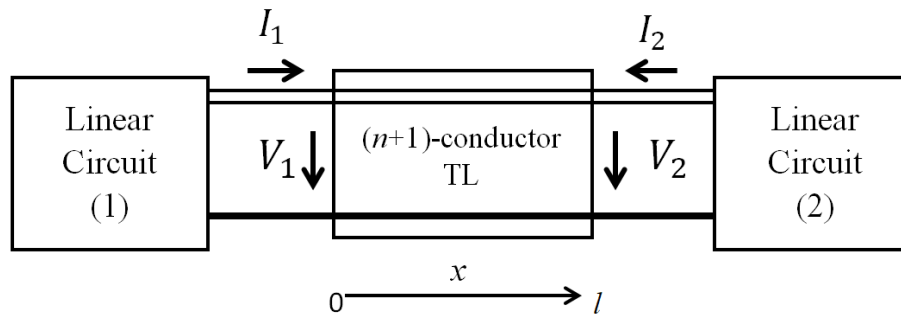


Fig. 4.16: General $(n + 1)$ -conductor TL system with linear terminations.

consider a MTL system containing an $(n + 1)$ -conductor TL with length l for each of the lines, which has the p.u.l. $n \times n$ matrices \mathbf{R} , \mathbf{L} , \mathbf{G} , and \mathbf{C} ; noting that the bold symbols here represent matrices, in contrast to the normal parameters used for a single TL in previous sections, [86].

Firstly, let us start with the description of a classical MTL, afterwards fractional-order elements will be incorporated. A uniform $(n + 1)$ -conductor TL can be presented by a pair of telegraph equations in the time domain with assuming zero initial conditions, i.e. $\mathbf{v}(0, x) = 0$ and $\mathbf{i}(0, x) = 0$.

$$-\frac{\partial \mathbf{v}(t, x)}{\partial x} = \mathbf{R}\mathbf{i}(t, x) + \mathbf{L}\frac{\partial \mathbf{i}(t, x)}{\partial t}, \quad (4.34)$$

$$-\frac{\partial \mathbf{i}(t, x)}{\partial x} = \mathbf{G}\mathbf{v}(t, x) + \mathbf{C}\frac{\partial \mathbf{v}(t, x)}{\partial t}, \quad (4.35)$$

where $\mathbf{v}(t, x)$ and $\mathbf{i}(t, x)$ are $n \times 1$ column vectors of the voltages and currents of n active wires at the distance x from the MTL’s left side, accordingly. For simplicity purposes, we can represent the above telegraph equations (4.34) and (4.35) in a

compact matrix form

$$\frac{\partial}{\partial x} \begin{bmatrix} \mathbf{v}(t, x) \\ \mathbf{i}(t, x) \end{bmatrix} = \begin{bmatrix} \mathbf{0} & -\mathbf{R} \\ -\mathbf{G} & \mathbf{0} \end{bmatrix} \cdot \begin{bmatrix} \mathbf{v}(t, x) \\ \mathbf{i}(t, x) \end{bmatrix} - \begin{bmatrix} \mathbf{0} & \mathbf{L} \\ \mathbf{C} & \mathbf{0} \end{bmatrix} \cdot \frac{\partial}{\partial t} \begin{bmatrix} \mathbf{v}(t, x) \\ \mathbf{i}(t, x) \end{bmatrix}, \quad (4.36)$$

transforming (4.36) into the Laplace domain with respect to the time variable t

$$\frac{d}{dx} \begin{bmatrix} \mathbf{V}(s, x) \\ \mathbf{I}(s, x) \end{bmatrix} = \begin{bmatrix} \mathbf{0} & -\mathbf{Z}(s) \\ -\mathbf{Y}(s) & \mathbf{0} \end{bmatrix} \cdot \begin{bmatrix} \mathbf{V}(s, x) \\ \mathbf{I}(s, x) \end{bmatrix}, \quad (4.37)$$

where the $n \times 1$ voltage and current vectors $\mathbf{V}(s, x) = \mathbf{L}\{\mathbf{v}(t, x)\}$ and $\mathbf{I}(s, x) = \mathbf{L}\{\mathbf{i}(t, x)\}$, respectively. The matrix $\mathbf{0}$ stands for the $n \times n$ order zero matrix, and the series impedance matrix and shunt admittance matrix are given, respectively, as follows

$$\mathbf{Z}(s) = \mathbf{R} + s\mathbf{L}, \quad (4.38)$$

$$\mathbf{Y}(s) = \mathbf{G} + s\mathbf{C}. \quad (4.39)$$

When considering the boundary condition at $x = 0$, $\mathbf{V}_1(s) = \mathbf{V}(s, 0)$ and $\mathbf{I}_1(s) = \mathbf{I}(s, 0)$, see Fig. 4.16, a formal solution is

$$\begin{bmatrix} \mathbf{V}(s, x) \\ \mathbf{I}(s, x) \end{bmatrix} = \exp\left(\begin{bmatrix} \mathbf{0} & -\mathbf{Z}(s) \\ -\mathbf{Y}(s) & \mathbf{0} \end{bmatrix} \cdot x\right) \cdot \begin{bmatrix} \mathbf{V}_1(s) \\ \mathbf{I}_1(s) \end{bmatrix}. \quad (4.40)$$

If the MTL is considered as a multiport then the matrix exponential function (4.40) can be considered as a chain matrix

$$\Phi(s, x) = \begin{bmatrix} \Phi_{11}(s, x) & \Phi_{12}(s, x) \\ \Phi_{21}(s, x) & \Phi_{22}(s, x) \end{bmatrix} = \exp\left(\begin{bmatrix} \mathbf{0} & -\mathbf{Z}(s) \\ -\mathbf{Y}(s) & \mathbf{0} \end{bmatrix} \cdot x\right), \quad (4.41)$$

where $\Phi_{ij}(s, x)$, $i, j = 1, 2$, are respective $n \times n$ square submatrices. noting that due to the MTL reciprocity, $\det(\Phi(s)) = 1$, though, in general $\Phi_{11}(s) \neq \Phi_{22}(s)$ due to some possible inhomogeneity.

Now, for simplicity, let us designate the chain matrix of the whole MTL of the length l as $\Phi(s, l) = \Phi(s)$. Then, by using e.g. a generalized Thévenin equivalents of both terminating linear circuits the formulae for the boundary vectors $\mathbf{I}_1(s)$ and $\mathbf{V}_1(s)$ can be determined as

$$\mathbf{I}_1(s) = \left[(\Phi_{11}(s) - \mathbf{Z}_{i2}(s)\Phi_{21}(s))\mathbf{Z}_{i1}(s) + \mathbf{Z}_{i2}(s)\Phi_{22}(s) - \Phi_{12}(s) \right]^{-1} \times \left[(\Phi_{11}(s) - \mathbf{Z}_{i2}(s)\Phi_{21}(s))\mathbf{V}_{i1}(s) - \mathbf{V}_{i2}(s) \right], \quad (4.42)$$

$$\mathbf{V}_1(s) = \mathbf{V}_{i1}(s) - \mathbf{Z}_{i1}(s)\mathbf{I}_1(s), \quad (4.43)$$

where $\mathbf{V}_{i1}(s)$, $\mathbf{V}_{i2}(s)$, and $\mathbf{Z}_{i1}(s)$, $\mathbf{Z}_{i2}(s)$ are internal voltage vectors and internal impedance matrices of the respective Thévenin equivalents, respectively.

Nevertheless, other combinations of Thévenin and/or Norton equivalents can be considered for both ends of the MTL, namely,

Norton left side \rightarrow Norton right side:

$$\mathbf{V}_1(s) = \left[\begin{array}{c} (\Phi_{22}(s) - \mathbf{Y}_{i2}(s)\Phi_{12}(s))\mathbf{Y}_{i1}(s) + \mathbf{Y}_{i2}(s)\Phi_{11}(s) - \Phi_{21}(s) \\ (\Phi_{22}(s) - \mathbf{Y}_{i2}(s)\Phi_{12}(s))\mathbf{I}_{i1}(s) + \mathbf{I}_{i2}(s) \end{array} \right]^{-1} \times \quad (4.44)$$

Thévenin left side \rightarrow Norton right side:

$$\mathbf{I}_1(s) = \left[\begin{array}{c} (\Phi_{21}(s) - \mathbf{Y}_{i2}(s)\Phi_{11}(s))\mathbf{Z}_{i1}(s) + \mathbf{Y}_{i2}(s)\Phi_{12}(s) - \Phi_{22}(s) \\ (\Phi_{21}(s) - \mathbf{Y}_{i2}(s)\Phi_{11}(s))\mathbf{V}_{i1}(s) + \mathbf{I}_{i2}(s) \end{array} \right]^{-1} \times \quad , \quad (4.45)$$

Norton left side \rightarrow Thévenin right side:

$$\mathbf{V}_1(s) = \left[\begin{array}{c} (\Phi_{12}(s) - \mathbf{Z}_{i2}(s)\Phi_{22}(s))\mathbf{Y}_{i1}(s) + \mathbf{Z}_{i2}(s)\Phi_{21}(s) - \Phi_{11}(s) \\ (\Phi_{12}(s) - \mathbf{Z}_{i2}(s)\Phi_{22}(s))\mathbf{I}_{i1}(s) + \mathbf{V}_{i2}(s) \end{array} \right]^{-1} \times \quad (4.46)$$

Incorporating fractional-order elements into the MTL model is done first by interchanging the p.u.l. series impedance $\mathbf{Z}(s)$ and shunt admittance $\mathbf{Y}(s)$ matrices with $Z_f(s)$ and $\mathbf{Y}_f(s)$, respectively, as follows

$$\mathbf{Z}_f(s) = \mathbf{R} + s^\alpha \mathbf{L}_\alpha \quad , \quad (4.47)$$

$$\mathbf{Y}_f(s) = \mathbf{G} + s^\beta \mathbf{C}_\beta \quad , \quad (4.48)$$

The skin effect of the MTL can be incorporated in a similar manner as done for the single TL by the modification of the series impedance (4.47) with the introduction of the term $\mathbf{K}\sqrt{s}$, though with \mathbf{K} as a matrix coefficient, i.e. $\mathbf{Z}_f(s) = \mathbf{R} + s^\alpha \mathbf{L}_\alpha + \mathbf{K}\sqrt{s}$. A second simplified approach to solve the MTL system equations can be also done by performing another Laplace transform with respect to the geometric coordinate x , [115], while considering fractional-order MTL elements, which leads to the following matrix equation in the (s, q) Laplace domain,

$$\begin{pmatrix} \mathbf{V}(s, q) \\ \mathbf{I}(s, q) \end{pmatrix} = \begin{pmatrix} q\mathbf{E} & \mathbf{Z}_f(s) \\ \mathbf{Y}_f(s) & q\mathbf{E} \end{pmatrix}^{-1} \cdot \begin{pmatrix} \mathbf{V}_1(s) \\ \mathbf{I}_1(s) \end{pmatrix}, \quad (4.49)$$

where \mathbf{E} is the identity matrix, and the voltage and current vectors that correspond to the left side of the MTL are obtained by computing the generalized Thévenin equivalents for both terminating linear circuits, as shown in (4.42) and (4.43), respectively. Henceforth, the time domain results can be obtained by undergoing the 2D *FFT*-NILT method in a fast and accurate process [116]; further details on utilizing the 2D NILT are available in the following Chapters 5 and 6.

4.6.1 Fractional-order MTL case study

A main characteristic of the proposed fractional-order MTL model and simulation is its direct support of several physical phenomena which have not been supported yet. In this case study we demonstrate the applicability of the NILT method to a practically-relevant MTL application.

Let us examine a (3+1)-conductor TL, as shown in Fig. 4.17, with the length $l = 1.2$ m. The MTL has the following terminal resistors $R_{1i} = R_{2i} = 1 \Omega$, where $i = 1, 2, 3$. The MTL's p.u.l. matrices are as follows: [55],

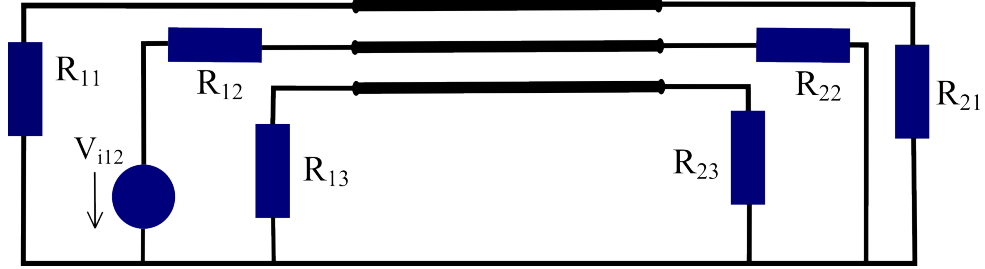


Fig. 4.17: A (3 + 1)-conductor TL system.

$$\begin{aligned} \mathbf{R} &= \begin{pmatrix} 41.7 & 0 & 0 \\ 0 & 41.7 & 0 \\ 0 & 0 & 41.7 \end{pmatrix} \frac{\Omega}{\text{m}}; & \mathbf{L}_\alpha &= \begin{pmatrix} 2.4 & 0.69 & 0.64 \\ 0.69 & 2.36 & 0.69 \\ 0.64 & 0.69 & 2.4 \end{pmatrix} \frac{\mu\text{H}}{\text{m}}; \\ \mathbf{C}_\beta &= \begin{pmatrix} 21 & -12 & -4 \\ -12 & 26 & -12 \\ -4 & -12 & 21 \end{pmatrix} \frac{\text{pF}}{\text{m}}; & \mathbf{G} &= \begin{pmatrix} 0.6 & 0 & 0 \\ 0 & 0.6 & 0 \\ 0 & 0 & 0.6 \end{pmatrix} \frac{\text{mS}}{\text{m}}. \end{aligned} \quad (4.50)$$

The voltage source $V_{i1,2}$ driving the second wire in Fig. 4.17 is excited by the waveform (4.30), and has the corresponding Laplace domain form as in (4.31). As this MTL is considered to have zero initial conditions, it is thus not required to compute matrix convolution integrals. The time-domain final results are obtained by using the 1D NILT method based on *FFT* accelerated with the Qd algorithm in its matrix form.

The simulation results of the voltage/current propagations along the different MTL wires are illustrated in Fig. 4.18 to Fig. 4.29, where three cases are shown; namely, the classic integer case, i.e. $\alpha = \beta = 1$, fractional-order case with $\alpha = \beta = 0.97$, and the fractional-order case $\alpha = \beta = 0.87$, respectively.

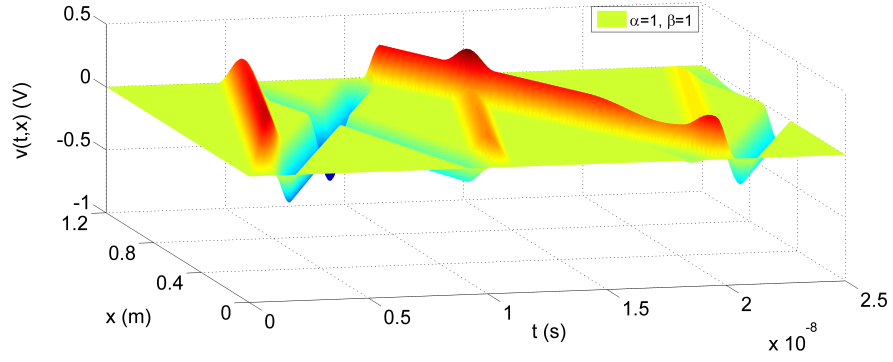


Fig. 4.18: Voltage distribution on the 1st and the 3rd line with integer-orders $\alpha = \beta = 1$.

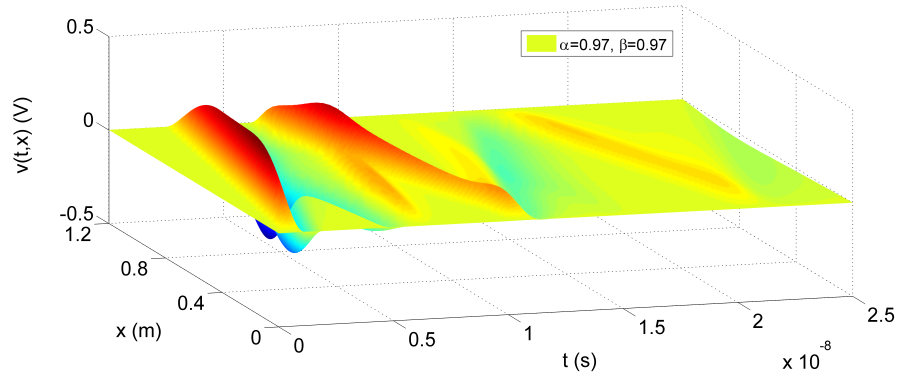


Fig. 4.19: Voltage distribution on the 1st and the 3rd line with fractional-orders $\alpha = \beta = 0.97$.

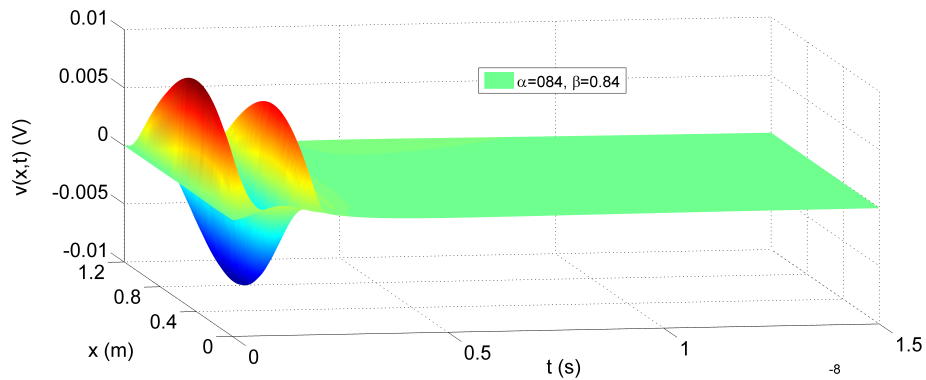


Fig. 4.20: Voltage distribution on the 1st and the 3rd line with fractional-orders $\alpha = \beta = 0.84$.

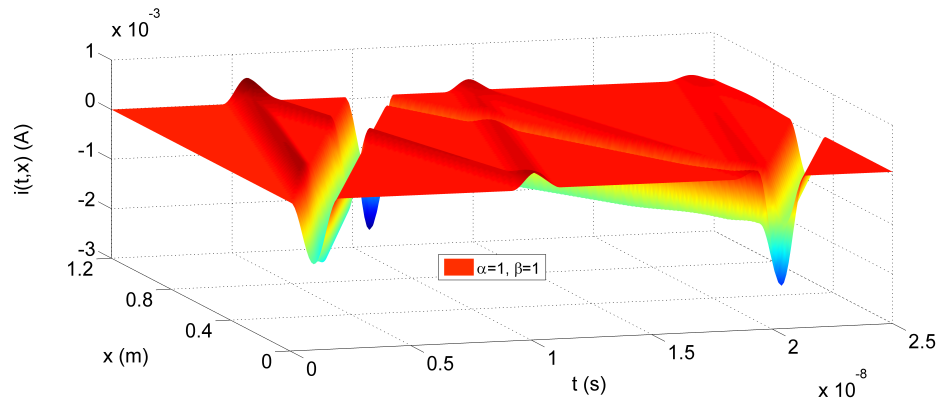


Fig. 4.21: Current distribution on the 1st and the 3rd line with integer-orders $\alpha = \beta = 1$.

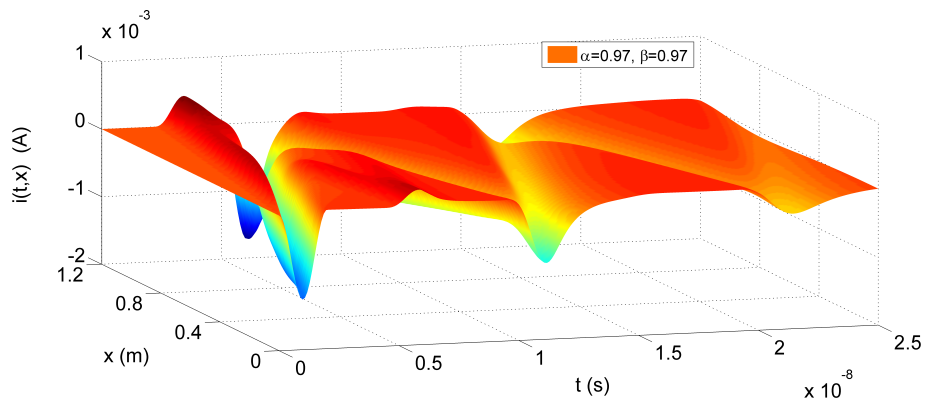


Fig. 4.22: Current distribution on the 1st and the 3rd line with fractional-orders $\alpha = \beta = 0.97$.

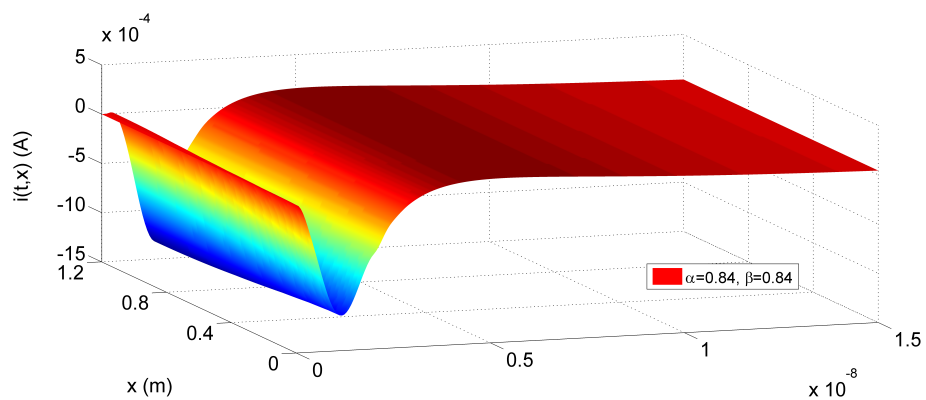


Fig. 4.23: Current distribution on the 1st and the 3rd line with fractional-orders $\alpha = \beta = 0.84$.

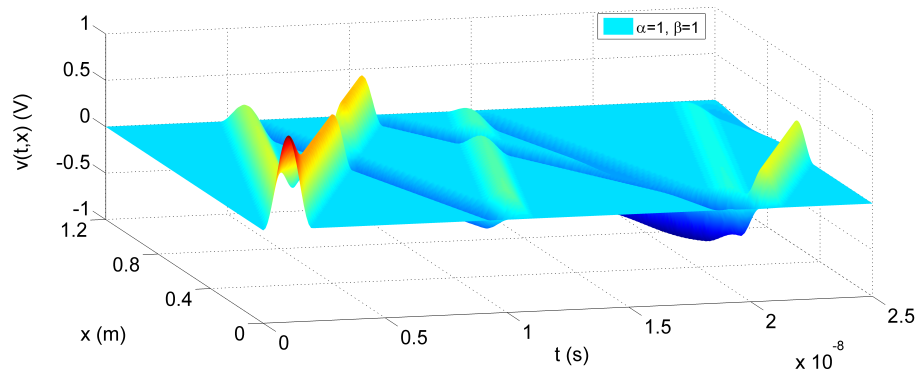


Fig. 4.24: Voltage distribution on the 2nd line with integer-orders $\alpha = \beta = 1$.

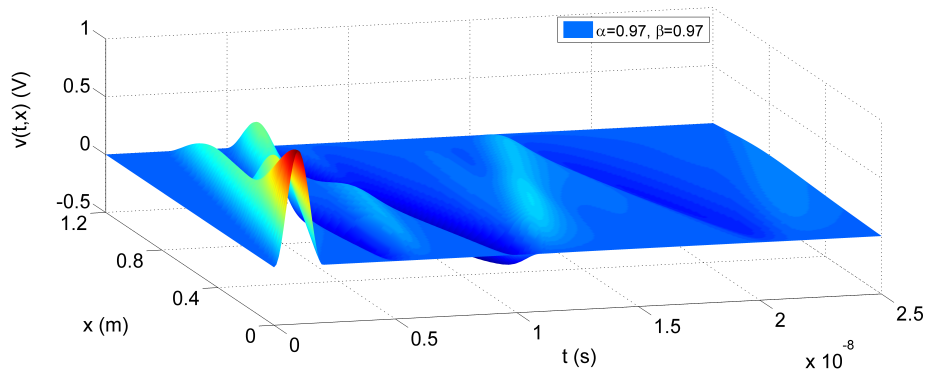


Fig. 4.25: Voltage distribution on the 2nd line with fractional-orders $\alpha = \beta = 0.97$.

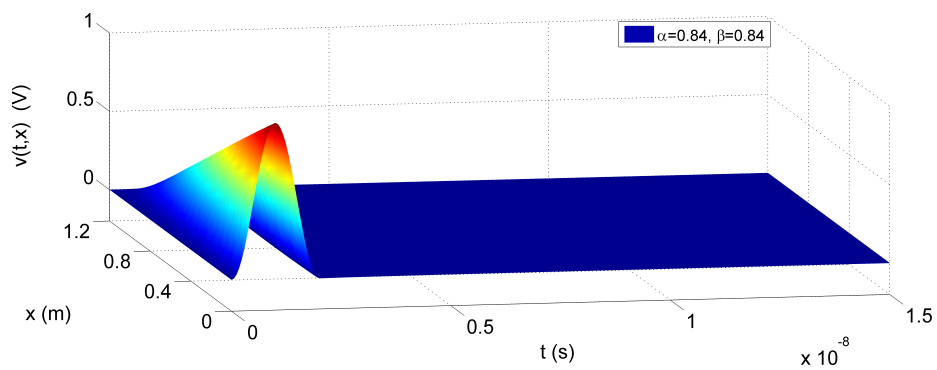


Fig. 4.26: Voltage distribution on the 2nd line with fractional-orders $\alpha = \beta = 0.84$.

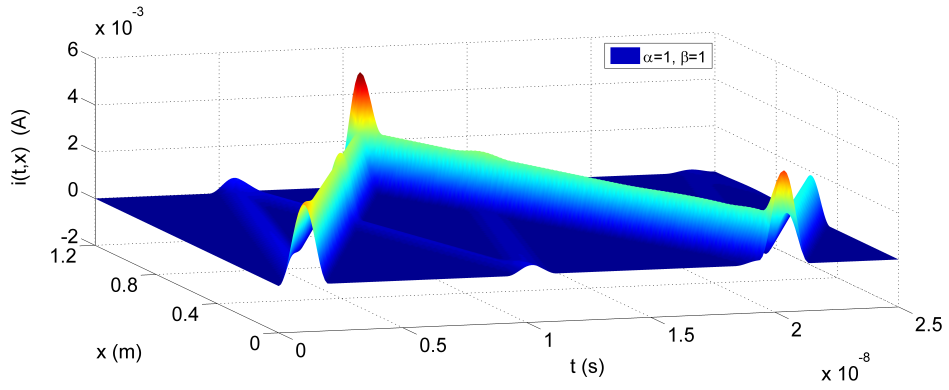


Fig. 4.27: Current distribution on the 2nd line with integer-orders $\alpha = \beta = 1$.

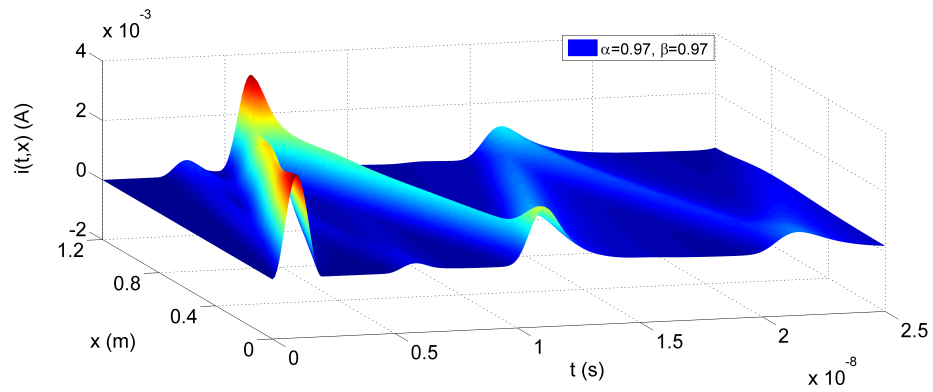


Fig. 4.28: Current distribution on the 2nd line with fractional-orders $\alpha = \beta = 0.97$.

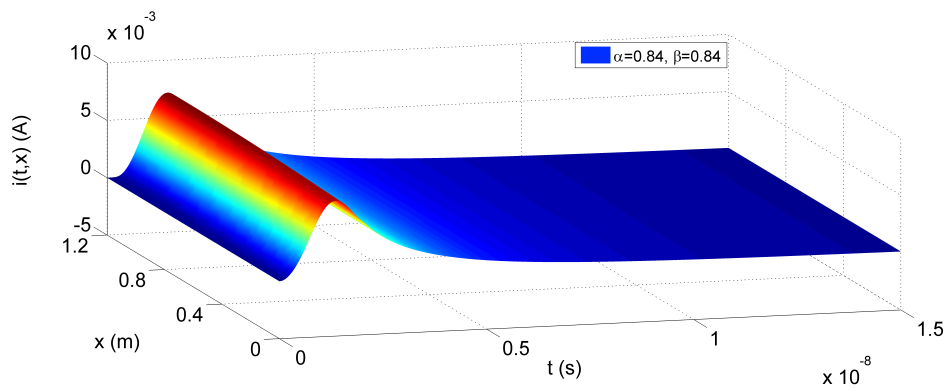


Fig. 4.29: Current distribution on the 2nd line with fractional-orders $\alpha = \beta = 0.84$.

In general, Fig. 4.18 to Fig. 4.29 exhibit the voltage and current waveform distribution along the MTL wires for $\alpha, \beta = 0.84, 0.97$ and 1; while, Fig. 4.18, Fig. 4.21, Fig. 4.24, and Fig. 4.27 show the solutions of voltage/current waveforms for the classical (integer-order) MTL. Comparing the MTL simulation result figures with regard to the change in fractional-orders, we can find out that with the increase of the fractional-orders from 0.84 to 0.97, the waveform has a faster spread at the beginning; this agrees with the results of the single TL simulations obtained in Sect. 4.4, and with the diffusion theory investigated in [78, 112]. Moreover, observing the results when introducing fractional-orders, such as a comparison between Fig. 4.27 and Fig. 4.28 for the current distributions, shows that the waveform exhibits more attenuation along the wire, and hence this compensates for power losses and gives a higher degree of optimization. Looking into Fig. 4.25 and Fig. 4.26, it is noticed that the superposition effect that happens on TL wires when the forward wave and reflected wave interact is obvious in these two figures; this further shows that the physical phenomenon of MTL is more accurately modeled using fractional-order techniques. The main advantage of utilizing the 1D *FFT*-NILT accelerated by the Qd algorithm [19], in its matrix form, can be seen from the obtained 3D MTL simulation results. The method allows us to solve the waves on all the MTL's wires in parallel. Depending on the defined resolution of the results and the number of terms considered for the 1D *FFT*-NILT computations, the average CPU time for the simulations is approximately 4 to 6 seconds running on a common PC. In principle, the 1D *FFT*-NILT method, presented in Sect. 1.1.1, is devised based on computing the inverse Laplace transform (ILT), of Bromwich definition integral, numerically on a whole given interval $(0, t_m)$. The original approach of this method was proposed in reference [21], where the *FFT* algorithm is applied in order to provide the solution in an accurate and fast way. Moreover, further improvements have been done on this method, such as incorporating acceleration techniques and a development into a matrix form.

4.7 Nonuniform multiconductor transmission line systems with possible external feedback

The subject of nonuniform MTL has been attracting renewed interest by microwave engineers in the last decades due to its large field of applications; for instance, impedance transformers [117], analog signal processing [118], filters [119], pulse shaping [120], VLSI interconnects [121], and many more [122]. In this section, the modeling and simulation of nonuniform MTL simplified by the use of NILT method is presented.

In order to develop the uniform MTL model into the nonuniform one, let us start by defining the time and also geometrically dependent p.u.l. matrices $\mathbf{R}(x)$, $\mathbf{L}(x)$, $\mathbf{G}(x)$, and $\mathbf{C}(x)$. Similarly, as shown in (4.34) and (4.35) in Sect. 4.6, though here considering the nonuniformity of the MTL's, the telegraph equations in a matrix form are [123],

$$-\frac{\partial \mathbf{v}(t, x)}{\partial x} = \mathbf{R}(x)\mathbf{i}(t, x) + \mathbf{L}(x)\frac{\partial \mathbf{i}(t, x)}{\partial t}, \quad (4.51)$$

$$-\frac{\partial \mathbf{i}(t, x)}{\partial x} = \mathbf{G}(x)\mathbf{v}(t, x) + \mathbf{C}(x)\frac{\partial \mathbf{v}(t, x)}{\partial t}, \quad (4.52)$$

where $\mathbf{v}(t, x)$ and $\mathbf{i}(t, x)$, see Fig. 4.30 [123], are the n^{th} -order column vectors of voltage and currents along the MTL, respectively. The telegraph equations can be, for simplicity, represented in a formal compact matrix form

$$\frac{\partial}{\partial x} \begin{bmatrix} \mathbf{v}(t, x) \\ \mathbf{i}(t, x) \end{bmatrix} = \begin{bmatrix} \mathbf{0} & -\mathbf{R}(x) \\ -\mathbf{G}(x) & \mathbf{0} \end{bmatrix} \cdot \begin{bmatrix} \mathbf{v}(t, x) \\ \mathbf{i}(t, x) \end{bmatrix} - \begin{bmatrix} \mathbf{0} & \mathbf{L}(x) \\ \mathbf{C}(x) & \mathbf{0} \end{bmatrix} \cdot \frac{\partial}{\partial t} \begin{bmatrix} \mathbf{v}(t, x) \\ \mathbf{i}(t, x) \end{bmatrix}, \quad (4.53)$$

To simplify the telegraph equations (4.53) we utilize the Laplace transform which

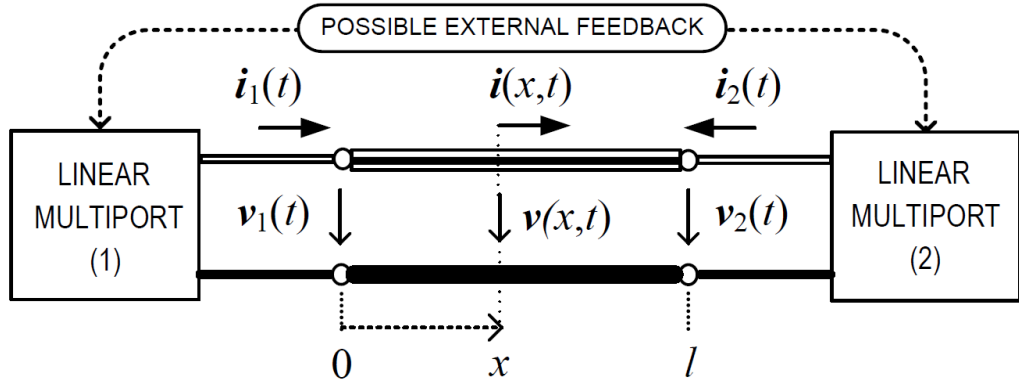


Fig. 4.30: MTL system with possible external feedback.

converts the equations from PDE to ODE, with the consideration of zero initial voltage and current distributions, i.e. $\mathbf{v}(0, x) = 0$ and $\mathbf{i}(0, x) = 0$, as follows

$$\frac{d}{dx} \begin{bmatrix} \mathbf{V}(s, x) \\ \mathbf{I}(s, x) \end{bmatrix} = \begin{bmatrix} \mathbf{0} & -\mathbf{Z}(s, x) \\ -\mathbf{Y}(s, x) & \mathbf{0} \end{bmatrix} \cdot \begin{bmatrix} \mathbf{V}(s, x) \\ \mathbf{I}(s, x) \end{bmatrix}, \quad (4.54)$$

where $\mathbf{Z}(s, x) = \mathbf{R}(x) + s\mathbf{L}(x)$ and $\mathbf{Y}(s, x) = \mathbf{G}(x) + s\mathbf{C}(x)$ denoting the series impedance and shunt admittance matrices, accordingly. Henceforth, incorporating

the frequency-dependent skin effect losses in the MTL's conductors the series impedance is modified as follows

$$\tilde{\mathbf{Z}}(s, x) = \mathbf{R}(x) + s\mathbf{L}(x) + \mathbf{K}(x)\sqrt{s} , \quad (4.55)$$

where $\mathbf{K}(x)$ represents high-frequency resistance and internal inductive reactance; hence (4.55) is used in (4.54) in the following solution.

For a nonuniform MTL, the chain matrix property can be used, in a similar manner as for the single nonuniform TL presented in Sect. 4.5. Primarily, let us represent the ODE (4.54) in a more formal manner, i.e.

$$-\frac{d\mathbf{W}(s, x)}{dx} = \mathbf{M}(s, x)\mathbf{W}(s, x) , \quad (4.56)$$

which has the following known solution

$$\mathbf{W}(s, x) = \Phi_0^x(s)\mathbf{W}(s, 0) , \quad (4.57)$$

where $\Phi_0^x(s)$ is a matrizant, or known as the fundamental matrix, which can be defined by the Volterra product integral [110], and $\mathbf{W}(s, 0)$ can be obtained from the boundary conditions. It can be noticed here that when the MTL is uniform, i.e. $\mathbf{M}(s, x) = \mathbf{M}(s)$ which is a constant matrix, then the matrizant becomes a matrix exponential function. In light of this, and considering the following property of a matrizant i.e. $\Phi_0^x = \Phi_y^x \Phi_0^y$, $x > y > 0$, it is then possible to consider the MTL to be divided on m small segments such that $\Delta x_r = x_r - x_{r-1}$, where $r = 1, 2, \dots, m$, $x_0 = 0$ and $x_m = l$, and then each segment can be approximately evaluated as a uniform part. Based on this, in a similar way as used for deriving (4.25), we get

$$\Phi_0^l(s) \approx e^{-\mathbf{M}(\zeta_m, s)\Delta x_m} e^{-\mathbf{M}(\zeta_{m-1}, s)\Delta x_{m-1}} \dots e^{-\mathbf{M}(\zeta_1, s)\Delta x_1} \quad (4.58)$$

where $\zeta_r \in \Delta x_r$, and Δx_r can be, for example, chosen as $\Delta x_r = h = l/m$, $\forall r$. Furthermore, based on circuit theory terminology, (4.58) is considered a chain matrix and can be simply labeled as $\Phi(s)$. Hence, at a specific point x , the partial chain matrix can be labeled as $\Phi(s, x)$, and accordingly $\Phi(s, l) = \Phi(s)$. Henceforth, to continue with the solution of (4.57), the boundary condition $\mathbf{W}(s, 0) = [\mathbf{V}_1^T(s), \mathbf{I}_1^T(s)]^T$, should be considered. This condition can be obtained by the linear multiport terminations of the MTL, as shown in Fig. 4.30. When linear terminations are evaluated then Thévenin and Norton combinations can be considered-see equations (4.42) up to (4.46). Choosing Thévenin equivalents on both sides of the MTL, we get the current vector $\mathbf{I}_1(s)$ entering the MTL and is given as in (4.42), and $\mathbf{V}_1(s)$ similarly as in (4.43) and hence solving the boundary condition $\mathbf{W}(s, 0)$.

The MTL solution presented so far was for MTL having simple linear multiport

terminations, if a more sophisticated terminating multiport or a MTL with an external feedback is investigated, then the boundary conditions ought to be incorporated by a more general method. A suggested method is the modified nodal analysis (MNA) used to describe lumped-parameter circuits around the MTL. Therefore, using the MNA, related to principles given in [124, 125], we get

$$(\mathbf{G} + s\mathbf{C})\mathbf{V}_N(s) + \mathbf{S}_B\mathbf{I}_B(s) + \mathbf{C}\mathbf{v}_N(0), \quad (4.59)$$

given that \mathbf{G} and \mathbf{C} are N^{th} -order square matrices with entry elements given by lumped resistive and reactive elements, respectively. Moreover, $\mathbf{V}_N(s) = \mathbf{L}\{\mathbf{v}_N(t)\}$ which is the Laplace transform of the N^{th} -order column vector of exciting sources, $\mathbf{S}_B = [\mathbf{S}_1, \mathbf{S}_2]$ is the $(N \times 2n)^{\text{th}}$ -order selector matrix, with entry elements $s_{ij} \in \{0, 1\}$, mapping the joint vector of boundary currents $\mathbf{I}_B(s) = [\mathbf{I}_1^T(s), \mathbf{I}_2^T(s)]^T$ to a nodal space of all the systems. The former value $\mathbf{v}_N(0)$, in (4.59), represents the N^{th} -order vector of initial conditions of the lumped-parameter part. In light of the foregoing, a joint vector of boundary voltages $\mathbf{V}_B(s) = [\mathbf{V}_1^T(s), \mathbf{V}_2^T(s)]^T$ is related to MNA variables by the following expression

$$\mathbf{V}_B(s) = \mathbf{S}_B^T \mathbf{V}_N(s). \quad (4.60)$$

At this point, in order to solve (4.59) and (4.60) we need to have a relation between $\mathbf{V}_B(s)$ and $\mathbf{I}_B(s)$; such a relation can be found by the MTL multiport admittance matrix,

$$\mathbf{I}_B(s) = \mathbf{Y}(s)\mathbf{V}_B(s), \quad (4.61)$$

where $\mathbf{Y}(s)$ is the admittance matrix and it is obtained from the chain matrix $\mathbf{\Phi}(s)$, as was developed in (4.41), namely

$$\mathbf{Y}(s) = \begin{bmatrix} \mathbf{Y}_{11}(s) & \mathbf{Y}_{12}(s) \\ \mathbf{Y}_{21}(s) & \mathbf{Y}_{22}(s) \end{bmatrix} \quad (4.62)$$

where the matrix elements are defined as follows:

- $\mathbf{Y}_{11}(s) = -\mathbf{\Phi}_{12}^{-1}(s)\mathbf{\Phi}_{11}(s)$,
- $\mathbf{Y}_{12}(s) = \mathbf{\Phi}_{12}^{-1}(s)$,
- $\mathbf{Y}_{21}(s) = \mathbf{Y}_{12}^T(s)$, and
- $\mathbf{Y}_{22}(s) = -\mathbf{\Phi}_{22}(s)\mathbf{\Phi}_{12}^{-1}(s)$.

Henceforth, first we substitute (4.60) to (4.61), and then both $\mathbf{V}_B(s)$ and $\mathbf{I}_B(s)$ are substituted back to (4.60), then the result is

$$\mathbf{V}_N(s) = \left(\mathbf{G} + s\mathbf{C} + \mathbf{S}_B\mathbf{Y}(s)\mathbf{S}_B^T \right)^{-1} \left(\mathbf{I}_N(s) + \mathbf{C}\mathbf{v}_N(0) \right). \quad (4.63)$$

As it can be noticed, based on (4.63), both $\mathbf{V}_B(s)$ and $\mathbf{I}_B(s)$ are solved, and hence $\mathbf{W}(s, 0)$ from (4.57) is determined. Finally a 1D NILT method can now be utilized to obtain the time domain solution, i.e. $\mathbf{w}(t, x) = \text{NILT}\{\mathbf{W}(s, x)\}$.

4.7.1 Nonuniform MTL case study

As an example of utilizing 1D NILT for simulating a nonuniform MTL with high frequency losses, let us consider a linear MTL, see Fig. 4.31, with two active conductors above a ground and terminated by resistive two-ports [123]. The length

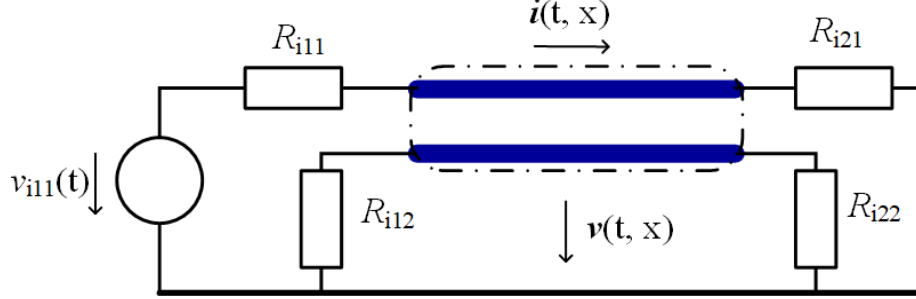


Fig. 4.31: Nonuniform MTL system with linear terminations.

of the MTL wires is $l = 0.4$ m, and is defined by the following p.u.l. parameter matrices [124]

$$\begin{aligned} \mathbf{R}_0 &= \begin{pmatrix} 0.1 & 0.02 \\ 0.02 & 0.1 \end{pmatrix} \frac{\Omega}{\text{m}}; \quad \mathbf{L}_0 = \begin{pmatrix} 494.6 & 63.3 \\ 63.3 & 494.6 \end{pmatrix} \frac{\text{nH}}{\text{m}}; \\ \mathbf{C}_0 &= \begin{pmatrix} 62.8 & -4.9 \\ -4.9 & 62.8 \end{pmatrix} \frac{\text{pF}}{\text{m}}; \quad \mathbf{G}_0 = \begin{pmatrix} 0.1 & -0.01 \\ -0.01 & 0.1 \end{pmatrix} \frac{\text{S}}{\text{m}}. \end{aligned} \quad (4.64)$$

The generalized Thévenin equivalent is applied in order to model the terminating circuits shown in Fig. 4.31, while considering the following internal parameters: $\mathbf{R}_{i1} = \text{diag}(R_{i11}, R_{i12})$, $\mathbf{R}_{i2} = \text{diag}(R_{i21}, R_{i22})$, $\mathbf{v}_{i1}(t) = [v_{i11}(t), 0]^T$, and $\mathbf{v}_{i2}(t) = [0, 0]^T$. The source resistance is equal to $R_{i11} = 1 \Omega$, whereas the other resistors are each $1 \text{ k}\Omega$. The MTL is excited with the following voltage waveform

$$v_{i11}(t) = \begin{cases} \sin^2\left(\frac{\pi t}{2 \cdot 10^{-9}}\right), & \text{if } 0 \leq t \leq 2 \cdot 10^{-9}. \\ 0, & \text{otherwise.} \end{cases} \quad (4.65)$$

The voltage waveform has the corresponding Laplace-domain transform: $V_{i11}(s) = \mathcal{L}\{v_{i11}(t)\} = 2\pi^2(1 - \exp(-2 \cdot 10^{-9}s))/s/((2 \cdot 10^{-9}s)^2 + 4\pi^2)$. The time domain simulation results, after undergoing the 1D NILT method, are shown in Fig. 4.32. Four cases are simulated; namely, the uniform MTL, nonuniform MTL, with and without skin effect loss for each of the MTL wires. As for the nonuniformity of the MTL, an exponential inhomogeneity is considered by following the relation $\mathbf{D}_0(x) = \mathbf{D}_0 e^{dx}$, where $\mathbf{D}_0 \in \{\mathbf{R}_0, \mathbf{L}_0, \mathbf{C}_0, \mathbf{G}_0\}$, $d \in \{d_R, d_L, d_C, d_G\}$, and the skin effect is expressed as $\mathbf{K}(x) = \mathbf{K}_0 e^{kx}$. For this example we choose $\mathbf{K}_0 = \text{diag}(2 \cdot 10^{-3}, 2 \cdot 10^{-3})$

$\Omega\sqrt{s}/m$ and $k = d = \ln(3)/l \approx 2.75$, in other words it gives three times higher values at the end of the MTL when compared to its beginning. The different MTL conditions simulated in Fig. 4.32, as can be noticed from the above equations, as follows when $k = 0$, the skin effect is constant along the MTL, when $\mathbf{K}_0 = \mathbf{0}$, then no skin effect is simulated, and if the exponential power $d = 0$, the MTL is a uniform one.

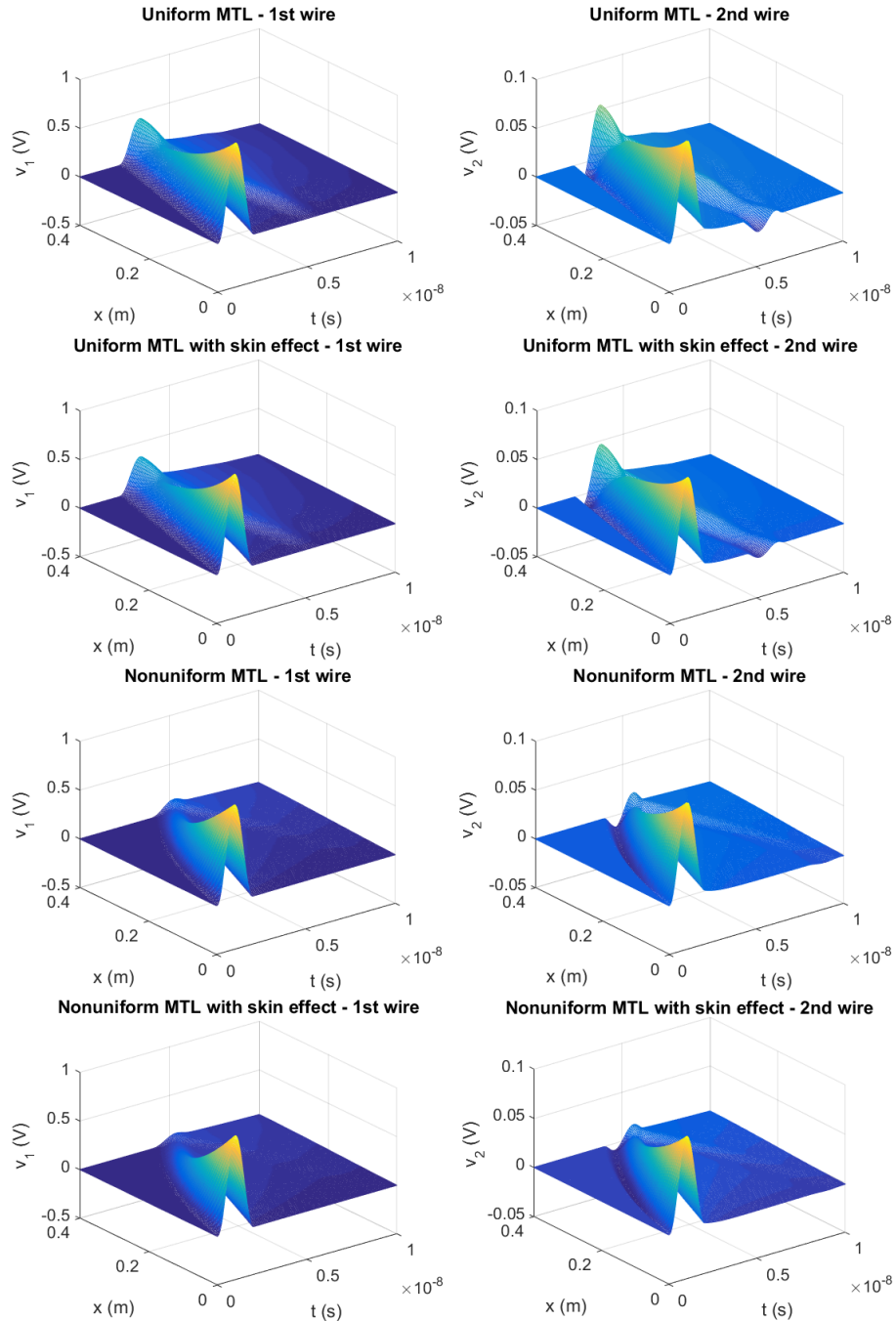


Fig. 4.32: MTL's wires voltage distributions under different conditions.

The time-domain solution was obtained by testing different 1D NILT methods, namely the NILT based on FFT/IFFT, and the 1D hyperbolic NILT method, both in conjunction with techniques for acceleration of convergence of infinite series [5, 13, 102, 123].

4.8 Summary

This chapter presented a wide range of applications of the developed 1D hyperbolic NILT method, and other ones. I have mathematically devised these applications in detail and developed their models by introducing several new features in contrast to the classical approach, e.g. frequency dependent parameters, fractional-order elements. These applications of the NILT method in the electrical engineering field, mainly, are to solve systems with distributed parameters in which transcendental and irrational functions arise. The NILT method was used to simulate voltage and /or current waveforms propagating along lossy transmission lines, these lines were developed to include frequency dependent parameters, and the nonuniformity of the lines was further introduced. Moreover, an expansion to multiconductor transmission lines was performed, and then a possibility of including nonuniformity of the lines and/or an external feedback model. All these applications I have improved also by including fractional-order elements of the transmission lines resulting in a greater flexibility to model these applications and also simulating different physical phenomenon on these models. Moreover, the fractional-order's range of choices was studied in detail and listed. The applications were possible to perform and all these features were possible to include in an easy manner due to the possibility of utilizing the Laplace transform and obtaining the original time-domain results via the NILT method.

5 EXPANSION OF HYPERBOLIC NILT METHOD INTO THE TWO DIMENSIONAL FORM

The fundamental importance of two dimensional NILT arise from its wide application on the solution of partial differential equations with two variables, solving slightly non-linear systems described by Volterra series expansion, fractional derivative operators, and many more. In this section a two-dimensional expansion of the hyperbolic NILT is conducted, and the static error analysis is investigated and computed. It will be shown that developing the Hyp-Eul NILT from the 1D field to the 2D field grants the ability of solving applications that contain two variables, such as continuous space-time systems simultaneously. The Hyp-Eul NILT has been verified and shows to give high accuracy results on the performed test functions and the relevant applications in the electrical engineering field, such as that for systems with distributed parameters and is applicable on a wide range of different functions [1, 104]. Having these results, The goal is to further expand the NILT method into a two-dimensional one. The first section will present the analysis and simulation results for 2D NILTs, and the following section will present the two-dimensional expansion algorithms of the proposed hyperbolic NILT method along with the error analysis of the algorithm.

5.1 Simulation and analysis of some 2D NILT methods

In this section some effective 2D NILT methods, which were presented in Sect. 1.3, are verified and simulated and the results of the inversions of the methods are displayed as 3D plots. The corresponding absolute errors are measured and used as an accuracy study, and their results are displayed as 3D plots on the whole region of calculation. The methods tested and simulated are 2D Moorthy-NILT, 2D Singhal-NILT, 2D FFT- ε NILT and 2D FFT-Qd NILT [126, 127]. The two variable test functions used are shown in Table 5.1, and the 3D plot simulation results are shown in Fig. 5.1 to Fig. 5.3 for the test functions F_1 , F_2 and F_3 , respectively.

For precise quantitative solutions an error measurement is introduced by following the function ζ_2 , namely

$$\zeta_2 = \sqrt{\frac{\sum_{i=1}^{128} \sum_{j=1}^{128} [f(t_i, x_j) - \tilde{f}(t_i, x_j)]^2}{128 \times 128}}. \quad (5.1)$$

Tab. 5.1: List of two variable test functions with their pre-known originals

	Functions in the Laplace domain	Original functions in the time domain
1	$F_1(s_1, s_2) = [(s_1 + 1) \cdot (s_2 + 1)]^{-2}$	$f_1(t, x) = t \cdot x \cdot e^{-(t+x)}$
2	$F_2(s_1, s_2) = \frac{\exp(-2s_1 - 2s_2)}{(s_1 \cdot s_2)}$	$f_2(t, x) = e^{-t-2x}$
3	$F_3(s_1, s_2) = \frac{1}{(s_1+1) \cdot (s_2+2)}$	$f_3(t, x) = e^{-t-2x}$.

The simulation tests are done on a grid of 128×128 points. Results of the absolute error measures are listed in Table 5.2. The parameters of the 2D NILTs

Tab. 5.2: Accuracy calculations of the simulated 2D NILTs

Method / ζ_2	Function 1	Function 2	Function 3
2D FFT-Qd NILT	$1.85 \cdot 10^{-10}$	$2.2 \cdot 10^{-3}$	$1.9 \cdot 10^{-3}$
2D FFT- ε NILT	$3.33 \cdot 10^{-10}$	$2.3 \cdot 10^{-3}$	$4.7 \cdot 10^{-4}$
2D Singhal-NILT	$2.91 \cdot 10^{-19}$	0.34	$1.16 \cdot 10^{-8}$
2D Moorthy-NILT	$4.68 \cdot 10^{-4}$	0.57	$1.1 \cdot 10^{-2}$.

implemented are optimized by performing the error analysis and/or the trial and error method, with the goal to obtain a high accuracy and stable inversion while maintaining a suitable calculation speed. Table 5.3 bellow expresses these measured values [126, 127].

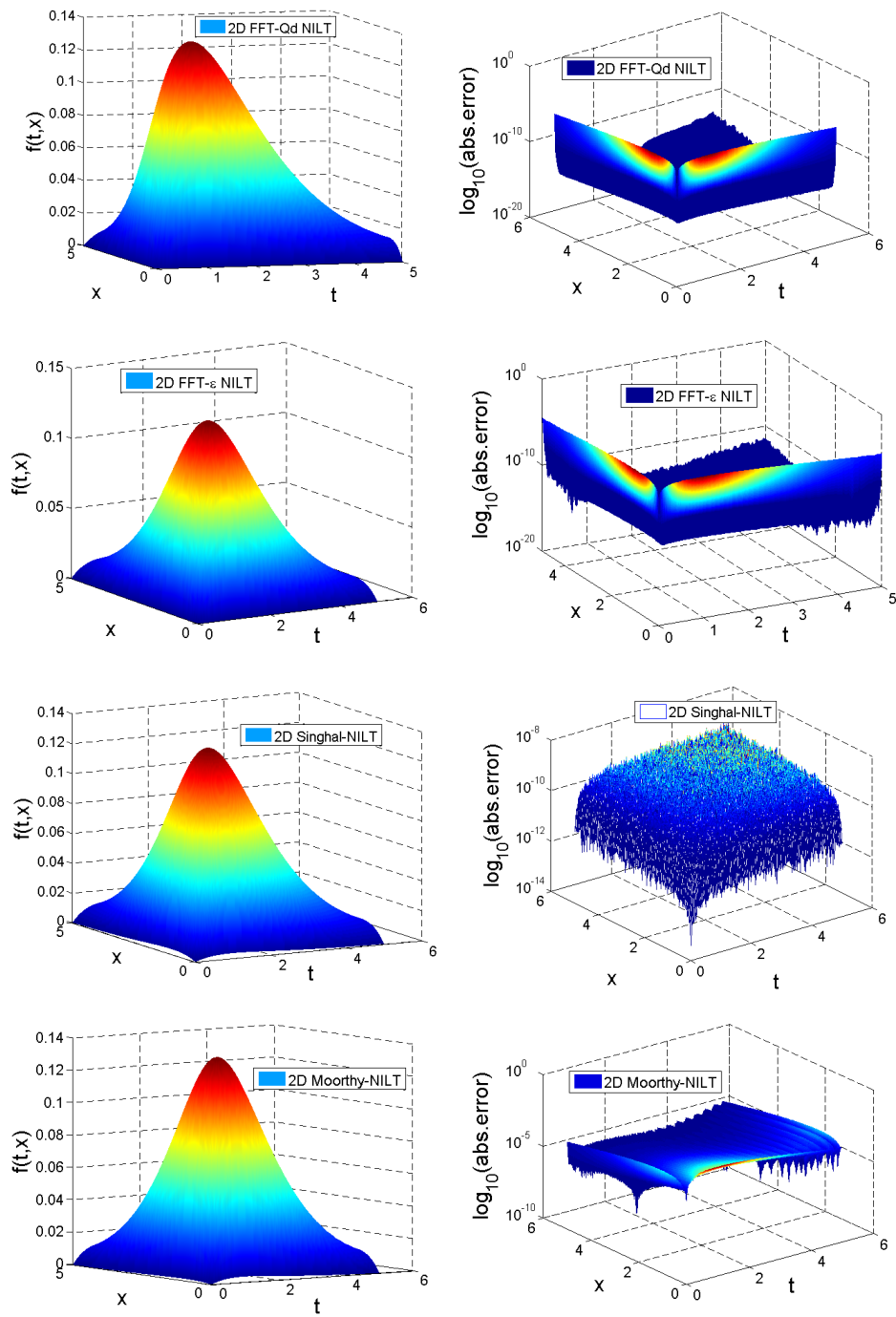


Fig. 5.1: Inversion and error analysis of 2D NILTs for F_1 .

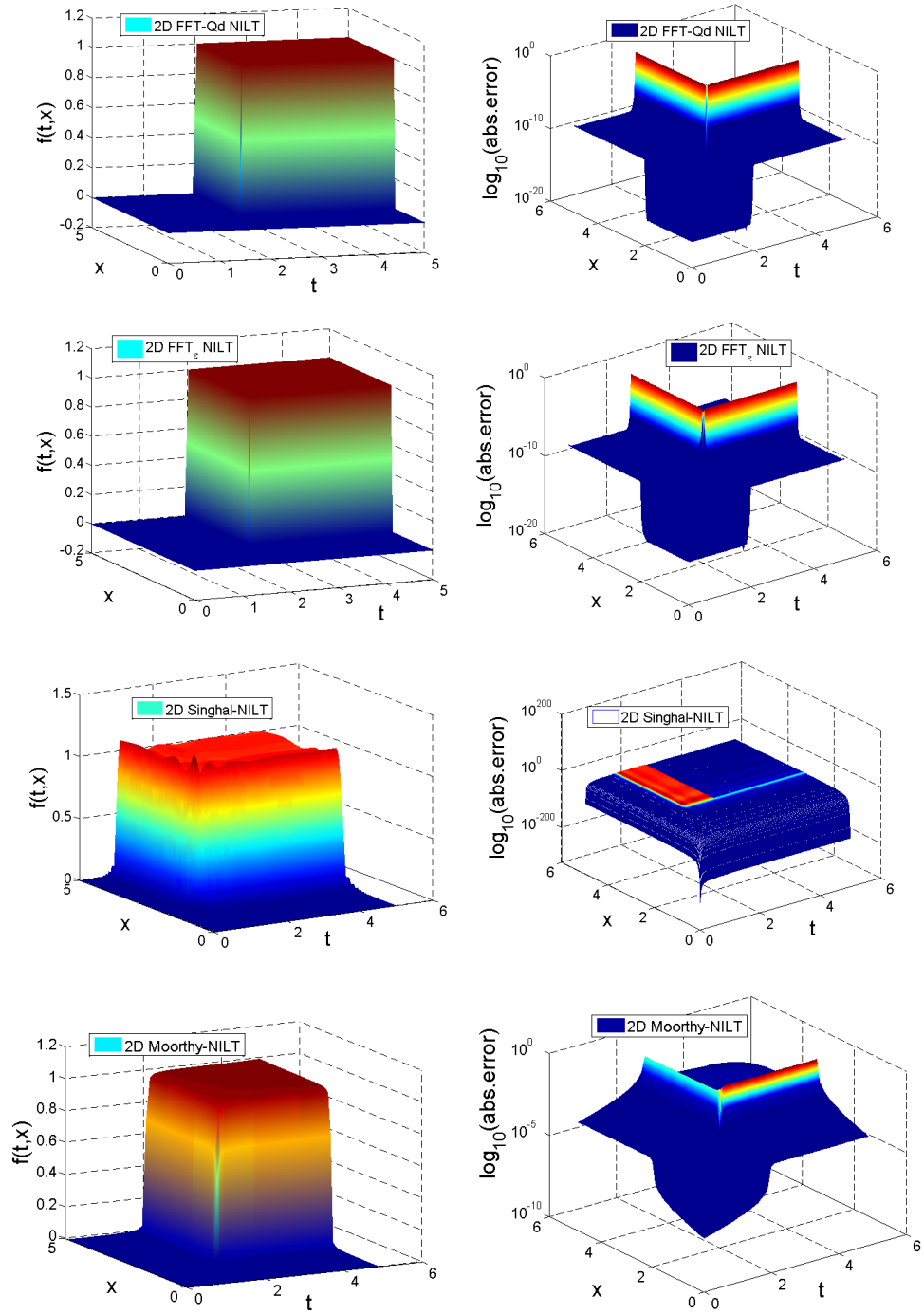


Fig. 5.2: Inversion and error analysis of 2D NILTs for F_2 .

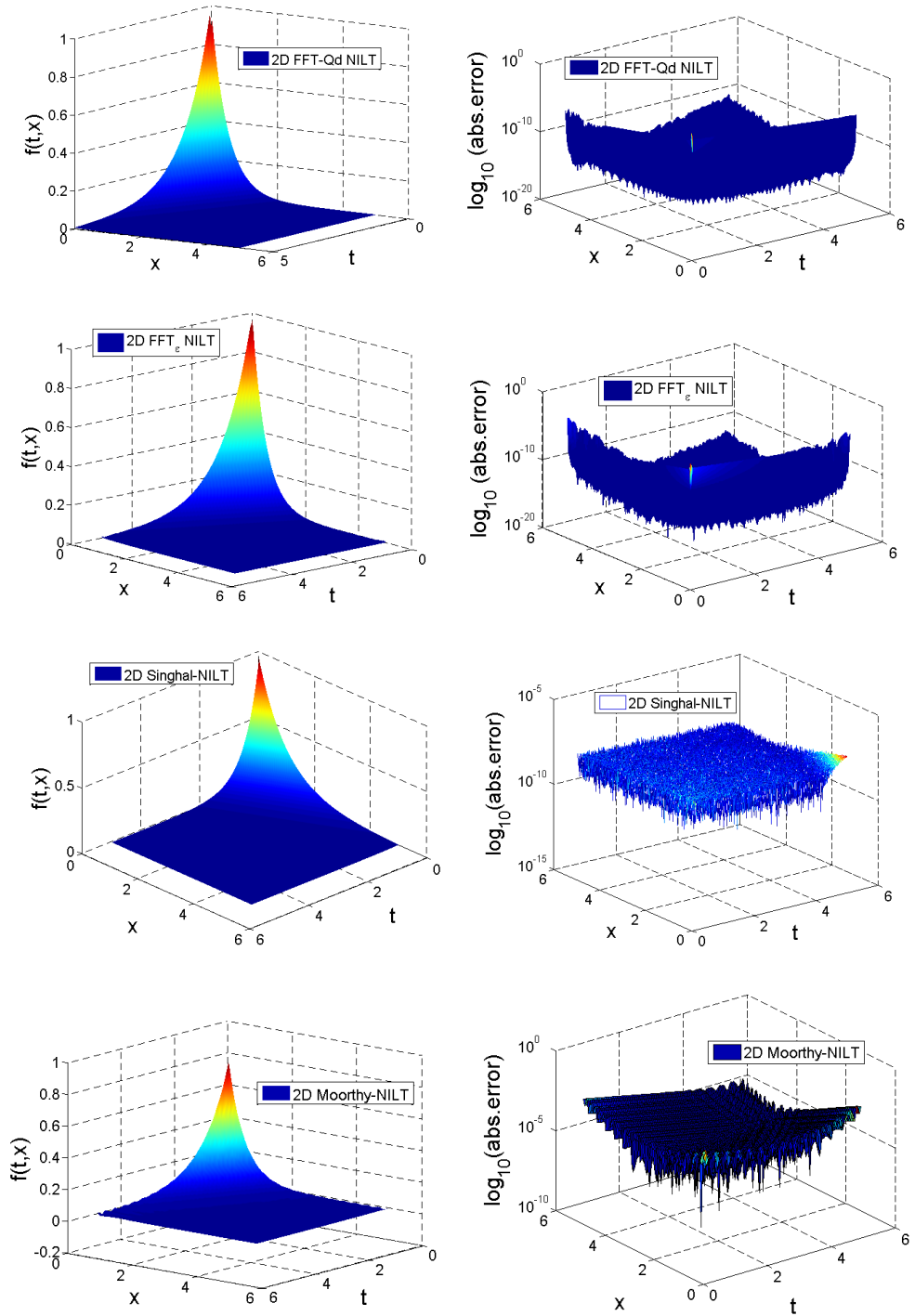


Fig. 5.3: Inversion and error analysis of 2D NILTs for F_3 .

Tab. 5.3: Parameter optimal choices used for the simulated 2D NILTs

2D NILT method	Optimised parameter values
2D FFT-Qd NILT	$P = 3, \alpha_1 = 0, \alpha_2 = 0, E_r = 1e^{-8}$
2D FFT- ε NILT	$P = 2, \alpha_1 = 0, \alpha_2 = 0, E_r = 1e^{-7}$
2D Singhal-NILT	$M = 10, N = 8,$
2D Moorthy-NILT	Function 1 and 3: $c_1 = 1, c_2 = 0, T = 3.5.$ Function 2, $c_1 = 15, c_2 = 10.21, T = 1.0.$

5.2 Numerical method of the hyperbolic NILT two-dimensional expansion

In this section, the two dimensional expansion of the proposed 1D hyperbolic NILT is conducted [104], inspired by the work done in [129], followed by a detailed error analysis.

5.2.1 Theoretical concept and basic formulae

The principal formula of a two-dimensional Laplace transform of a two variable function $f(t_1, t_2)$ where $t_1, t_2 \geq 0$, is given as

$$F(s_1, s_2) = \int_0^\infty \int_0^\infty f(t_1, t_2) e^{-s_1 t_1 - s_2 t_2} dt_1 dt_2. \quad (5.2)$$

Considering the assumption $|f(t_1, t_2)| < M e^{\alpha_1 t_1 + \alpha_2 t_2}$, where M, α_1 and α_2 are positive real constants, the object function $f(t_1, t_2)$ can be given by [130]

$$f(t_1, t_2) = -\frac{1}{4\pi^2} \int_{\gamma_1 - j\infty}^{\gamma_1 + j\infty} \int_{\gamma_2 - j\infty}^{\gamma_2 + j\infty} F(s_1, s_2) e^{s_1 t_1 + s_2 t_2} ds_1 ds_2, \quad (5.3)$$

where $s = \gamma + j\omega$. A practical technique for the evaluation of the double integral (5.3) is done by rearranging it to the forms

$$\begin{aligned}
f(t_1, t_2) &= \frac{1}{2\pi j} \int_{\gamma_1-j\infty}^{\gamma_1+j\infty} \left(\frac{1}{2\pi j} \int_{\gamma_2-j\infty}^{\gamma_2+j\infty} F(s_1, s_2) e^{s_2 t_2} ds_2 \right) e^{s_1 t_1} ds_1 \\
&= \frac{1}{2\pi j} \int_{\gamma_2-j\infty}^{\gamma_2+j\infty} \left(\frac{1}{2\pi j} \int_{\gamma_1-j\infty}^{\gamma_1+j\infty} F(s_1, s_2) e^{s_1 t_1} ds_1 \right) e^{s_2 t_2} ds_2
\end{aligned} \tag{5.4}$$

and then we introduce the partial inverse Laplace transform as follows

$$L_2^{-1}\{F(s_1, s_2)\} = F_2(s_1, t_2) = \frac{1}{2\pi j} \int_{\gamma_2-j\infty}^{\gamma_2+j\infty} F(s_1, s_2) e^{s_2 t_2} ds_2, \tag{5.5}$$

and

$$L_1^{-1}\{F(s_1, s_2)\} = F_1(t_1, s_2) = \frac{1}{2\pi j} \int_{\gamma_1-j\infty}^{\gamma_1+j\infty} F(s_1, s_2) e^{s_1 t_1} ds_1, \tag{5.6}$$

consequently, the two equivalent formulae can be given as

$$\begin{aligned}
f(t_1, t_2) &= L_1^{-1}\{F_2(s_1, t_2)\} = \frac{1}{2\pi j} \int_{\gamma_1-j\infty}^{\gamma_1+j\infty} F_2(s_1, t_2) e^{s_1 t_1} ds_1 \\
&= L_2^{-1}\{F_1(t_1, s_2)\} = \frac{1}{2\pi j} \int_{\gamma_2-j\infty}^{\gamma_2+j\infty} F_1(t_1, s_2) e^{s_2 t_2} ds_2.
\end{aligned} \tag{5.7}$$

A symbolic expression is given as [42, 131]

$$f(t_1, t_2) = L_1^{-1}\left\{L_2^{-1}\{F(s_1, s_2)\}\right\} = L_2^{-1}\left\{L_1^{-1}\{F(s_1, s_2)\}\right\}. \tag{5.8}$$

5.2.2 The numerical method

In order to expand the hyperbolic NILT method into a 2D form, let us first start with a recapitulation of the hyperbolic relations used to approximate the exponential kernel of the i. L. t. Bromwich integral; namely, $E_{sh}(st, a) = \frac{e^a}{2\sinh(a-st)}$, $E_{ch}(st, a) = \frac{e^a}{2\cosh(a-st)}$. First we start with the $E_{ch}(st, a)$ approximation for a 2D NILT expansion, then after the first 2D NILT is devised we proceed with the second approximation i.e. the $E_{sh}(st, a)$. Henceforth, the reciprocal hyperbolic function appearing in $E_{ch}(st, a)$ is expressed by the infinite sum of rational functions

$$\frac{1}{\cosh z} = 2\pi \sum_{n=0}^{\infty} \frac{(-1)^n (n+0.5)}{(n+0.5)^2 \pi^2 + z^2}. \tag{5.9}$$

Replacing both exponential kernels that appear in the double integral (5.4), by their respective approximations E_{ch2} and E_{ch1} , we get

$$f_{ch}(t_1, t_2) = \frac{1}{2\pi j} \int_{\gamma_1-j\infty}^{\gamma_1+j\infty} \left(\frac{1}{2\pi j} \int_{\gamma_2-j\infty}^{\gamma_2+j\infty} F(s_1, s_2) E_{ch2} ds_2 \right) E_{ch1} ds_1, \tag{5.10}$$

where the respective exponential kernels are given by

$$E_{ch2}(s_2 t_2, a) = \pi e^a \sum_{n_2=0}^{\infty} \frac{(-1)^{n_2} (n_2 + 0.5)}{(n_2 + 0.5)^2 \pi^2 + (a - s_2 t_2)^2}, \quad (5.11)$$

$$E_{ch1}(s_1 t_1, a) = \pi e^a \sum_{n_1=0}^{\infty} \frac{(-1)^{n_1} (n_1 + 0.5)}{(n_1 + 0.5)^2 \pi^2 + (a - s_1 t_1)^2}. \quad (5.12)$$

By performing the first partial i. L. t. based on (5.5) , with the intention to reach the symbolic expression (5.8), we get

$$F_{ch2}(s_1, t_2, a) = \frac{e^a}{2j} \int_{\gamma_2 - j\infty}^{\gamma_2 + j\infty} F(s_1, s_2) \sum_{n_2=0}^{\infty} \frac{(-1)^{n_2} (n_2 + 0.5)}{(n_2 + 0.5)^2 \pi^2 + (a - s_2 t_2)^2} ds_2, \quad (5.13)$$

interchanging the sequence of summation and integration for the variable s_2 we get

$$F_{ch2}(s_1, t_2, a) = \frac{e^a}{2j} \sum_{n_2=0}^{\infty} (-1)^{n_2} (n_2 + 0.5) I_{2n}, \quad (5.14)$$

where I_{2n} is

$$\begin{aligned} I_{2n} &= \int_{\gamma_2 - j\infty}^{\gamma_2 + j\infty} \frac{F(s_1, s_2)}{(n_2 + 0.5)^2 \pi^2 + (a - s_2 t_2)^2} ds_2 \\ &= \int_{\gamma_2 - j\infty}^{\gamma_2 + j\infty} \frac{F(s_1, s_2)}{G_{2n}(s_1, s_2)} ds_2 = \int_{\gamma_2 - j\infty}^{\gamma_2 + j\infty} H_{2n}(s_1, s_2) ds_2, \end{aligned} \quad (5.15)$$

while, for this integral, we consider s_1 a constant parameter and s_2 as a variable. To evaluate this integral we complete the integration path by a semi-circle with an infinite radius, where the function $F(s_1, s_2)$ equals zero along this semi-circle. Using the residual theorem the result of I_{2n} is equal to the sum of the residua of $H_{2n}(s_1, s_2)$ in the poles lying inside the integration contour multiplied by $2\pi j$ [5]. In our case the poles of $H_{2n}(s_1, s_2)$ are formed by poles of $F(s_1, s_2)$ and roots of $G_{2n}(s_1, s_2)$, see (5.15). On principle, the poles of $F(s_1, s_2)$ lay on the left side of the Gaussian plane, because $F(s_1, s_2)$ represents mainly stable systems, whereas the roots of $G_{2n}(s_1, s_2)$ lay on the right side of the complex plane, namely

$$s_{21} = \frac{a + j(n_2 + 0.5)\pi}{t_2}, \quad s_{22} = \frac{a - j(n_2 + 0.5)\pi}{t_2}. \quad (5.16)$$

The process we follow when applying the residual theorem is to choose the contour of integration around the poles of $H_{2n}(s_1, s_2)$, i.e. the roots of $G_{2n}(s_1, s_2)$, while multiplying the result by minus $2\pi j$. The reason of multiplying by minus sign is due to integrating in a mathematically opposite direction, we integrate on the right side of the complex plane. Solving for I_{2n} and substituting back to (5.14) we get

$$F_{ch2}(s_1, t_2, a) = -\frac{e^a}{t_2} \sum_{n_2=0}^{\infty} (-1)^{n_2} \text{Im} \left\{ F \left(s_1, \left[\frac{a + j(n_2 + 0.5)\pi}{t_2} \right] \right) \right\}. \quad (5.17)$$

Performing the 2nd partial i.L.t. with respect to s_1 and considering t_2 here to be a parameter we get

$$f_{ch}(t_1, t_2, a) = \frac{-e^{2a}}{2jt_2} \int_{\gamma_1-j\infty}^{\gamma_1+j\infty} \left(\sum_{n_2=0}^{\infty} (-1)^{n_2} \operatorname{Im} \left\{ F \left(s_1, \left[\frac{a}{t_2} + j(n_2 + 0.5) \frac{\pi}{t_2} \right] \right) \right\} \right) \cdots \\ \times \left(\sum_{n_1=0}^{\infty} \frac{(-1)^{n_1}(n_1 + 0.5)}{(n_1 + 0.5)^2\pi^2 + (a - s_1 t_1)^2} \right) ds_1 . \quad (5.18)$$

Interchanging the sequence of summation and integration,

$$f_{ch}(t_1, t_2, a) = \frac{-e^{2a}}{2jt_2} \sum_{n_1=0}^{\infty} \sum_{n_2=0}^{\infty} (-1)^{n_2} \int_{\gamma_1-j\infty}^{\gamma_1+j\infty} \operatorname{Im} \left\{ F \left(s_1, \left[\frac{a}{t_2} + j(n_2 + 0.5) \frac{\pi}{t_2} \right] \right) \right\} \cdots \\ \times \left(\frac{(-1)^{n_1}(n_1 + 0.5)}{(n_1 + 0.5)^2\pi^2 + (a - s_1 t_1)^2} \right) ds_1 , \quad (5.19)$$

$$f_{ch}(t_1, t_2, a) = \frac{-e^{2a}}{2jt_2} \sum_{n_1=0}^{\infty} \sum_{n_2=0}^{\infty} (-1)^{n_2} (-1)^{n_1} (n_1 + 0.5) I_{n_1} , \quad (5.20)$$

where I_{n_1} is

$$I_{n_1} = \int_{\gamma_1-j\infty}^{\gamma_1+j\infty} \frac{\operatorname{Im} \left\{ F \left(s_1, \left[\frac{a}{t_2} + j(n_2 + 0.5) \frac{\pi}{t_2} \right] \right) \right\}}{(n_1 + 0.5)^2\pi^2 + (a - s_1 t_1)^2} , \quad (5.21)$$

now, similarly as done for the first partial i.L.t., i.e. evaluating the integral by completing the integration path on a semi-circle with an infinite radius and using the residual theorem and then performing some mathematical manipulations the resulting approximate algorithm is, [104],

$$f_{ch}(t_1, t_2, a) = \frac{e^{2a}}{t_1 t_2} \sum_{n_1=0}^{\infty} \sum_{n_2=0}^{\infty} (-1)^{n_1+n_2} \cdots \\ \times \operatorname{Im} \left\{ F \left(\frac{[a + j(n_1 + 0.5)\pi]}{t_1}, \frac{[a + j(n_2 + 0.5)\pi]}{t_2} \right) \right\} , \quad (5.22)$$

noting that the parameter a can be same or different valued for each variable, which can help optimize the results. Furthermore, we continue with the 2D expansion of the second i.L.t. Bromwich integral exponential kernel, i.e. the $E_{sh}(st, a)$ part. Henceforth, the reciprocal hyperbolic function appearing in $E_{sh}(st, a)$ is expressed by the infinite sum of rational functions

$$\frac{1}{\sinh z} = \frac{1}{z} + 2z \sum_{n=1}^{\infty} \frac{(-1)^n}{n^2\pi^2 + z^2} , \quad (5.23)$$

Replacing both exponential kernels that appear in the double integral (5.4), by their respective approximations E_{sh2} and E_{sh1} , we get

$$E_{sh2}(s_2 t_2, a) = e^{2a} \left[\frac{1}{2(a - s_2 t_2)} + (a - s_2 t_2) \sum_{n_2=1}^{\infty} \frac{(-1)^{n_2}}{n_2^2\pi^2 + (a - s_2 t_2)^2} \right] , \quad (5.24)$$

$$E_{sh1}(s_1 t_1, a) = e^{2a} \left[\frac{1}{2(a - s_1 t_1)} + (a - s_1 t_1) \sum_{n_1=1}^{\infty} \frac{(-1)^{n_1}}{n_1^2 \pi^2 + (a - s_1 t_1)^2} \right], \quad (5.25)$$

Afterwards, following similar process as done for the first derivation i.e. from (5.13) to (5.22), namely performing the first and second partial i. L. t. with the similar assumptions and considerations, then the second approximation is obtained and the resulting algorithm is given as, [104],

$$\begin{aligned} f_{sh}(t_1, t_2, a) = & \frac{e^{2a}}{2t_1 t_2} \left[\frac{1}{2} F\left(\frac{a}{t_1}, \frac{a}{t_2}\right) + \sum_{n_2=1}^{\infty} (-1)^{n_2} \operatorname{Re} \left\{ F\left(\frac{a}{t_1}, \left[\frac{a + j n_2 \pi}{t_2}\right]\right) \right\} \dots \right. \\ & + \sum_{n_1=1}^{\infty} (-1)^{n_1} \operatorname{Re} \left\{ F\left(\left[\frac{a + j n_1 \pi}{t_1}\right], \frac{a}{t_2}\right) \right\} \dots \\ & \left. + 2 \sum_{n_1=1}^{\infty} \sum_{n_2=1}^{\infty} (-1)^{n_1+n_2} \operatorname{Re} \left\{ F\left(\left[\frac{a + j n_1 \pi}{t_1}\right] \left[\frac{a + j n_2 \pi}{t_2}\right]\right) \right\} \right]. \quad (5.26) \end{aligned}$$

Finally, for a higher accuracy of the method, the arithmetic mean of (5.22) and (5.26) is considered as the 2D hyperbolic NILT algorithm, and Euler transform is used to accelerate the convergence of infinite series, since it has shown the best results for the 1D hyperbolic NILT. It is worth mentioning that the original variables i.e. t_1, t_2 can be any two variables, such as time and space for instance.

5.3 Error analysis of devised 2D hyperbolic NILT method

Investigating the 2D NILT algorithm (5.22) and its derivation steps, it can be noticed that there exist two sources of errors, namely, the static error and the dynamic error [5]. The latter resulting from the practical truncation of the infinite series of the algorithm up to a certain number of terms when performing a practical computation, this error can be significantly reduced by successfully adapting suitable convergence acceleration techniques, such as those presented in Sect. 3.2 for the 1D hyperbolic NILT method. In contrast, the static error is caused by the approximation of the exponential kernel e^{st} by the proposed hyperbolic relation approximations, and this can be decreased by an optimization of the parameter a , as will be investigated in more details in this section [104].

In order to efficiently compute the static error of (5.22), first, we start by expressing the approximate kernels $E_{ch1}(s_1 t_1, a)$ and $E_{ch2}(s_2 t_2, a)$ both by an alternative manner, namely

$$e^{st} \approx E_{ch}(st, a) = \frac{e^a}{2 \cosh(a - st)} = \frac{e^{st}}{1 + e^{-2a} e^{2st}}, \quad (5.27)$$

When the parameter $a > \gamma t$, it is possible to expand the fraction in (5.27) by a convergent MacLaurin series

$$E_{ch}(st, a) = e^{st} + \sum_{n=1}^{\infty} (-1)^n e^{-2na} e^{(2n+1)st}, \quad (5.28)$$

Considering the alternative approximation of the exponential kernel, and performing the first partial i.L.t. with respect to s_2 we get

$$F_{ch2}(s_1, t_2, a) = F_2(s_1, t_2) + \varepsilon_{ch2}(s_1, t_2, a), \quad (5.29)$$

where the expression $\varepsilon_{ch2}(s_1, t_2, a) = -e^{-2a} F_2(s_1, 3t_2) + e^{-4a} F_2(s_1, 5t_2) - \dots$. Assuming $e^{-2a} \ll 1$ and continuing for the second partial i.L.t. with respect to s_1 , the result is

$$\begin{aligned} f_{ch}(t_1, t_2, a) &= f(t_1, t_2) - e^{-2a} f(t_1, 3t_2) + \sum_{n_1=1}^{\infty} \left((-1)^{n_1} e^{-2n_1 a} f([2n_1 + 1]t_1, t_2) \right) \cdots \\ &- e^{-2a} \sum_{n_1=1}^{\infty} \left((-1)^{n_1} e^{-2n_1 a} f([2n_1 + 1]t_1, 3t_2) \right) = f(t_1, t_2) + \varepsilon_{ch}(t_1, t_2, a). \end{aligned} \quad (5.30)$$

At this point the static error can be theoretically computed through the resulting absolute error, namely

$$\begin{aligned} \varepsilon_{ch}(t_1, t_2, a) &= f_{ch}(t_1, t_2, a) - f(t_1, t_2) \approx -e^{-2a} f(3t_1, t_2) - e^{-2a} f(t_1, 3t_2) \\ &\approx 2M e^{-2a}, \end{aligned} \quad (5.31)$$

where M is a maximal absolute value of an original function $f(t_1, t_2)$. It is evident that the static error declines rapidly by increasing the parameter a .

In previous work [5], it was shown that the hyperbolic NILT method can be considered to behave as a low-pass filter with the cutoff frequency varying with time, i.e. $f_{\text{cut}} = \frac{n_{\text{sum}}}{2t}$. Taking this point into consideration can have a more clear understanding for the derived theoretical static error for the 2D hyperbolic NILT and its relation to the appointed number of terms and the cutoff frequency. Namely, when multiplicative constants at the variables t_i , $i = 1, 2$, increase in the error formula (5.31), its corresponding harmonic component disappears earlier. For instance, considering the approximate static error $\varepsilon_{ch}(t_1, t_2, a) = -e^{-2a} f(3t_1, t_2) - e^{-2a} f(t_1, 3t_2) \cdots$ when $n_{\text{sum}} = 120$ we get $t_1 = \frac{n_{\text{sum}}}{(2 \cdot 3)} = 20$ s, $t_2 = \frac{n_{\text{sum}}}{(2 \cdot 1)} = 60$ s and so on. In Table 5.4 the theoretical absolute static errors of the proposed 2D hyperbolic NILT method for some typical 2D Laplace transforms and their known originals are shown.

In the next section, the developed 2D hyperbolic NILT accelerated with Euler transform is compared with some other available 2D NILT methods as for their accuracy and computational efficiency. As these compared methods do not have any open access program codes available for use, thus, they were programmed in the Matlab language in order to fairly test them.

Tab. 5.4: Absolute static errors of the hyperbolic 2D NILT

Function	I	II
$F(s_1, s_2)$	$\frac{1}{(s_1+1)(s_2+2)}$	$\frac{1}{((s_1+1)(s_2+1))^2}$
$f(t_1, t_2)$	$e^{-t_1-2t_2}$	$t_1 t_2 e^{-(t_1+t_2)}$
Abs.error	$-e^{-(3t_1+2t_2+2a)} - e^{-(t_1+6t_2+2a)}$	$-3t_1 t_2 e^{-2a} (e^{-(3t_1+t_2)} + e^{-(t_1+3t_2)})$

5.4 Comparative analysis of the 2D hyperbolic NILT method

The developed 2D hyperbolic NILT method under discussion is compared with two other methods; namely, the 2D NILT method from K. Singhal et al. [14], and the 2D-NILT proposed by M. Moorthy [44]. To evaluate the accuracy, the ζ_2 measure with a grid of 64×64 points is used, and is expressed as follows

$$\zeta_2 = \sqrt{\frac{\sum_{i=1}^{64} \sum_{j=1}^{64} [f(t_{1i}, t_{2j}) - \hat{f}(t_{1i}, t_{2j})]^2}{(64 \times 64)}} \quad (5.32)$$

where f is the original function and \hat{f} is the corresponding 2D-NILT result. Three test functions with known originals are used for the accuracy test; namely,

- $F_1(s_1, s_2) = [(s_1^2 + 1)(s_2^2 + 1)]^{-1} \rightarrow f_1(t_1, t_2) = \sin(t_1)\sin(t_2)$,
- $F_2(s_1, s_2) = (s_1 + s_2)[(s_1^2 + 1)(s_2^2 + 1)]^{-1} \rightarrow f_2(t_1, t_2) = \sin(t_1)\cos(t_2)$, and
- $F_3(s_1, s_2) = (s_2^2 - 1)[(s_1 + 0.2)^2 + 1]^{-1}(s_2^2 + 1)^{-2} \rightarrow f_3(t_1, t_2) = t_2 e^{-0.2t_1} \sin(t_1)\sin(t_2)$.

Respective accuracy results for each of the 2D NILT methods, using the test functions F_1 , F_2 and F_3 , are shown in Table 5.5.

Tab. 5.5: Accuracy measures of 2D NILT methods using three test functions

2D NILT Method	F_1	F_2	F_3
Proposed	$2.33 \cdot 10^{-1}$	0.462	0.233
2D Singhal-NILT	$1.56 \cdot 10^{-3}$	0.499	0.291
2D Moorthy-NILT	0.6706	0.984	0.124

5.5 Summary

In this chapter some 2D NILT methods were simulated and an optimization of their free parameter choices was presented. The main focus of this chapter was on the mathematical expansion of the 1D hyperbolic NILT method into a two-dimensional one. The technique used to expand this method was by following a repeated application of a partial inverse Laplace transformation. The error analysis of the 2D hyperbolic NILT method was performed and studied. Furthermore, the method was accelerated via the Euler transform which proves to have a high performance. A main advantage of the 2D NILT method arises from its ability to simulate distributed systems with two variables, such as transmission lines or multiconductor transmission lines, e.g. time and space. The leverage of a 2D NILT is that from systems described by linear partial differential equations, we get completely algebraic equations leading to a much simpler solution in the Laplace domain. Moreover, the method provides the possibility of easily incorporating frequency dependent parameters of even fractional-order primary parameters in the system of equations. The method compared to other ones and the efficiency of the method was verified.

6 APPLICATION OF THE MNILT METHODS IN THE ELECTRICAL ENGINEERING FIELD

The multidimensional NILT (MNILT) methods have some potential advantages, in contrast to the 1D NILT method, which lay on the type of applications that can be solved, e.g. nonlinear circuit solution, and the ability of solving systems mathematically described by two variables, such as continuous space-time related systems. Moreover, using MNILT applications described by more than two variables can be solved, for example using 3D NILT to solve nearly nonlinear systems using Volterra series expansion. The following sections are structured as follows: first the application of 2D hyperbolic NILT on simulating a lossy TL is presented [104], second a possibility of simulating weakly nonlinear circuit via MNILT methods [132].

6.1 Transmission line simulation using the 2D hyperbolic NILT method

Here, the 2D hyperbolic NILT method will be used to simulate voltage/current distributions along the TLs, as shown on a Laplace-domain TL model in Fig. 6.1 [104, 127].

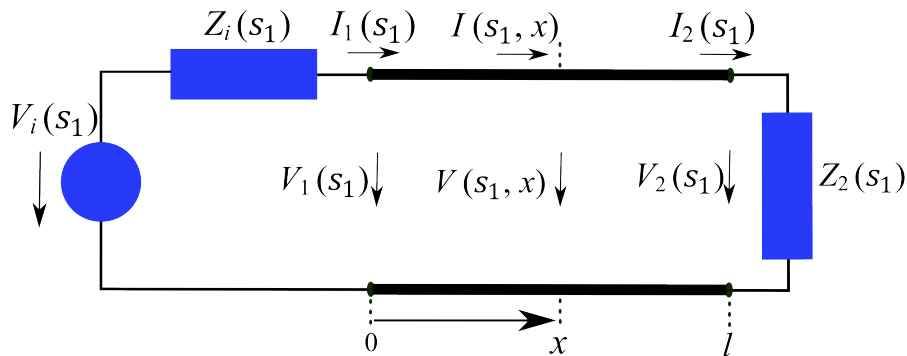


Fig. 6.1: Transmission line model in Laplace-domain with respect to the time variable.

As it is known, a TL can be described mathematically by a pair of partial differential equations (telegraphic equations) of the form

$$-\frac{\partial v(t, x)}{\partial x} = R_0 i(t, x) + L_0 \frac{\partial i(t, x)}{\partial t}, \quad -\frac{\partial i(t, x)}{\partial x} = G_0 v(t, x) + C_0 \frac{\partial v(t, x)}{\partial t}; \quad (6.1)$$

the Laplace-domain TL model in Fig. 6.1 results from the application of the Laplace transform, with respect to time, on the set of telegraphic equations (6.1), which is also represented by the equations (4.3) and (4.4) given in Chapt. 4; henceforth, these equations can be further simplified by transforming them not only with respect to the time t , but also with respect to the geometric coordinate x , resulting with fully algebraic equations,

$$V(s, q) = \frac{qV_1(s) - \gamma(s)Z_c(s)I_1(s)}{q^2 - \gamma^2(s)}, \quad (6.2)$$

$$I(s, q) = \frac{qI_1(s) - \frac{\gamma(s)}{Z_c(s)}V_1(s)}{q^2 - \gamma^2(s)}, \quad (6.3)$$

where zero initial conditions is considered and the boundary conditions are incorporated based on the terminating circuits. $Z_c(s_1)$ and $\gamma(s_1)$ are the characteristic impedance and the propagation constant, respectively. $V_1(s_1)$ and $I_1(s_1)$ are given as follows

$$V_1(s_1) = V_i(s_1) \frac{Z_c(s_1)}{Z_i(s_1) + Z_c(s_1)} \cdot \frac{1 + \rho_2(s_1)e^{-\gamma(s_1)2l}}{1 - \rho_1(s_1)\rho_2(s_1)e^{-2\gamma(s_1)l}} \quad (6.4)$$

$$I_1(s_1) = V_i(s_1) \frac{1}{Z_i(s_1) + Z_c(s_1)} \cdot \frac{1 - \rho_2(s_1)e^{-\gamma(s_1)2l}}{1 - \rho_1(s_1)\rho_2(s_1)e^{-2\gamma(s_1)l}}. \quad (6.5)$$

where $\rho_1(s_1)$ and $\rho_2(s_1)$ are reflection coefficients at the beginning and end of the TL respectively. It is evident from the devised TL equations that the solution in the original domain is not possible to obtain analytically, though it is feasible by utilizing the 2D hyperbolic NILT method, and hence obtaining the simulations of the voltage/current waveform distributions along the TL numerically.

6.1.1 Transmission line via 2D hyperbolic NILT case study

As an example let us consider a TL, as in Fig. 6.1., with length of $l = 1$ m [104]. The TL is characterized by the following p.u.l. parameters: $R_0 = 1$ m Ω /m, $L_0 = 600$ nH/m, $G_0 = 2$ mS/m, $C_0 = 80$ pF/m. The TL is terminated by the impedances $Z_i = 10$ Ω , $Z_2 = 1$ k Ω . The TL is excited with the source voltage waveform:

$$v_i(t) = \begin{cases} \sin^2\left(\frac{\pi t}{2 \cdot 10^{-9}}\right), & \text{for } 0 \leq t \leq 2 \cdot 10^{-9}. \\ 0, & \text{otherwise.} \end{cases} \quad (6.6)$$

The voltage waveform (6.6) has the corresponding Laplace-domain transform: $V_i(s_1) = \frac{2\pi^2[1 - \exp(-2 \cdot 10^{-9}s_1)]}{s_1[(2 \cdot 10^{-9}s_1)^2 + 4\pi^2]}$. After undergoing the 2D hyperbolic NILT the simulation results of the voltage/current propagation profiles along the TL are shown, respectively, in Fig. 6.2 and Fig. 6.3.

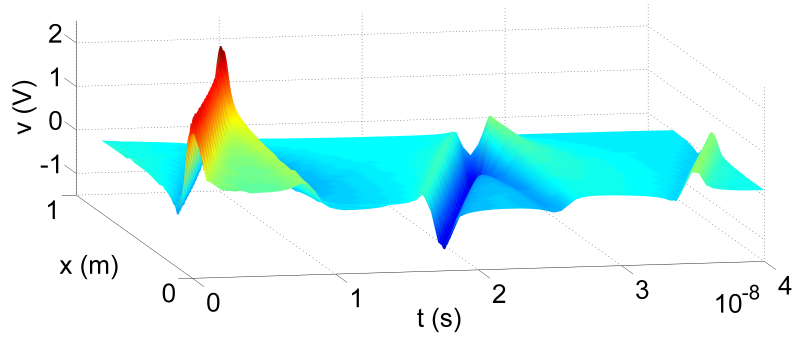


Fig. 6.2: Voltage distribution along the TL via 2D hyperbolic NILT.

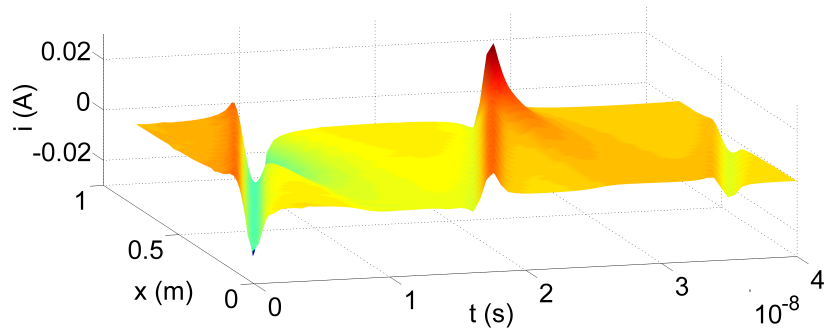


Fig. 6.3: Current distribution along the TL via 2D hyperbolic NILT.

6.2 Weakly nonlinear-circuit solution via MNILT

Predicting the response of nonlinear systems has been a challenge for scientists and researchers alike for many years, due to the analytical difficulties in analysing such systems. The significant importance of analysing nonlinear systems mainly arises due to the fact that, in the physical world, several systems are to some extent nonlinear ones. In this section, it will be demonstrated the possibility of utilizing a MNILT method for the simulation of nonlinear networks based on a classical approach of Volterra series expansion [132].

There exist several approaches to solve and analyze nonlinear circuits; these approaches are based mainly on specific numerical techniques that can solve nonlinear differential equations. When considering a nearly nonlinear system, a method based on Volterra series expansion can mathematically describe the system accurately enough from a practical point of view. Nevertheless, the main limitation of this approach lies on the difficulty of obtaining the time domain results, and hence comes the advantage of using an MNILT method.

A weakly nonlinear circuit has the leverage that it can be described by third order Volterra kernels with a very reasonable accuracy. Another advantage is based on the fact that these Volterra kernels can be experimentally obtained by measuring the X -parameters through the use of a nonlinear vector network analyzer (NVNA) and afterwards transferring the results properly [132, 133]. In theory, the process of the solution is as follows: By utilizing the multidimensional Laplace transform (MLT) of a time domain nonlinear impulse response a result is a respective Laplace domain transfer function, and this, in fact, helps to obtain the needed Volterra kernels [134], by using, for example, a harmonic input method [135]. Then, after solving the system in the Laplace domain, the final step is to transfer the solution back into the time domain. This process will be mathematically shown in more detail in this section.

Assuming a response $y(t)$ to a stimulus $x(t)$ [136], has the form

$$y(t) = \sum_{n=1}^{\infty} y_n(t) , \quad (6.7)$$

the infinite sum has the following terms

$$y_n(t) = \int_{-\infty}^{\infty} \xrightarrow{n\text{-fold}} \int_{-\infty}^{\infty} h_n(\tau_1, \tau_2, \dots, \tau_n) \prod_{i=1}^n x(t - \tau_i) d\tau_i , \quad (6.8)$$

with $h_n(\tau_1, \tau_2, \dots, \tau_n)$ representing a nonlinear impulse response, also known as the n -th order Volterra kernel. These equations are shown more clearly as a flow chart in Fig. 6.4. In order to perform the Laplace-domain approach new variables are introduced by $t_1 = t_2 = \dots = t_n = t$, and then an n -dimensional Laplace transform is applied transforming the n -fold convolution integral (6.8) into a multidimensional Laplace-domain response [134],

$$Y_n(s_1, s_2, \dots, s_n) = H_n(s_1, s_2, \dots, s_n) \prod_{i=1}^n X(s_i) , \quad (6.9)$$

with $H_n(s_1, s_2, \dots, s_n)$ as a nonlinear transfer function, which can be solved for some nonlinear circuit using for instance the harmonic input method [137]. At this point the time-domain terms $y_n(t_1, t_2, \dots, t_n)$ can be obtained by an n -D ILT, while considering $t_1 = t_2 = \dots = t_n = t$ in the final results; a graphical representation is shown in Fig. 6.4. As we are limiting our computations to weakly nonlinear networks, i.e. considering Volterra series expansion up to the 3rd order, thus the NILTs of 1D, 2D and 3D are needed to get the required time-domain response; for more clarity, a block diagram of this process is depicted in Fig. 6.4.

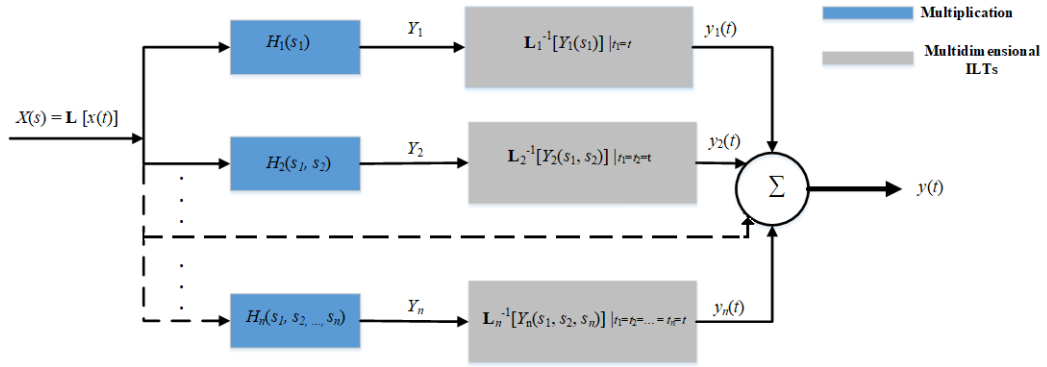


Fig. 6.4: Diagram of a nonlinear circuit solution by using Volterra series expansion and multidimensional ILTs.

6.2.1 Weakly nonlinear circuits using 1D to 3D NILTs case study

In order to demonstrate the approach presented in Sect. 6.2, a solution of a weakly nonlinear circuit by using 1D, 2D and 3D NILTs is presented. Let us consider a nonlinear serial LR circuit, see Fig. 6.5 [132]. The network consists of a linear inductor L , a linear resistor R , and a nonlinear resistive element R_n , the network is excited by the voltage source $v_i(t)$. Assuming square nonlinearity, i.e. the resistive element R_n having a quadratic characteristics: $v_{R_n}(t) = R_n i^2(t)$.

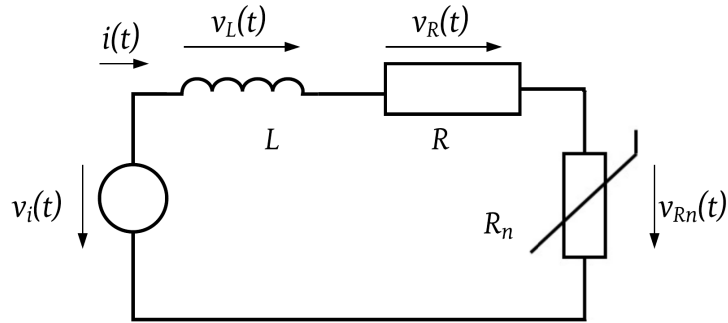


Fig. 6.5: Electrical circuit with nonlinear resistive element R_n .

In light of the foregoing, the first-order nonlinear ordinary differential equation (NODE) is given as follows,

$$L \frac{di(t)}{dt} + Ri(t) + R_n i^2(t) = v_i(t) . \quad (6.10)$$

In association with the block diagram in Fig. 6.4, it can be noticed that the excitation voltage $v_i(t)$ and the current $i(t)$ represent the stimulus $x(t)$ and the response $y(t)$, accordingly. Henceforth, with respect to (6.9), and assuming a third-order expansion, the following Laplace-domain partial solutions ought to be resolved,

$$I_1(s_1) = H_1(s_1)V_i(s_1), \quad (6.11a)$$

$$I_2(s_1, s_2) = H_2(s_1, s_2)V_i(s_1)V_i(s_2), \quad (6.11b)$$

$$I_3(s_1, s_2, s_3) = H_3(s_1, s_2, s_3)V_i(s_1)V_i(s_2)V_i(s_3) . \quad (6.11c)$$

With the use of a suitable method, for e.g. here the harmonic input method is used, and hence, the transfer functions (6.11) are solved,

$$H_1(s_1) = \frac{1}{s_1L + R} , \quad (6.12a)$$

$$H_2(s_1, s_2) = -R_n H_1(s_1)H_1(s_2)H_1(s_1 + s_2) , \quad (6.12b)$$

$$H_3(s_1, s_2, s_3) = -\frac{R_n}{3} [H_1(s_1)H_2(s_2, s_3) + H_1(s_2)H_2(s_1, s_3) \cdots \\ + H_1(s_3)H_2(s_1, s_2)]H_1(s_1 + s_2 + s_3) . \quad (6.12c)$$

Suppose that an exponential pulse is chosen as the excitation voltage source $v_i(t)$, with its Laplace transform given as follows,

$$v_i(t) = V_0 e^{-at} \underline{1}(t) \xrightarrow{\mathbf{L} \{ \cdot \} } V_i(s) = \frac{V_0}{s + a} , \quad (6.13)$$

where $a \geq 0$, and then substituting (6.13) back into (6.11), solving the respective sub-equations. The Laplace-domain responses will undergo the 1D, 2D and 3D NILT methods to obtain the resultant time-domain current response, namely,

$$i(t) = \mathbf{L}_1^{-1}[I_1(s_1)]|_{t_1=t} + \mathbf{L}_2^{-1}[I_2(s_1, s_2)]|_{t_1=t_2=t} + \mathbf{L}_3^{-1}[I_3(s_1, s_2, s_3)]|_{t_1=t_2=t_3=t} \\ = i_1(t_1)|_{t_1=t} + i_2(t_1, t_2)|_{t_1=t_2=t} + i_3(t_1, t_2, t_3)|_{t_1=t_2=t_3=t} \\ = i_1(t) + i_2(t) + i_3(t) . \quad (6.14)$$

For the simulation tests, the following parameters are considered: $L = 100$ mH, $R = 100$ m Ω , $R_n = 100$ m Ω A $^{-1}$, $V_0 = 10$ mV, and $a = 1$. The results are illustrated in Fig. 6.6 and Fig. 6.7, showing individual terms $i_i(t)$, namely: $i_1(t)$, $i_2(t)$, and $i_3(t)$, respectively. Two cases are simulated first is with $a = 1$ (an exponential impulse), and the second one with $a = 0$ (a unit step), see (6.13), where the results are depicted in Fig. 6.6 and Fig. 6.7, respectively.

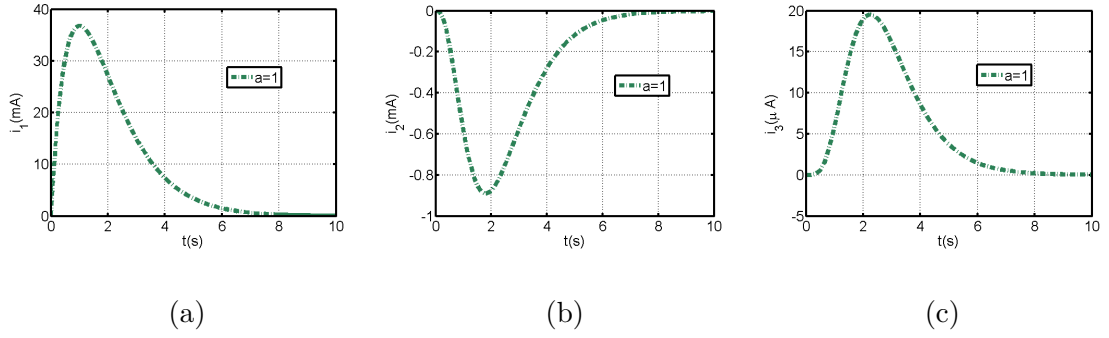


Fig. 6.6: Numerical inversions leading to current response Volterra series terms by (a) 1D NILT, (b) 2D NILT, (c) 3D NILT, for an exponential impulse.

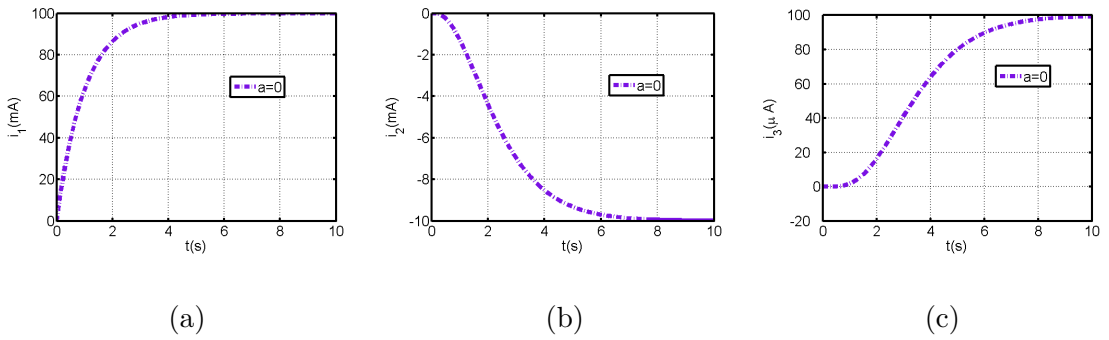


Fig. 6.7: Numerical inversions leading to current response Volterra series terms by: (a) 1D NILT, (b) 2D NILT, (c) 3D NILT, for a unit step.

The resultant current responses, computed according to (6.14), are depicted in Fig. 6.8, for both cases accordingly.

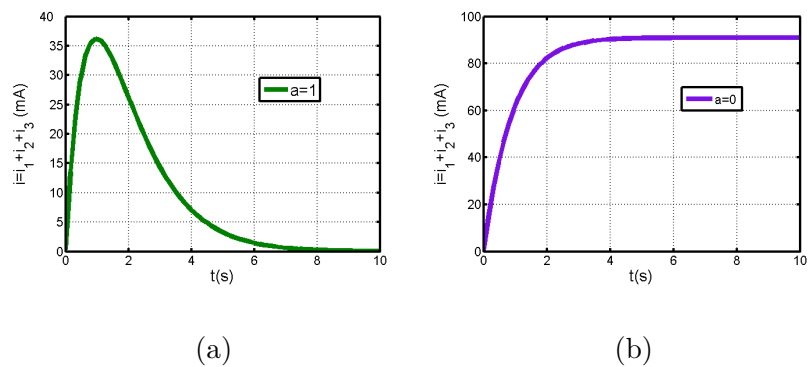


Fig. 6.8: Resulting current response for: (a) an exponential impulse, (b) a unit step.

Furthermore, the resulting current response is computed, and the accuracy of the method, considering the exponential input case $a = 1$, is verified by comparing

the resultant current response of NODE, in (6.10), computed by a Matlab built-in function, particularly, the ODE45 Runge-Kutta function, which is applied directly to the NODE, and then analyzing the relative errors, the results are shown in Fig. 6.9 [132].

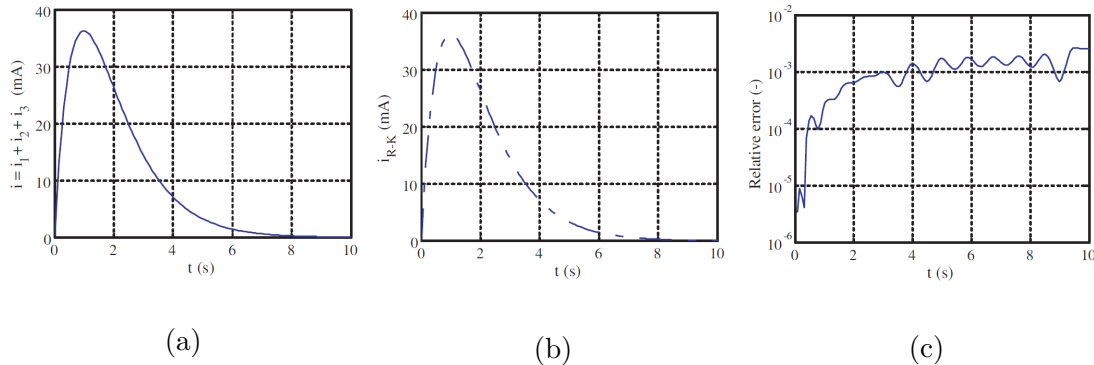


Fig. 6.9: Resultant current response for the case $a = 1$ by: (a) Volterra series solution, (b) Runge-Kutta method, and (c) the relative error.

The simulation results were obtained using Matlab language on a common PC, and the CPU computation times were generally less than one min, while considering 64 points of time division. The 1D NILT up to 3D NILT programming codes used are available in [132].

6.3 Summary

This chapter clearly demonstrates the outputs of utilizing multidimensional NILTs, i.e. two-dimensional or higher. The advantage is mainly due to the possibility of transforming linear partial differential equations with two variables into completely algebraic ones, leading to a much simpler solution in the Laplace domain. Moreover, it was shown that the MNILT method allows to simulate nonlinear electrical circuits. The process relies on the possibility of describing a nonlinear system via a Volterra series expansion, in conjunction with MNILT, in relatively very accurate manner. For a weakly nonlinear system, usually the Volterra kernels up to a third order yield very reasonable results. The Laplace-domain Volterra kernels are simply determined using the harmonic input method, and thus a three-dimensional NILT method is used to obtain the original time-domain results, more effectively as when compared to the associate variable method. These applications were presented in detail in this chapter, and the simulation results were performed using Matlab programming language.

7 RESEARCH CHALLENGES AND CONCLUSIONS

In this chapter, the conclusions of the doctoral thesis are presented and summarized. The main goals can be listed as follows:

- Research and development of effective numerical inverse Laplace transform methods.
- Development of a promising 1D NILT method, including the detailed study of its error analysis and its successful program implementation and verification.
- Enhancements on the NILT method by incorporating different infinite series convergence acceleration techniques.
- Expansion of the proposed hyperbolic NILT method to a higher dimension, including detailed error analysis, adjustment of Euler transform acceleration method and the program implementation of the obtained 2D NILT method.
- Experimental implementation of the developed NILT methods by the successful application on different potential electrical engineering topics, including those that require the solution of ODE, PDE and even weakly nonlinear systems via MNILT method.
- Incorporating fractional-order calculus on different NILT method field of applications to improve the modeling and simulation of these applications.

The first chapter focused on different methodological techniques for Numerical Inverse Laplace Transforms (NILT). A high-level description is presented for different NILTs, with the categorization of these methods regarding their bases of derivation, and a general analysis of the accuracy, stability and the range of application of these NILTs on different types of functions. The different methods of interest are implemented and experimentally tested with optimization of their free parameters. Several 1D NILT methods have been tested and analyzed, mainly, regarding their accuracy, computation speed and the types of functions supported. It is clear that most available NILT methods are based on the necessity that the inverse transform of polynomial time functions up to a specific and relatively high power is accurate. Moreover, most of the available methods suffer from some limitations such as the accuracy of the method itself, the range of different functions that can be correctly inverted and the large computational time (see practical accuracy results in Fig. 3.6 to Fig. 3.8).

Based on the findings, a proposed hyperbolic NILT method that differs from other similar algorithms, namely, by reacting as a nearly ideal low pass filter with time-variable cutoff frequency, was developed and generalized. Mainly, this

numerical method is based on approximation of the Bromwich integral exponential kernel by suitable hyperbolic approximations. The hyperbolic NILT has the benefit of not only inverting functions along a time period but also at a specific chosen point. Furthermore, this method was generalized by reducing the integration step, while providing higher accuracy of the results. After performing several tests on different types of functions, this numerical method has proved to yield results with a higher degree of accuracy and stability, including a wide range of types of functions that can be inverted, e.g. rational, irrational and transcendental functions in the Laplace domain; this is verified in Fig. 3.6 to Fig. 3.8. The hyperbolic NILT method is tested and compared to other highly cited 1D NILT methods. Furthermore, the error analysis of the approximate inversion formulae, including both sources of error, namely, the ‘static’ and the ‘dynamic’ were presented in detail, specifically in Section 3.1.1.

Additionally, further enhancements to the hyperbolic NILT method were performed by adapting several infinite series convergence accelerating algorithms. These algorithms include the quotient difference algorithm, the epsilon algorithm and the Euler transform. The former proved to be a method with high stability, while the latter, the Euler transform, improved the method with a much higher precise inversion accuracy (the results were depicted in Fig. 3.3 to Fig. 3.5). The 1D hyperbolic NILT, among other methods, was used in several applications in the electrical engineering and electronics field. These applications include the solution of transient processes in linear time invariant system.

Once a given problem is resolved in the Laplace domain, the difficult part is to obtain the original results in the time-domain, as, analytically, it is usually impractical, hard or even impossible to obtain. Thus, it was verified that by using the NILT it is possible to overcome these difficulties and obtain the required solution and simulations of these applications in the time domain. The applications that have been solved include: lossy TL, fractional-order TL, frequency dependent TL, nonuniform TL, and furthermore, an expansion to MTL with fractional-order elements and possible external feedback were performed. These successfully preformed simulations were presented in detail in Chapter 4.

Furthermore, in Chapter 5, an innovative approach to the numerical computation of the hyperbolic NILT method two-dimensional expansion was performed. The technique involves the repeated application of partial inverse Laplace transform operations. The detailed error analysis of the method was devised and studied in Section 5.3. The 2D hyperbolic NILT was verified by utilizing it in more sophisticated applications, such as multiconductor transmission lines with simulations that contain both time and space variables obtained by a single computation step (see Fig. 6.2 and Fig. 6.3). Moreover, the n D NILT is used for

potential applications such as weakly non-linear circuits, while using Volterra series method; these applications were presented and a case study was done in Chapter 6.

A novel approach of modeling some applications using the fractional-order domain, in contrast to the classical integer-orders of the electronic components, was effectively incorporated in the conducted applications in a straightforward manner. It was shown that with the benefit of utilizing the Laplace domain, it is feasible to include these fractional-order elements in the respective models, due to the advantage of obtaining the original time domain results with the different NILT methods. It was verified that including fractional-order elements in the simulation tests provides a better representation of the physical phenomena in such applications. Moreover, imposing fractional-order elements gives a higher degree of freedom for the optimization of these applications and a better control of its characteristics; such applications were simulated and the results were depicted in Chapter 4. All the results displayed in this doctoral thesis were programmed and implemented in the Matlab language package. For practical requirements, a CD is attached which includes all the original programming codes along with the exercises and experiments performed in this doctoral thesis.

The original contributions to the doctoral thesis are:

- The development of a NILT method with an achievable high degree of accuracy, which is possible to increase according to need at the cost of the number of arithmetic operations performed.
- The discovery that the hyperbolic NILT method can be enhanced by adapting suitable infinite series convergence acceleration techniques, for instance, by providing an absolute error of about 10^{-8} or even less for some tested functions.
- The demonstration that the NILT method is a computationally effective method able to solve mathematical models of interconnects based on telegraphic equations or on RLCG lumped elements.
- The discovery that using the NILT method followed by the simulation of TL/MTL high-frequency losses, nonuniformity of the wires, and inclusion of fractional-order TL elements, in contrast to the conventional integer ones, can be all done in a novel and simple manner.
- Implementation of previous findings into the new developed 2D hyperbolic NILT method, followed by a detailed error analysis of the method and verification by solving practical applications in the electrical engineering field.
- The possibility of solving weakly nonlinear systems using MNILT method of up to three variables accurately enough from a practical point of view with the assistance of Volterra series expansion method.
- Optimization of the free parameter values for some 1D and 2D NILT methods.

Future work recommendations:

- Generalization of the hyperbolic 2D NILT method to three variables based on partial inversions and including the error analysis.
- Familiarization with parallel programming techniques and the possible deployment to MNILT methods.
- Programming implementations of the method and the simulation of potential applications requiring MNILTs with a possibility of modeling in the fractional-order domain.
- Possible future collaboration with the Department of Engineering Science and Mechanics, Pennsylvania State University for the application of the hyperbolic NILT method in direct and inverse heat conduction and thermoelasticity with prof. A. E. Segall.
- Possible future collaboration with the Department of Radiology, University of Pennsylvania, USA, for using NILT methods with research on myelin water mapping in brain with prof. D. Kumar.

Bibliography

- [1] L. Brančik, and N. Al-Zubaidi R-Smith, “Two approaches to derive approximate formulae of NILT method with generalization,” *38th International Convention on Information and Communication Technology, Electronics and Microelectronics (MIPRO)*, Croatia, pp. 155–160, 2015.
- [2] J. Toutain, J.-L. Battaglia, C. Pradere, J. Pailhes, A. Kusiak, W. Aregba, and J.- C. Batsale, “Numerical inversion of Laplace transform for time resolved thermal characterization experiment,” *Journal of Heat Transfer*, vol. 133, no. 4, ID: 044504, 2011.
- [3] G. V. Milovanovic, and A. S. Cvetkovic, “Numerical inversion of the Laplace transform,” *Facta. Univ. Ser. Electr. Energ.*, vol. 18, No. 3, pp. 515-530, 2005.
- [4] R. G. Campos, and A. Huet, “Numerical inversion of the Laplace transform and its application to fractional diffusion,” *Journal Applied Mathematics and Computation*, vol. 327, pp. 70-78, 2018.
- [5] J. Valsa, and L. Brančik, “Approximate formulae for numerical inversion of Laplace transforms,” *International Journal of Numerical Modelling: Electronic Networks, Devices and Fields*, vol. 11, pp. 153-166, 1998.
- [6] G. Honig, and U. Hirdes, “A method for the numerical inversion of Laplace transforms,” *Journal of Computational and Applied Mathematics*, vol. 10, pp. 113-132, 2// 1984.
- [7] T. Hosono, “Numerical inversion of Laplace transform and some applications to wave optics,” *Radio Science*, vol. 16, pp. 1015-1019, 1981.
- [8] L. Brančik, “Programs for fast numerical inversion of two-dimensional Laplace transforms in Matlab language environment with some applications,” *in Proceedings of the 23rd International Conference on Fundamentals of Electrotechnics and Circuit Theory SPETO’2000*, Gliwice-Ustroń, Poland, pp. 197-200, 2000.
- [9] K. Singhal, and J. Vlach, “Computation of time domain response by numerical inversion of the Laplace transform,” *Journal of the Franklin Institute*, vol. 299, pp. 109-126, 2// 1975.
- [10] L. Brančik, “An improvement of FFT-based numerical inversion of two-dimensional Laplace transforms by means of ϵ -algorithm,” *in Proceedings of IEEE ISCAS’2000*, Geneva, Switzerland, pp. 581-584, 2000.

- [11] A. M. Cohen, *Numerical methods for Laplace transform inversion*, New York, N.Y: Springer, 2007.
- [12] J. Abate, G. L. Choudhury, and W. Whitt, “Numerical inversion of multidimensional Laplace transforms by the Laguerre method,” *Performance Evaluation*, vol. 31, pp. 229-243, 1// 1998.
- [13] L. Brančák, “Numerical Inverse Laplace Transforms for Electrical Engineering Simulation,” *in MATLAB for Engineers-Applications in Control, Electrical Engineering, IT and Robotics*, Edited by Karel Perutka, Rijeka: InTech, pp. 51-74, 2011.
- [14] K. Singhal, J. Vlach, and M. Vlach, “Numerical inversion of multidimensional Laplace transform,” *Proceedings of the IEEE*, vol. 63, pp. 1627-1628, 1975.
- [15] B. Davies, and B. Martin, “Numerical inversion of the Laplace transform: a survey and comparison of methods,” *Journal of computational physics*, vol. 33, pp. 1-32, 1979.
- [16] P. P. Valkó, and J. Abate, “Numerical inversion of 2-D Laplace transforms applied to fractional diffusion equations,” *Applied Numerical Mathematics*, vol. 53, pp. 73-88, 4// 2005.
- [17] H. Dubner and J. Abate, “Numerical Inversion of Laplace Transforms by Relating Them to the Finite Fourier Cosine Transform,” *Journal of the ACM*, vol. 15, pp. 115-123, 1968.
- [18] L. Brančák, “Programs for fast numerical inversion of Laplace transforms in MATLAB language environment,” *Conference Matlab 99*, Prague, Czech Republic, pp. 27-39, 1999.
- [19] L. Brančák, “Utilization of quotient-difference algorithm in FFT based numerical ILT method,” *in Proceedings of the 11th International Czech-Slovak Scientific Conference Radioelektronika 01*, Brno, Czech Republic, pp. 352-355, 2001.
- [20] K. S. Crump, “Numerical Inversion of Laplace Transforms Using a Fourier Series Approximation,” *Journal of the ACM*, vol. 23, pp. 89-96, 1976.
- [21] L. Brančák, “The fast computing method of numerical inversion of Laplace transforms using FFT algorithm,” *in Proceedings of the 5th EDS 98 International Conference*, Brno, Czech Republic, pp. 97-100, 1998.

- [22] L. Brančık, “An improvement of FFT-based numerical ILT procedure by application of ϵ -algorithm,” in *Proceedings of the Seminar STO-7*, pp. 196-199, Brno, Czech Republic, 1999.
- [23] L. Brančık, “Error analysis and optimal parameter evaluation in FFT-based 2D-nilt method,” in *Proceedings of 2004 IEEE Asia-Pacific Conference on Circuits and Systems*, Tainan, Taiwan, pp. 809-812, 2004.
- [24] O. Taiwo, J. Schultz, and V. Krebs, “A comparison of two methods for the numerical inversion of Laplace transforms,” *Computers and Chemical Engineering*, vol. 19, pp. 303-308, 3// 1995.
- [25] R. M. Simon, M. T. Stroot, and G. H. Weiss, “Numerical inversion of Laplace transforms with application to percentage labeled mitoses experiments,” *Computers and Biomedical Research*, vol. 5, pp. 596-607, 1972.
- [26] F. R. d. Hoog, J. H. Knight, and A. N. Stokes, “An Improved Method for Numerical Inversion of Laplace Transforms,” *Journal on Scientific and Statistical Computing SIAM*, vol. 3, pp. 357-366, 1982.
- [27] H. Stehfest, “Algorithm 368: Numerical inversion of Laplace transforms [D5],” *Communications of the ACM*, vol. 13, pp. 47-49, 1970.
- [28] D. P. Gaver Jr, “Observing stochastic processes, and approximate transform inversion,” *Operations Research*, vol. 14, pp. 444-459, 1966.
- [29] P. P. Valko and J. Abate “Comparison of sequence accelerators for the Gaver method of numerical Laplace transform inversion,” *Computers and Mathematics with Applications*, vol. 48, pp. 629-636, 2004.
- [30] V. Zakian, “Numerical inversion of Laplace transform,” *Electronics Letters*, vol. 5, pp. 120-121, 1969.
- [31] D. J. Halsted, and D. E. Brown, “Zakian’s technique for inverting Laplace transforms,” *The Chemical Engineering Journal*, vol. 3, pp. 312-313, // 1972.
- [32] Q. Wang, and H. Zhan, “On different numerical inverse Laplace methods for solute transport problems,” *Advances in Water Resources*, vol. 75, pp. 80-92, 1// 2015.
- [33] Y. Feng, W. Xinhai, and L. Hong, “Application of Laplace transform in well test interpretation - an example of the oilfield cavity-fractured reservoirs in tarim basin,” in *International Conference on Multimedia Technology (ICMT)*, pp. 1988-1991, 2011.

- [34] J. Weideman, “Optimizing Talbot’s contours for the inversion of the Laplace transform,” *SIAM Journal on Numerical Analysis*, vol. 44, pp. 2342-2362, 2006.
- [35] P. O. Kano, M. Brio, P. Dostert, and J. Cain, “Dempster–Shafer evidential theory for the automated selection of parameters for Talbot’s method contours and application to matrix exponentiation,” *Computers and Mathematics with Applications*, vol. 63, pp. 1519-1535, 2012.
- [36] W. T. Weeks, “Numerical Inversion of Laplace Transforms Using Laguerre Functions,” *Journal of the ACM*, vol. 13, pp. 419-429, 1966.
- [37] V. Zakian, “Solution of homogeneous ordinary linear differential systems by numerical inversion of Laplace transforms,” *Electronics Letters*, vol. 7, pp. 546-548, 1971.
- [38] J. Vlach, “Numerical method for transient responses of linear networks with lumped, distributed or mixed parameters,” *Journal of the Franklin Institute*, vol. 288, pp. 99-113, 1969.
- [39] P. O. Kano, and M. Brio, “Application of Post’s formula to optical pulse propagation in dispersive media,” *Computers and mathematics with applications*, vol. 59, pp. 629-650, 2010.
- [40] G. L. Choudhury, D. M. Lucantoni, and W. Whitt, “Multidimensional Transform Inversion with Applications to the Transient M/G/1 Queue,” *The Annals of Applied Probability*, vol. 4, pp. 719-740, 1994.
- [41] E. Huntley, and A. S. I. Zinober, “Applications of numerical double Laplace transform algorithms to the solution of linear partial differential equations,” *Computing*, vol. 21, pp. 245-258, 1979.
- [42] L. Brančík, “Numerical Inversion of Two-Dimensional Laplace Transforms Based on Partial Inversions,” in *Proceedings of the 17th International Conference Radioelektronika’07*, Brno, Czech Republic, pp. 451-454, 2007.
- [43] C. Hwang, and M.-J. Lu, “Numerical inversion of 2-D Laplace transforms by fast Hartley transform computations,” *Journal of the Franklin Institute*, vol. 336, pp. 955-972, 8// 1999.
- [44] M. V. Moorthy, “Numerical inversion of two-dimensional Laplace transforms–Fourier series representation,” *Applied Numerical Mathematics*, vol. 17, pp. 119-127, 5// 1995.

- [45] V. Zakian, "Optimisation of numerical inversion of Laplace transforms," *Electronics Letters*, vol. 6, pp. 677-679, 1970.
- [46] P. Gomez, L. Vergara, R. Nuricumbo-Guillen, and F. P. Espino-Cortes, "Two-Dimensional Definition of the Numerical Laplace Transform for Fast Computation of Transient Profiles Along Power Transmission Lines," *IEEE Transactions on Power Delivery*, vol. 31, pp. 412-414, 2016.
- [47] L. Brančík, "Multiconductor Transmission Lines Sensitivity via Two-Dimensional Laplace Transform," in *the 13th IEEE International Conference on Electronics, Circuits and Systems ICECS'06*, Nice, France, pp. 17-20, 2006.
- [48] C. Zhang, S.h. Hu, Y. Xiao, and X. f. Wang, "The application of 2-D numerical inversion of Laplace transform," in *9th International Conference on Signal Processing ICSP'08*, Beijing, China, pp. 60-63, 2008.
- [49] I. Y. Korotyeyev, "Process analysis in PWM inverters based on two dimensional Laplace transform," in *International School on Nonsinusoidal Currents and Compensation (ISNCC)*, Zielona Gora, Poland, pp. 1-5, 2013.
- [50] C. Hwang, T. Y. Guo, and Y. P. Shih, "Numerical inversion of multidimensional Laplace transforms via block-pulse functions," *Control Theory and Applications, IEE Proceedings D*, vol. 130, no. 5, pp. 250-254, 1983.
- [51] L. Brančík, "Numerical inversion of 3D Laplace transforms for weakly nonlinear systems solution," in *Proceedings of the 20th International Conference Radioelektronika'10*, Brno, Czech Republic, pp. 221-224, 2010.
- [52] G. L. Choudhury, D. M. Lucantoni, and W. Whitt, "Multidimensional transform inversion with applications to the transient M/G/1 queue," *The Annals of Applied Probability*, vol. 4, pp. 719-740, 1994.
- [53] T.J. Freeborn, B. Maundy, and A.S. Elwakil, "Field programmable analogue array implementations of fractional step filters," *IET Circuits, Devices and Systems*, vol. 4, no.6, pp. 514-524, 2010.
- [54] K. Oldham, and J. Spanier, *The Fractional Calculus: Theory and Applications of Differentiation and Integration to Arbitrary Order*, (New York: Academic Press, 1974).
- [55] M. Ortigueira, *Fractional Calculus for Scientists and Engineers*, Springer, 2011.
- [56] J. A. T. Machado, V. Kiryakova, and F. Mainardi, "Recent history of fractional calculus," *Communications in Nonlinear Science and Numerical Simulation*, vol. 16, no. 3, pp. 1140-1153, 2011.

- [57] R. K. Saxena, and A. M. Mathai, *Generalized hypergeometric functions with applications in statistics and physical sciences*, Springer-Verlag, Berlin, 1973.
- [58] A. A. Kilbas, and M. Saigo, *H-Transforms: Theory and Applications, Analytic Methods and Special Functions*, Chapman and Hall, CRC Press, Boca Raton, Florida, USA, 2004.
- [59] R. Metzler and J. Klafter, "The random walk's guide to anomalous diffusion: A fractional dynamics approach," *Physics Reports*, vol. 339, pp. 1-77, 2000.
- [60] R. E. Gutierrez, J. M. Rosario, and J. T. Machado, "Fractional order calculus: basic concepts and engineering applications," *Mathematical Problems in Engineering*, vol. 2010, Article ID 375858, 19 pages, 2010.
- [61] N. Sebaa, Z. E. A. Fellah, W. Lauriks, and C. Depollier, "Application of fractional calculus to ultrasonic wave propagation in human cancellous bone," *Signal Processing*, vol. 86, no. 10, pp. 2668-2677, 2006.
- [62] S. Abbisso, R. Caponetto, O. Diamante, L. Fortuna, and D. Porto, "Non-integer order integration by using neural networks," in *Proceedings of IEEE International Symposium Circuits Systems*, Sydney, Australia, pp. 688-691, 2001.
- [63] J.F. G. Aguilar, J.J.B. Alvarado, J.J.R. Garcia, and T.C. Fraga, "Modeling and simulation of equivalent circuits in description of biological systems-a fractional calculus approach," *Journal of Electrical Bioimpedance*, vol. 3, pp. 2-11, 2012.
- [64] A. Radwan, A. Soliman, and A. Elwakil, "First-order filters generalized to the fractional domain," *Journal of Circuits, Systems and Computers JCSC*, vol. 17, no. 1, pp. 55-66, 2008.
- [65] G. Tsirimokou, R. Sotner, J. Jerabek, J. Koton, and C. Psychalinos, "Programmable analog array of fractional-order filters with CFOAs," *Proceedings of the 40th International Conference on Telecommunications and Signal Processing TSP*, Barcelona, Spain, pp.706-709, 2017.
- [66] I. Podlubny, I. Petras, B. Vinagre, P. O. Leary, and L. Dorcak, "Analogue realizations of fractional-order controllers," *Nonlinear Dynamics*, vol. 29, pp. 281-296, 2002.
- [67] N. Sugimoto, "Burgers equation with a fractional derivative; hereditary effects on non-linear acoustic waves," *Journal of Fluid Mechanics*, vol. 225, pp. 631-653, 1991.

- [68] J.F. Gmez-Aguilar, J.J. Rosales-Garca, J.J. Bernal-Alvarado, T. Crdova-Fraga, and R. Guzmán-Cabrera, “Fractional mechanical oscillators,” *Revista Mexicana de Fsica*, vol. 58, pp. 348-352, 2012.
- [69] Y. Xu, Y. Lil, and D. Liu, “Response of fractional oscillators with viscoelastic term under random excitation,” *Journal Computational and Nonlinear Dynamics*, vol. 9, no. 3, paper ID CND-13-1213, 8 pages, 2013.
- [70] A. G. Radwan, A. M. Soliman, and A.S. Elwakil, “Design equations for fractional-order sinusoidal oscillators: four practical circuits examples,” *International Journal of Circuit Theory and Applications*, vol. 36, pp. 473-492, 2007.
- [71] W. Ahmad, R. El-Khazali, and A.S. Elwakil, “Fractional-order Wien-bridge oscillator,” *Electronics Letters*, vol. 37, pp. 1110-1112, 2001.
- [72] A.G. Radwan, A.S. Elwakil, and A.M. Soliman, “Fractional-order sinusoidal oscillators: design procedure and practical examples,” *IEEE Trans. on Circuits and Systems I: Regular Papers*, vol. 55, pp. 2051-2063, 2008.
- [73] A.S. Elwakil, A. Agambayev, A. Allagui, and K.N. Salama, “Experimental demonstration of fractional-order oscillators of orders 2.6 and 2.7,” *Chaos, Solitons and Fractals*, vol. 96, pp. 160-164, 2017.
- [74] A. Kartci, N. Herencsar, J. Koton, L. Brančík, K. Vrba, G. Tsirimokou, and C. Psychalinos, “Fractional-order oscillator design using unity-gain voltage buffers and OTAs,” *Proceedings of the 2017 60th IEEE International Midwest Symposium on Circuits and Systems MWSCAS*, Boston, USA, pp. 555-558, 2017.
- [75] Y. Shang, W. Fei, and H. Yu, “A fractional-order RLGC model for terahertz transmission line,” *IEEE MTT-S International Microwave Symposium Digest IMS*, Seattle, USA, pp. 1-3, 2013.
- [76] C. Yang-Yang, and S-H. Yu, “A compact fractional-order model for terahertz composite right/left handed transmission line,” *General Assembly and Scientific Symposium URSI GASS, 2014 XXXIth URSI*, Beijing, China, pp. 1-4, 2014.
- [77] R. Ismail, and R. A. El-Barkouky, “Fractional-order transmission line modeling,” *International Journal of Advances in Computer Science and Technology IJACST*, vol. 2, no. 11, pp. 18-24, 2013.

- [78] Z. Yanzhu, and X. Dingyu, “Dynamical simulation analysis based on time fractional transmission line model,” *7th International Symposium on Antennas, Propagation and EM Theory, ISPE’06*, Guilin, China, pp. 1-4, 2006.
- [79] I. Podlubny, *Fractional Differential Equations: An Introduction to Fractional Derivatives, Fractional Differential Equations, Some Methods of Their Solution and Some of Their Applications*, New York: Academic, 1999.
- [80] R. Hermann, *Fractional Calculus an Introduction for Physicists*, Singapore: World Scientific, 2011.
- [81] M. Meerschaert, and A. Sikorskii, *Stochastic Models for Fractional Calculus*, Berlin, Germany: De Gruyter, 2011.
- [82] B. T. Krishna and K. V. V. S. Reddy, “Active and Passive Realization of Fractance Device of Order 1/2,” *Active and Passive Electronic Components*, vol. 2008, Article ID 369421, 5 pages, 2008.
- [83] S. M. Cvetianin, D. Zorica, and M. R. Rapaić, “Generalized time-fractional telegraphers equation in transmission line modeling,” *Nonlinear Dynamics*, vol. 88, no. 2, pp. 1453-1472, 2017.
- [84] X. Liu, X. Cui, L. Qi, G. Liang, and L. Yan, “Wide-band modeling of cables based on the fractional order differential theory,” *Proceedings of the 7th International Conference IEEE Asia-Pacific Lightning APL*, Chengdu, China, pp. 604-608, 2011.
- [85] E. C. Levy, “Complex-curve fitting,” *IRE Transactions on Automatic Control*, vol. AC-4, no. 1, pp. 37-43, 1959.
- [86] N. Al-Zubaidi R-Smith, A. Kartci, and L. Brančík, “Application of Numerical Inverse Laplace Transform Methods for Simulation of Distributed Systems with Fractional-Order Elements,” *Journal of Circuits, Systems, and Computers JCSC*, vol. 27, no. 11, pp 1-25. 2018.
- [87] L. Brančík, A. Kartci, and N. Al-Zubaidi R-Smith, “Matlab simulation of transmission lines with skin effect via fractional telegraph equations and NILT,” *27th EAEEIE Annual Conference*, Grenoble, France, pp. 1-5, 2017.
- [88] M. Caputo, *Elasticita e Dissipazione*, Bologna: Zanichelli, 1969.
- [89] M. Nakagawa, and K. Sorimachi, “Basic characteristics of a fractance device,” *IEICE Trans. On Fundamentals of Electronics, Communications and Computer Sciences*, vol. 75, pp. 1814–1819, 1992.

- [90] M. Sugi, Y. Hirano, Y. F. Miura, and K. Saito, "Simulation of fractal immittance by analog circuits: An approach to the optimized circuits," *IEICE Trans. On Fundamentals of Electronics, Communications and Computer Sciences*, vol. E82-A, No. 8, pp. 1627–1635, 1999.
- [91] N. Al-Zubaidi R-Smith, A. Kartci, and L. Brančik, "Fractional-order lossy transmission line with skin effect using NILT method," *Proceedings of the 40th International Conference on Telecommunications and Signal Processing TSP*, Barcelona, Spain,, pp.730-734, 2017.
- [92] I. Petras, *Engineering Education and Research Using MATLAB.*, InTech, ch. Fractional Derivatives, Fractional Integrals, and Fractional Differential Equations in Matlab, pp. 239–264, 2011.
- [93] H. Sheng, Y. Li, and Y. Q. Chen, "Application of numerical inverse Laplace transform algorithms in fractional calculus," *Journal Franklin Institute*, vol. 348, pp. 315–330, 2011.
- [94] H. Hassanzadeh, and M. Pooladi-Darvish, "Comparison of different numerical Laplace inversion methods for engineering applications," *Applied Mathematics and Computation*, vol. 189, no. 2, pp. 1966-1981, 2007.
- [95] L. Brančik, and N. Al-Zubaidi R-Smith, "Commentary on method of numerical inverse Laplace transformation - possible generalization and error analysis," *in Electronic Horizon*, vol. 70, no. 4, pp. 6-10, 2014.
- [96] N. Al-Zubaidi R-Smith, and L. Brančik, "Comparative study on one-dimensional numerical inverse Laplace transform methods for electrical engineering," *in Elektrovrevue e-journal*, vol. 18, no. 1, pp. 1-8, 2016.
- [97] P. Wynn, "A note on the generalized Euler transformation," *Computer Journal*, vol. 14, pp. 437-441, 1971.
- [98] P. Henrici, "Quotient-difference algorithms," *in Mathematical Methods for Digital Computers*, vol. 2, A. Ralston and H. S. Wilf, eds., J. Wiley, N. York, pp. 37-62, 1967.
- [99] H. Rutishauser *Der Quotienten-Differenzen-Algorithmus*, Basel, Birkhauser Verlag, 1957.
- [100] L. Brančik, "Technique of 3D NILT based on complex Fourier series and quotient-difference algorithm," *17th IEEE Int. Conference on Electronics, Circuits, and Systems (ICECS)*, Athens, pp. 203-206, 2010.

- [101] J. R. Macdonald, “Accelerated convergence, divergence, iteration, extrapolation, and curve fitting,” *Journal Applied Physics*, vol.10, pp. 3034-3041, 1964.
- [102] N. Al-Zubaidi R-Smith, and L. Brančik, “Convergence acceleration techniques for proposed numerical inverse Laplace transform method,” 24th *Telecommunications Forum (TELFOR)*, Belgrade, Serbia, IEEE, pp. 1-4, 2016.
- [103] P. Wynn, “The epsilon algorithm and operational formulas of numerical analysis,” *Mathematics of Computation*, vol.15, no.74, pp. 151-158, 1961.
- [104] N. Al-Zubaidi R-Smith, and L. Brančik, “Proposed hyperbolic NILT method—acceleration techniques and two-dimensional expansion for electrical engineering applications,” *IEICE Transactions on Fundamentals of Electronics, Communications and Computer Sciences*, vol. E101-A, no.5, pp. 763-771, 2018.
- [105] J. A. C. Weideman, “Optimizing Talbot’s Contours for the Inversion of the Laplace Transform,” *SIAM Journal on Numerical Analysis*, vol. 44, pp. 2342-2362, 2006.
- [106] N. Nahman, and D. Holt, “Transient analysis of coaxial cables using the skin effect approximation,” *Circuit Theory, IEEE Transactions*, vol. 19, no. 5, pp. 443-451, 1972.
- [107] C. R. Paul, *Analysis of Multiconductor Transmission Lines*, John Wiley and Sons, New York, 1994.
- [108] N. Al-Zubaidi R-Smith, “Accelerated hyperbolic NILT method used for frequency-dependent transmission line simulation,” *Proceedings of the 23rd Conference Student EEICT*, Brno University of Technology, Brno, Czech Republic, pp. 634 – 639, 2017.
- [109] N. Al-Zubaidi R-Smith, and L. Brančik, “Nonuniform Lossy Transmission Lines with Fractional-order Elements Using NILT Method,” *Progress in Electromagnetic Research Symposium (PIERS)*, Singapore, Singapore, IEEE, pp. 2540-2547, 2017.
- [110] F. R. Gantmacher, *The Theory of Matrices*, Chelsea Publishing Company, New York, 1984.
- [111] Y. Zhang, and D. Xue, “Dynamical simulation analysis based on time fractional transmission line model,” 7th *International Symposium on Antennas, Propagation and EM Theory, ISPE’06*, Guilin, China, 1-4, 2006.

- [112] O. P. Agrawal, "A general solution for a fourth-order fractional diffusion-wave equation defined in a bounded domain," *Computers and Structures*, vol. 79, no. 16, 1497-1501, 2001.
- [113] J. A. B. Faria, *Multiconductor Transmission-Line Structures: Modal Analysis Techniques*, John Wiley and Sons, New York, 1993.
- [114] L. Brančák, and B. Ševčík, "Computer simulation of nonuniform MTLs via implicit Wendroff and state-variable methods," *Radioengineering*, vol. 20, no. 1, pp. 221-227, 2011.
- [115] L. Brančák, "Improved method of numerical inversion of two-dimensional Laplace transforms for dynamical systems simulation," *Proceedings of the 9th IEEE ICECS'02*, Dubrovnik, Croatia, pp. 385-88, 2002.
- [116] L. Brančák, "Simulation of multiconductor transmission lines using two-dimensional Laplace transformation," *Proceedings of the 15th European Conference Circuit Theory and Design ECCTD'01*, Espoo, Finland, pp. 133-136, 2001.
- [117] J. Willis, and N. K. Sinha, "Non-uniform transmission lines as impedance transformers," *Proceedings IEE (London)*, vol. 103, pt. B, pp. 166-172, 1956.
- [118] L. A. Hayden, and V. K. Tripathi, "Nonuniformly coupled microstrip transversal filters for analog signal processing," *IEEE Transactions Microwave Theory Tech.*, vol. 39, pp. 47-53, 1991.
- [119] P. P. Roberts, and G. E. Town, "Design of microwave filters by inverse scattering," *IEEE Transactions on Microwave Theory and Techniques* vol. 43, no.4, 739-743, 1995.
- [120] S. C. Burkhart, and R. B. Wilcox, "Arbitrary pulse shape synthesis via nonuniform transmission lines," *IEEE Transactions on Microwave Theory and Techniques* vol. 38, pp. 1514-1518, 1990.
- [121] T. Dhaene, L. Martens, and D. D. Zutter, "Transient simulation of arbitrary nonuniform interconnection structures characterized by scattering parameters," *IEEE Transactions Circuits Systms I* vol. 39, pp. 928-937, 1992.
- [122] M. Khalaj-Amirhosseini, "Analysis of coupled or single nonuniform transmission lines using step-by-step numerical integration," *Progress In Electromagnetics Research, (PIER)* vol. 58, pp. 187-198, 2006.

- [123] L. Brančık, N. Al-Zubaidi R-Smith, and A. Kartci, “Numerical simulation of nonuniform multiconductor transmission lines with HF losses in Matlab,” *28th International Conference Radioelektronika18*, Prague, Czech Republic, pp.1-5, 2018.
- [124] S. Lum, M. S. Nakhla, and Q. J. Zhang, “Sensitivity analysis of lossy coupled transmission lines,” *IEEE Transactions on Microwave Theory and Techniques*, vol. 39, no. 12, pp. 2089-2099, 1991.
- [125] L. Brančık, and N. Al-Zubaidi R-Smith, “Comparative simulations of hybrid systems with nonuniform MTLs via Wendroff and NILT based techniques,” *In 2016 Progress in Electromagnetics Research Symposium (PIERS)*. Shanghai, China, pp. 4067-4072, 2016.
- [126] N. Al-Zubaidi R-Smith, “Accuracy comparison of some 2D numerical inverse Laplace transform methods,” *22nd Conference Student EEICT16*. The Faculty of Electrical Engineering and Communication, Brno University of Technology, pp. 282-287, 2016.
- [127] N. Al-Zubaidi R-Smith, and L. Brančık, “On two-dimensional numerical inverse Laplace transforms with transmission line applications,” *In 2016 Progress in Electromagnetics Research Symposium (PIERS)*. Shanghai, China, pp. 227-231, 2016.
- [128] E. L. Koh, and J. Conlan, “Fractional derivatives, Laplace transforms and association of variables,” *International Journal of Systems Science*, vol. 7, no. 5, pp. 591-596, 1976.
- [129] J. Valsa, “Numerical inversion of multivariable Laplace transforms,” *Proceedings of the 5th Electronic Devices and Systems International Conference EDS98*, Brno, Czech Republic, pp. 337-340, 1998.
- [130] V. A. Ditkin, and A. P. Prudnikov, *Operational Calculus in Two Variables and its Applications*, New York, Pergamon, 1962.
- [131] L. Brančık, “Error analysis at numerical inversion of multidimensional Laplace transforms based on complex Fourier series approximation,” *IEICE Transactions on Fundamentals of Electronics, Communications and Computer Sciences*, vol. E94-A, no. 3, pp. 999-1001, 2011.

- [132] L. Brančik, N. Al-Zubaidi R-Smith, and F. Záplata, “Matlab Simulation of Nonlinear Electrical Networks via Volterra Series Expansion and Multidimensional NILT,” *Progress in Electromagnetic Research Symposium (PIERS)* Singapore, Singapore, pp. 2822-2829, IEEE, 2017.
- [133] L. Sang, J. Wang, Y. Xu, and R. Xu, “Extracting Volterra Series Representation from X -parameters for the Modeling of Microwave Device,” *Journal of Electromagnetic Waves and Applications*, vol. 27, no. 3, 299-308, 2013.
- [134] S. B. Karmakar, “Laplace transform solution of nonlinear differential equations,” *Indian Journal of Pure and Applied Mathematics*, vol. 11, no. 4, 407-412, 1980.
- [135] J. Debnath, and N. C. Debnath, “Associated transforms for solution of nonlinear equations,” *International Journal of Mathematics and Mathematical Sciences*, vol. 14, no. 1, 177-190, 1991.
- [136] M. Schetzen, *The Volterra and Wiener Theories of Nonlinear Hybrid Systems*, Krieger Publishing Company, New York, 2006.
- [137] J. J. Bussgang, L. Ehrman, and J. W. Graham, “Analysis of nonlinear systems with multiple inputs,” *Proceedings of the IEEE*, vol. 62, no. 8, 1088-1119, 1974.

List of abbreviations

NILT	Numerical Inverse Laplace Transform
MNILT	Multidimensional Numerical Inverse Laplace Transform
ILT	Inverse Laplace Transform
MLT	Multidimensional Laplace Transform
FFT	Fast Fourier Transform
Qd	Quotient-difference
IFFT	Inverse Fast Fourier Transform
FHT	Fast Hartley Transform
CST	Continuous Space–Time
PWM	Pulse Width Modulation
Hyp-Qd	Hyperbolic Quotient-difference
Hyp-Eul	Hyperbolic Euler
Hyp – ε	Hyperbolic Epsilon
TL	Transmission Line
MTL	Multiconductor Transmission Line
SE	Skin Effect
PCB	Printed Circuit Board
ODE	Ordinary Differential Equation
PDE	Partial Differential Equation
NODE	Nonlinear Ordinary Differential Equation
NVNA	Nonlinear Vector Network Analyzer

List of appendices

A Curriculum Vitae	125
B List of Publications	128
C Achievements	132

A Curriculum Vitae

Nawfal Al-Zubaidi R-Smith

Technicka 3082/12,
616 00, Brno
Czech Republic
Phone: +420 5 4114 6556. Mobile: +4367762681530
Email: alzubaidi@phd.feec.vutbr.cz
Email: nawfal.smith@gmail.com

RESEARCH INTERESTS

Numerical methods for electrical engineering, computer-aided simulation, signal integrity issues in electronic circuits, transmission lines and fractional calculus.

EDUCATION

Since 2014: Brno University of Technology, Brno, Czech Republic.

- Postgraduate studies at the Department of Radio Electronics, Study Programme: Electrical, Electronic, Communication and Control Technology (PhD Candidate).
- Thesis: Methods of numerical inversion of Laplace transforms for electrical engineering and their applications.

2010-2013: Blekinge Institute of Technology, Karlskrona, Sweden.

- Master of Science (MSc.), Electrical Engineering with Emphasis on Radio Communication.
- Thesis: An Efficient Scheme in IEEE 802.22 WRAN for Real Time and Non-Real Time Traffic Delay.

2004-2009: Yarmouk University, Irbid, Jordan.

- Bachelor of Science (BSc.), Electrical Engineering and Communications.
- Thesis: Ad Hoc Networks – Performance & Analysis.

ACADEMIC APPOINTMENTS

- Since 9/2014: Department of Radio Electronics, Brno University of Technology.
- 5/2013-9/2013: Research assistant, department of computer science, Aarhus University, Aarhus, Denmark.

RESEARCH STAY

- 4/2018 - 8/2018: Exchange Fellow at Johannes Kepler University, Linz, Austria.

COMPUTER SKILLS

- Matlab – Intermediate
- MS Office, LaTeX- Advanced
- OrCad PSpice, AutoCad – Intermediate
- Adobe InDesign – Intermediate
- Adobe Photoshop – Intermediate
- Salesforce and Siebel – Advanced

WORK & EXPERIENCE

- 2/2009 – 8/2009 Orange Telecommunications Co, Jordan.
- 2/2014 – 12/2014 Lindberg International A/S, Denmark.
- 2018 Zebra Technologies Europe Limited, Czech Republic.

LANGUAGE SKILLS

- Arabic – Native speaker.
- Spanish – Native speaker.
- English – Advanced.
- German – Basic knowledge.
- Italian – Basic Knowledge.

B List of Publications

PUBLICATIONS

2018

N. Al-Zubaidi R-Smith, A. Kartci and L. Brančík, Application of Numerical Inverse Laplace Transform Methods for Simulation of Distributed Systems with Fractional-Order Elements, *Journal of Circuits, Systems, and Computers*, vol. 27, no. 11, pp 1-25. 2018.

N. Al-Zubaidi R-Smith and L. Brančík, “Proposed hyperbolic NILT method–acceleration techniques and two-dimensional expansion for electrical engineering applications,” *IEICE Trans. on Fundamentals of Electronics, Communications and Computer Sciences*, vol. E101-A, no.5, pp. 763-771, 2018.

L. Brančík, N. Al-Zubaidi R-Smith and A. Kartci, “Numerical Simulation of Nonuniform Multiconductor Transmission Lines with HF Losses in Matlab,” *28th International Conference Radioelektronika*, Prague, Czech Republic, pp. 1-5, 2018.

2017

N. Al-Zubaidi R-Smith and L. Brančík, “Nonuniform Lossy Transmission Lines with Fractional-order Elements Using NILT Method,” *Progress in Electromagnetic Research Symposium (PIERS)*, Singapore, Singapore, pp. 2540-2547, IEEE, 2017.

L. Brančík, A. Kartci and N. Al-Zubaidi R-Smith, “Matlab simulation of transmission lines with skin effect via fractional telegraph equations and NILT,” *27th EAEEIE Annual Conference*, Grenoble, pp. 1-5, 2017.

L. Brančík, N. Al-Zubaidi R-Smith, and Filip Záplata, “Matlab Simulation of Nonlinear Electrical Networks via Volterra Series Expansion and Multidimensional NILT,” *Progress in Electromagnetic Research Symposium (PIERS)*, Singapore, Singapore, pp. 2822-2829, IEEE, 2017.

N. Al-Zubaidi R-Smith, A. Kartci and L. Brančík, "Fractional-order lossy transmission line with skin effect using NILT method," *Proceedings of the 40th International Conference on Telecommunications and Signal Processing TSP*, (Barcelona, Spain), pp. 730-734, 2017.

Al Zubaidi-Polli, A.M., Verdezoto, N., Al Zubaidi R-Smith, N., Anderst-Kotsis, G., "Ex-situ Technology Appropriation of an e-Deliberation platform in an Art Gallery," *Proceedings of the 19th International Conference on Information Integration and Web-Based Applications & Services (iiWAS2017)*, Salzburg, Austria, pp. 1-10, 2017.

N. Al-Zubaidi R-Smith, "Accelerated hyperbolic NILT method used for frequency-dependent transmission line simulation," *Proceedings of the 23rd Conference Student EEICT, Brno University of Technology*, Brno, Czech Republic, pp. 634-639, 2017, ISBN: 978-80-214-5496-5.

2016

N. Al-Zubaidi R-Smith and L. Brančík, "Convergence acceleration techniques for proposed numerical inverse Laplace transform method," *24th Telecommunications Forum (TELFOR)*, Belgrade, Serbia, IEEE, pp. 1-4, 2016.

N. Al-Zubaidi R-Smith and L. Brančík, "On two-dimensional numerical inverse Laplace transforms with transmission line applications," *Progress in Electromagnetic Research Symposium (PIERS)*, Shanghai, China, pp. 227-231, IEEE, 2016.

L. Brančík and N. Al-Zubaidi R-Smith, "Comparative simulations of hybrid systems with nonuniform MTLs via Wendroff and NILT based techniques," *Progress in Electromagnetic Research Symposium (PIERS)*, Shanghai, China, pp. 4067-4072, IEEE, 2016.

N. Al-Zubaidi R-Smith, "Accuracy comparison of some 2D numerical inverse Laplace transform methods". *Proceedings of the 22nd Conference Student EEICT, Brno University of Technology*, Brno, Czech Republic, pp. 282-287, 2016, ISBN: 978-80-214-5350-0.

N. Al-Zubaidi R-Smith and L. Brančík, "Comparative study on one-dimensional numerical inverse Laplace transform methods for electrical engineering," in *Elektrorevue e-journal*, vol. 18, no. 1, pp. 1-8, 2016, ISSN: 1213-1539.

2015

L. Brančík and N. Al-Zubaidi R-Smith, "Two approaches to derive approximate formulae of NILT method with generalization," in *38th International Convention on Information and Communication Technology, Electronics and Microelectronics (MIPRO)*, Opatija, Croatia, IEEE, pp. 155-160, 2015

L. Brančík, E. Kolářová and N. Al-Zubaidi R-Smith, "SDE-based variance simulation in transmission line models with random excitations," *25th International Conference Radioelektronika*, Pardubice, Czech Republic, IEEE, pp. 85-88, 2015.

L. Brančík, J. Šebesta, T. Göthans, E. Kolářová, N. R-Smith, A. Povalač, M. Kubíček, and B. Ševčík, Research of Signal Integrity at High-Speed Interconnects. In PRIDE – Project Information and Dissemination Event, 38th International Convention MIPRO, May 25-29, 2015, Opatija, Croatia (poster).

2014

N. Al-Zubaidi R-Smith and A. Polli, "From Beer to Electricity- An Energy Harvesting Experiment in the Forest," in *Elektrorevue e-journal*, vol. 5, no. 4, pp. 42-47, 2014, ISSN: 1213-1539.

L. Brančík and N. Al-Zubaidi R-Smith, "Commentary on method of numerical inverse Laplace transformation-possible generalization and error analysis," in *Electronic Horizon*, vol. 70, no. 4, pp. 6-10, 2014. (Czech).

C Achievements

- I. Best paper award at the 40th international conference on telecommunications and signal processing (TSP) 2017, supported by IEEE.
- II. EEICT student conference 2017 winning best work certificate for 3rd position.